UNIVERSIDAD AUTONOMA DE MADRID

Aspects of global dynamics in nonautonomous dynamical systems

Applied Mathematics

Author

Carlos Lopesino Jiménez de Zadava Lissón

Advisors

Dr. Ana María Mancho Sánchez
Prof. Stephen Wiggins

February 11, 2018

ICMAT INSTITUTO DE CIENCIAS MATEMÁTICAS

CSIC CONSEJO SUPERIOR DE INVESTIGACIONES CIENTÍFICAS

EXCELENCIA SEVERO OCHOA

This Ph.D. thesis has been partially supported by MINECO under grant MTM2014-56392-R, MINECO: ICMAT Severo Ochoa project SEV-2011-0087 and ONR grant N00014-17-1-3003. The research stays along this Ph.D. programme have been financed by MINECO programme: Subprograma Estatal de Movilidad (announcements in 2015 and 2016) and ONR Grant No. N00014-01-1-0769.

Abstract

Lagrangian descriptors (LDs) are a recent tool that has been used in multiple applications as a method to uncover the phase space of time-dependent dynamical systems. The main goal of this work is to provide rigorous results about this technique in the discrete and continuous time setting.

First we extend the definition of LD to apply it in two dimensional, area-preserving, autonomous and nonautonomous discrete time dynamical systems. We then proceeded to prove rigorous results by considering four different model problems: a hyperbolic saddle point for a linear, area-preserving autonomous map, a hyperbolic saddle point for a nonlinear, area-preserving autonomous map, a hyperbolic saddle point for a linear, area-preserving nonautonomous map, and a hyperbolic saddle point for a nonlinear, area-preserving nonautonomous map. The choice of a specific norm allows us to provide a rigorous setting for the notion of "singular sets" that correspond to invariant manifolds of hyperbolic points. From the computational point of view, we also analyze the performance of LDs to reveal chaotic invariant sets.

We then extend these results to the continuous setting by also considering analogous particular cases: a hyperbolic saddle point for linear autonomous systems, a hyperbolic saddle point for nonlinear autonomous systems, a hyperbolic saddle point for linear nonautonomous systems and a hyperbolic saddle point for nonlinear nonautonomous systems. Additionally, we discuss further rigorous results which show the ability of LDs to highlight other invariant sets, such as n-tori. These results are an extension of the ergodic partition theory which we illustrate by applying LDs to some examples, such as the planar field of the harmonic oscillator and the 3D ABC flow. We also provide a discussion on the requirement of the objectivity (frame-invariance) property for tools designed to reveal phase space structures.

Finally, we address the challenge of rigorously proving the presence of chaotic invariant sets in aperiodically time-dependent systems. In the context of discrete dynamical systems, we prove the existence of a chaotic saddle for a well-known piecewise-linear map of the plane, named the Lozi map. This is studied in its orientation and area-preserving version. We apply the first and second Conley-Moser conditions to obtain the proof of the existence of a chaotic saddle in the autonomous setting. Then we generalize the Lozi map to its nonautonomous version and prove that the first and the third Conley-Moser conditions are satisfied, thus implying the existence of a chaotic saddle. Lastly, equipped with a discrete LD, we numerically demonstrate how the structure of this nonautonomous chaotic saddle varies as parameters are varied.

Resumen

Los descriptores Lagrangianos (LDs) son una técnica desarrollada recientemente capaz de dibujar una estructura geométrica que caracteriza el espacio de fases de un sistema dinámico. El principal objetivo de esta tesis es proporcionar un marco teórico para los LDs en el caso discreto y continuo.

Generalizaremos la definición de descriptor Lagrangiano para aplicarlo en el caso de mapas en dos dimensiones, discretos que preservan el área, tanto en su versión autónoma como no autónoma. Consideramos cuatro modelos básicos: el punto hiperbólico silla para el caso de un mapa autónomo y lineal, el punto hiperbólico silla para el caso de un mapa autónomo no lineal, el punto hiperbólico silla para el caso de un map no autónomo lineal y el punto hiperbólico silla para el caso de un mapa no autónomo no lineal. La elección de una p-norma específica nos permite proporcionar un marco teórico para la noción de "conjunto singular" que se corresponde con variedades invariantes de puntos hiperbólicos. Además, analizamos desde el punto de vista computacional el funcionamiento de los LDs para revelar los conjuntos caóticos invariantes.

Nuestro trabajo continúa con la extensión de estos resultados al caso continuo por medio del estudio de cuatro casos particulares: el punto hiperbólico silla para el caso de sistema mapa autónomo y lineal, el punto hiperbólico silla para el caso de un sistema autónomo no lineal, el punto hiperbólico silla para el caso de un sistema no autónomo lineal y el punto hiperbólico silla para el caso de un sistema no autónomo no lineal. Además, discutimos otros resultados rigurosos que demuestran la capacidad de los LDs para resaltar otros conjuntos invariantes, como los n-toros. Estos resultados son una extensión de la teoría de partición ergódica y, los ilustramos mediante la aplicación de los LDs a algunos ejemplos, como el oscilador armónico plano y el flujo ABC tres dimensional. También proporcionamos una discusión sobre el requisito de la propiedad de objetividad (frame-invariance) para herramientas diseñadas a la hora de revelar estructuras geométricas del espacio de fases.

Finalmente, demostramos la existencia de un conjunto caótico invariante para un mapa conocido como el mapa de Lozi en la versión que preserva el área y su orientación. Aplicamos la primera y segunda condición de Conley-Moser para obtener la demostración de la existencia de un conjunto caótico invariante de tipo silla. Posteriormente, generalizamos el mapa de Lozi a su versión no autónoma y demostramos que, aplicando la primera y la tercera condición de Conley-Moser, obtenemos la existencia del conjunto caótico invariante de tipo silla. Finalmente, ilustraremos numéricamente cómo varía la estructura de este conjunto caótico de tipo silla no autónomo a medida que variamos los parámetros.

Agradecimientos

En estas breves líneas querría dar las gracias a todas aquellas personas que han hecho posible que llegue a este punto de mi vida, que me han hecho ser como soy y que esta tesis se haya podido realizar.

En primer lugar, agradecer a mis directores de tesis, Ana María Mancho y Stephen Wiggins por su seguimiento, dedicación y orientación a lo largo de estos cuatro años. Gracias por apostar por mí y darme la oportunidad que me disteis cuando todo este viaje comenzó. Vuestra paciencia, consejos y experiencia han hecho posible no sólo que este trabajo salga a la luz sino que además me pueda formar como investigador.

Dentro del mundo de la investigación he podido conocer a gente maravillosa que me han ayudado durante todo este tiempo. A mis compañeros del ICMAT, sobre todo, gracias a Miguel y a Paco (mis compañeros de despacho), hemos pasado muy buenos momentos durante nuestra estancia en el centro; conversaciones, risas, paseos y alguna que otra cerveza. Además, Paco, tú me acogiste cuando llegué a Madrid; no olvido nuestras discusiones sobre los problemas a resolver, las barreras que nos ha puesto la burocracia y las estancias en Bristol; nada de esto hubiera sido posible sin tu ayuda. Mis compañeros del grupo de investigación, Víctor y Jezabel: Jezabel siempre estabas dispuesta a ayudarme con lo que fuese y me diste todo el apoyo que necesitaba para empezar y Víctor, me sacaste de todos los problemas que tenía con el ordenador y con tus consejos me hiciste la labor mucho más sencilla.

Trinidad Cámara Meseguer y Paco Balibrea Gallego; vosotros me inculcasteis mi amor por las Matemáticas, en el instituto y en la universidad respectivamente. Trini, ya desde el instituto me ponías a prueba con los problemas de las Olimpiadas Matemáticas y ya en el máster de educación me adoptaste, junto con Lucía, para enseñarme la parte docente. Paco, tú me enseñaste el mundo de las Ecuaciones Diferenciales y me aconsejaste, y con qué ojo, para que hiciera mi especialización en Opava, toda una experiencia. No me quiero olvidar del resto de profesores que también participaron en mi formación matemática: Víctor Jiménez, su examen con ejercicio sin solución incluído y Antonio Linero, nuestro centrocampista todoterreno.

También extiendo los agradecimientos a mis excompañeros y alumnos del IES Beatriz Galindo del año pasado: con ellos empecé mi experiencia en la docencia y me ayudaron en mis primeros pasos en este mundo. De la misma manera agradezco a mis compañeros de este año del IES Santamarca, en particular, a los profesores del departamento de Matemáticas: seguiremos con las cenas y las cañas de los viernes.

No me puedo olvidar de mis compañeros de la universidad, en particular, de ti Jesús: siempre estabas dispuesto a coger el teléfono cuando me surgía una duda o quedar para ver el fútbol o para ayudarme con alguna asignatura complicada, siempre has sido mucho mejor que yo en esto de las matemáticas pero a la play todavía estás a años luz de mí; ¡¡hala Madrid y nada más!!. También me quiero acordar en estas líneas de mis compañeros de fiestas universitarias: Miriam (y minica) conversaciones y secretillos (siempre seré tu tutorcillo), JM (y marido) sabes que seguiré siendo un cenutrio pero aún así nos lo pasamos bien de crucero, y cómo no Miguelito de la Roda (y mujer) cuántos momentos y viajes juntos (Galicia, Albacete y criucero), necesitaría todo un libro para hablar de nuestra amistad. Los partidos de fútbol tampoco se olvidan, eliminados en cuartos del Trofeo Rector, estuvimos muy cerca de llevar una copa de fútbol a la facultad de Matemáticas, y vivan esos Skulls y Ondiñas Veñen (pronto cambiaremos el nombre por Anchoiñas, es cuestión de tiempo).

Parte de lo que soy ha sido gracias a los veranos rillanos: las fiestas de los pueblos en que hemos estado, los viajes al río y por el campo descubriendo siempre nuevos sitios y la Peña de "El Puntillo" (con casita

incluída): Vicente, Álex, Emma, Diana, Fran y Carmen, Sara y Laura, Celia, María, Laura, Inés, Edu, Víctor, Lorena y mis dos primitos, Andrés e Inés. Muchas gracias a vosotros porque, a pesar de ser el peque de la peña siempre me cuidasteis y me hicisteis un hueco en ella. ¡Las fiestas de nuestro pueblo siempre serán las mejores!

Gracias a Murcia y Madrid: estas dos ciudades siempre las llevaré en mi corazón, una la que me vio crecer desde que nací y la otra la que me dio las oportunidades laborales que siempre busqué. Y gracias a mis dos familias, la política que me acogió desde el primer día como si fuera su hijo y la biológica. Muchísimas gracias a mis abuelos: siempre me hicisteis muy feliz y me cuidasteis como si fueseis mis padres. A ti Elena; gracias por estos ocho años tan maravillosos que llevamos juntos y que espero que sean muchísimos más a tu lado. Y por último, a mi hermano, a mi padre y a mi madre (que has sido muy pesada): gracias por vuestros consejos, vuestro cariño y vuestra confianza depositada en mí. Siempre estuvisteis y estáis ahí y nunca me faltó nada para que pudiera tener éxito en la vida; os estoy a todos eternamente agradecido.

Gracias por todo.

Contents

List of Figures

CHAPTER 1

Introduction

This Ph.D Thesis is written as a compendium of three articles and its structure is as follows: This introductory chapter briefly reviews the state of the art of some selected topics on nonautonomous dynamical systems that are the focus of study in this thesis. These topics are chosen for their significance in applications. Chapter 2 describes the objectives of this study. More specifically, the emphasis is on providing formal results which are relevant in the context of aperiodically time-dependent dynamical systems.

At the end of the 19th century, Poincaré (1890) opened up new ways of studying solutions by exploring geometrical and topological properties of the phase space of dynamical systems. A dynamical system may be understood as a system which evolves in time and is deterministic, i.e., given an initial condition, one can find the evolution in any future time by solving the ordinary differential equation:

$$\frac{d\mathbf{x}}{dt} = v(\mathbf{x}, t), \quad \mathbf{x} \in \mathbb{R}^{\mathbf{n}}, t \in \mathbb{R}, \tag{1.1}$$

The dynamical system expressed in Eq. 1.1 is nonautonomous when the vector field $v(\mathbf{x}, t)$ depends explicitly on time t. The study of nonautonomous dynamics is a topic of high interest, and a motivation for such work is the understanding of fluid transport in time-dependent flows. Let us explain further how nonautonomous dynamical systems describe transport phenomena. A fluid parcel, neglecting molecular diffusion, evolves according to trajectories that are solutions to the system (1.1). In this equation, the vector field $v(\mathbf{x}, \mathbf{t})$ represents the fluid velocity field. If the flow is incompressible and particle motions are restricted to a plane, the velocity field is obtained from a streamfunction $\psi(x, y, t)$ (Batchelor, 1967) and satisfies that $v = (v_x, v_y) = (\partial_y\psi, -\partial_x\psi)$. In this case, equations of motions (1.1) are rewritten as:

$$\begin{cases} \dot{x} &= \dfrac{\partial\psi}{\partial y}(x, y, t) \\ \\ \dot{y} &= -\dfrac{\partial\psi}{\partial x}(x, y, t) \end{cases} \tag{1.2}$$

In regard to dynamical systems theory, formally equations (1.2) have the structure of Hamilton's canonical equations, where $\psi(x, y, t)$ is the Hamiltonian function. These equations are applicable in many oceanic and atmospheric contexts (Ottino, 1989a,b; Wiggins, 1992; Branicki and Wiggins, 2010; Wiggins, 2005) where motion is quite frequently two-dimensional. Typically in these settings, the velocity fields (or the streamfunction) are time-dependent and aperiodic. Furthermore, these velocity fields are frequently given as data sets in a finite time interval. For instance, they are obtained as the solution of a set of partial differential equations that describe the dynamical evolution of the velocity field, or by observation through remote sensing of some region of the ocean.

As addressed in Wiggins and Mancho (2014), in the early eighties, this "Hamiltonian dynamical systems" point of view generated a great deal of interest; in particular, after the work by Aref (1984) focusing on time-dependent periodic flows. Adopting Aref's point of view, one may "see" that phase space structures such as elliptic periodic orbits and hyperbolic periodic orbits with their stable and unstable manifolds as well

Dynamical System Theory	**Physical observation**
Stable and unstable manifolds	Barriers for fluid transport
Elliptic regions and KAM Tori	Trapping fluid regions
Chaos and Smale horseshoes	Rapid stirring and lobe dynamics

Table 1.1: Dynamical Systems concepts and implication in fluid transport (Mancho *et al.*, 2006).

as KAM tori, have an immediate interpretation in terms of "structures" in the flow that influences transport and mixing. For instance, intersecting stable and unstable manifolds gave rise to "partial" barriers to transport and "lobe dynamics" (Rom-Kedar *et al.*, 1990), which means that transversely intersecting stable and unstable manifolds of hyperbolic periodic orbits could be linked to chaotic fluid particle trajectories through the construction of Smale horseshoes (Smale, 1967), while KAM tori were linked to regions trapping fluid particles, thereby preventing them from "mixing" with surrounding fluid. This connection between dynamical system theory and physical observation is summarized in Table 1.1 (Mancho *et al.*, 2006). Reviews of the dynamical system approach to Lagrangian transport and mixing for time periodic incompressible flows can be found in Aref (2002); Ottino (1989a,b); Wiggins and Ottino (2004); Sturman *et al.* (2006).

The task of finding these geometrical structures characterizing transport processes in the context of geophysical flows is a difficult challenge due to their aperiodic character, which in the literature has been addressed in several ways. Miller *et al.* (1997) applied numerical methods to obtain invariant manifolds of hyperbolic fixed points, as did Coulliette and Wiggins (2001) in geophysical relevant flows. Malhotra and Wiggins (1998) computed stable and unstable manifolds in aperiodic flows applied to Rossby wave flow, while examples of direct computation of manifolds can be found in Mancho *et al.* (2004, 2006) as well as Mendoza and Mancho (2012), all of which has provided valuable insights into oceanic problems (Mancho *et al.*, 2008; Mendoza *et al.*, 2010).

Finite size Lyapunov exponents (FSLE) (Aurell *et al.*, 1997) and finite time Lyapunov exponents (FTLE) (Nese, 1989) have been successfully applied in oceanic and atmospheric contexts (d'Ovidio *et al.*, 2004; Shadden *et al.*, 2009; Tew Kai *et al.*, 2009; Beron-Vera *et al.*, 2010; de la Cámara *et al.*, 2010). Rigorous results on the ability of FTLE to highlight Lagrangian Coherent Structures (LCSs) are discussed in Shadden *et al.* (2005); Lekien *et al.* (2007) and their objectivity property is discussed by Hadjighasem *et al.* (2017). Other approaches in this field consist of geodesic and variational theories of LCSs (Haller and Beron-Vera, 2012; Farazmand and Haller, 2012), trajectory complexity measures (Rypina *et al.*, 2011), mesohyperbolicity measures and ergodic partitions (Mezic and Wiggins, 1999; Levnajić and Mezić, 2010) and transfer operator methods Froyland *et al.* (2012); Froyland and Padberg-Gehle (2014).

A recent tool that reveals phase space structures of general time-dependent dynamical systems are Lagrangian descriptors (LDs). Lagrangian descriptors were first introduced in the literature by Madrid and Mancho (2009) in the form of a function, denoted by M, that was used to provide a definition for distinguished trajectories, which also included trajectories with an elliptic type of stability. Distinguished trajectories were highlighted by special minima of the function M referred to as limit coordinates. In the past few years, the applicability of the concept of Lagrangian descriptor has been extended and has become a method for detecting invariant manifolds of hyperbolic trajectories (Mendoza and Mancho, 2010). Invariant manifolds were highlighted by "singular features" of both the function M and some of its generalizations (Mendoza and Mancho, 2012; Mancho *et al.*, 2013). Since these early papers, numerous applications of Lagrangian descriptors have been given, e.g. in de la Cámara *et al.* (2012), where they were used in the context of atmospheric sciences to reveal the Lagrangian structures defining transport routes across the Antarctic polar vortex. This work was extended in de la Cámara *et al.* (2013), where LDs were applied to analyze the Lagrangian structures associated with a Rossby wave breaking in the stratosphere. Figure 1.1 a) shows the manifold geometry of the Antarctic Polar vortex as revealed by LDs (de la Cámara *et al.*, 2012). These studies have been continued by Curbelo *et al.* (2017a) with the study of the three-dimensional Lagrangian geometry of the Antarctic Polar Vortex. Other uses of the M function in atmospheric studies are those by Smith and Mc Donald (2014) and Manney and Lawrence (2016). In the field of magnetohydrodynamics, Lagrangian descriptors have also been shown to be useful for studying the influence of coherent structures on the saturation of a nonlinear dynamo in Rempel *et al.* (2013). There are also several applications in

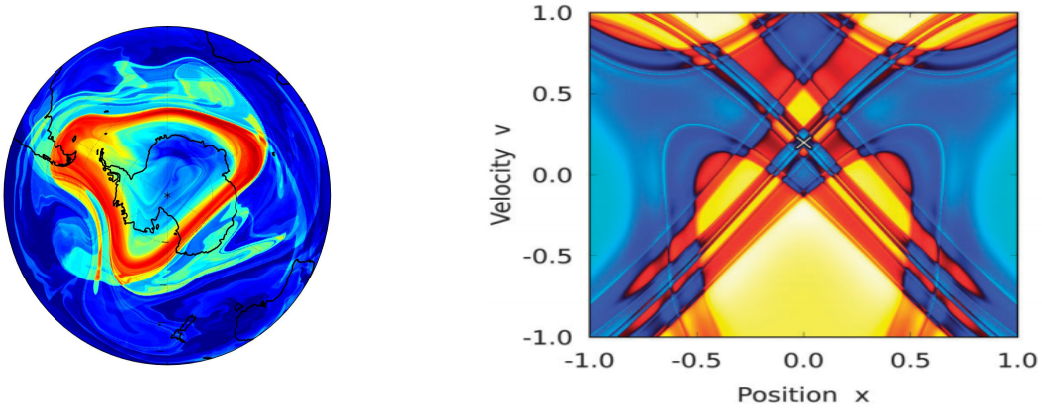

(a) (b)

Figure 1.1: Application of LDs in different contexts: (a) The manifold geometry of the Antartic Polar vortex as it is shown in de la Cámara *et al.* (2013) (courtesy of A. de la Cámara) and (b) Transition-state geometry of a chemical reaction as depicted in Junginger *et al.* (2016) (courtesy of A. Junginger).

oceanography. In Mendoza *et al.* (2014), LDs were used to analyze transport in a region of the Gulf of Mexico regarding the Deepwater Horizon oil spill. Garcia-Garrido *et al.* (2015) applied this tool to analyze the strategy followed by the Australian Maritime Authorities when searching for debris from the missing MH370 flight, and recently Garcia-Garrido *et al.* (2016) studied the role played by LDs in the management of the Oleg Naydenov oil spill that took place offshore to the south of Gran Canaria. All these works are related to various aspects of fluid dynamics. However, Lagrangian descriptors can be applied to the general study of the phase space structure of dynamical systems in different contexts. This has recently been illustrated in several applications of the tool to fundamental problems in chemical reaction dynamics. In particular, it has been applied to a study of chemical reactions under external time-dependent driving in Craven and Hernandez (2015); Junginger *et al.* (2016); Craven and Hernandez (2017). Figure 1.1 b) illustrates the kind of visualizations provided by LDs in this context. Other studies of phase space structure and reaction dynamics for a class of "barrierless reactions" are found in Junginger and Hernandez (2016), and for the isomerization dynamics of ketene in Craven and Hernandez (2016).

The ability of LDs to reveal invariant manifolds has been established in the references above from a phenomenological and numerical point of view; however, a rigorous framework is missing in these works. Our first goal in this thesis is to provide a mathematical framework for this tool. To this end, the initial result described in the first paper presented in Chapter 3 starts by extending the definition of LDs to discrete dynamical systems for which obtaining exact results is more tractable. In particular, discrete dynamical systems (maps) are given by

$$x_{n+1} = f(x_n) \tag{1.3}$$

where f is a continuous function. Eq. (1.4) is an autonomous system, i.e., this system does not depend explicitly on the time variable which in the map notation is n. If the system (1.4) is modified as follows

$$x_{n+1} = f(x_n, n) = f_n(x_n) \tag{1.4}$$

then the system becomes nonautonomous. In this system, f_n is a sequence of functions.

The second result discussed in the second paper in Chapter 3 extends these formal results obtained for discrete dynamical systems to the context of continuous-time dynamical systems. In this article we also trace back links of LDs with the ergodic partition theory (Mezic and Wiggins, 1999) and its ability to detect not only invariant manifolds of hyperbolic trajectories but also KAM tori.

Figure 1.2: The forwards and backwards Smale horseshoe map acting on the unit square D.

Most of the applications cited above are described for dynamical systems that depend on time in an aperiodic manner. Understood from the dynamical systems point of view, fluid transport for aperiodically time-dependent flows posses challenges such as rigorously proving the presence of chaotic invariant sets in this context. Results in this regard are reported in the third article presented in Chapter 3. Discrete dynamical systems, i.e. maps, provide a framework in which the presence of "chaotic invariant sets" (a notion that is precisely defined later) can be rigorously stated. The prototypical map possessing a chaotic invariant set is the Smale horseshoe, a map based on stretching and folding, which are the essential ingredients associated with chaos. The construction of the horseshoe map (Smale, 1967), and also the contributions by Alekseev (1968a,b, 1969) when applying Smale's ideas, provided new techniques to prove chaos in different contexts such as problems from celestial mechanics. We now provide a brief description of the Smale horseshoe map. The Smale horseshoe map is a map such that $f : D \to \mathbb{R}^2$ where $D = [0, 1] \times [0, 1]$. This map f converts the unit square D into a folded rectangle that intersects with same square giving two vertical strips (a vertical strip V is a piece of area surrounded by two vertical curves and two horizontal lines). In the same way, f^{-1} acting on the square produces another folded rectangle that intersects the square in two horizontal strips (a horizontal strip H is a piece of area surrounded by two horizontal curves and two vertical lines). This effect is visualized in Figure 1.2. By means of considering the forward and backward iteration of this map we may define the set:

$$\Lambda = \bigcap_{n=-\infty}^{+\infty} f^n(D) \tag{1.5}$$

which is a Cantor set having the following properties:

- Λ is invariant under the action of a map f, that is, $f(\Lambda) = \Lambda$.
- The dynamics of the map restricted to Λ is topologically conjugate to the shift map acting on the space of bi-finite sequences of 0's and 1's. This property enables us to prove the sensitive dependence on initial conditions restricted to this invariant set, and is thus called chaotic (see Wiggins (2003) Chapter 23).

An illustration of the iteration procedure defining the Cantor set is given in Figure 1.3.

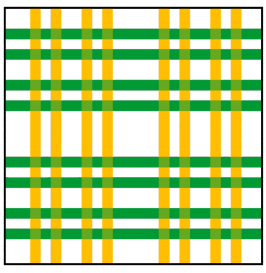

Figure 1.3: Illustration of the procedure defining the Cantor set for two forward and backward iterations.

Conley-Moser conditions are sufficient conditions for a map f to posses a chaotic invariant set Λ (Moser, 1973; Wiggins, 1999, 2003; Balibrea-Iniesta *et al.*, 2015). A detailed description of the autonomous version

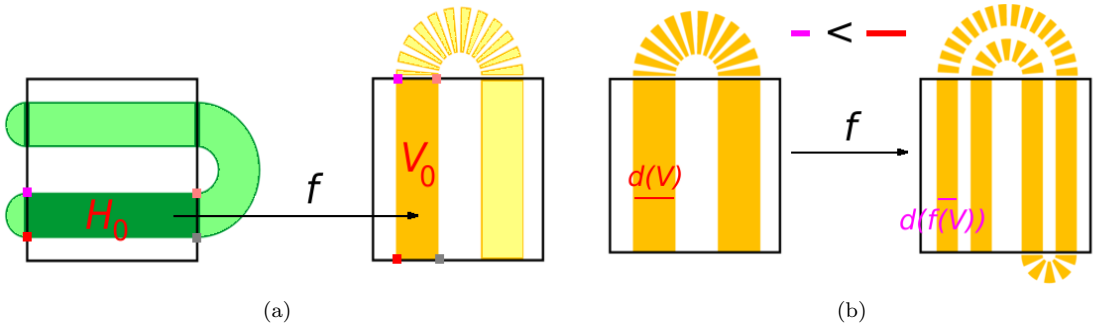

Figure 1.4: First and second Conley-Moser conditions: a) f maps horizontal strips to vertical strips and b) f converts vertical strips to thinner vertical strips.

of the three Conley Moser conditions is found in Wiggins (2003), and nonautonomous versions of the first and second conditions are given in Wiggins (1999). Conley–Moser conditions have been used by Devaney and Nitecki (1979) to show the existence of a chaotic invariant set for the Hénon map and by Holmes (1982), Chastaing *et al.* (2015) to show the existence of a chaotic invariant set for the bouncing ball map and Koon *et al.* (2000) to show the existence of a chaotic invariant set in the restricted three-body problem. Earlier work on chaos in nonautonomous systems can be found in Stoffer (1988a,b) and Lerman and Silnikov (1992). First and second conditions, which are illustrated in Figure 1.4, imply the existence of a chaotic invariant set Λ under the action of the map f. Moreover, if the first and the third condition are satisfied then the second condition is satisfied, and therefore the existence of a chaotic saddle is assured. The last result presented in Chapter 3 of this thesis proves, by means of these conditions, the presence of a chaotic saddle in the autonomous and nonautonomous versions of the Lozi map.

Finally, Chapter 4 provides a discussion on the results in Chapter 3, and Chapter 5 presents the conclusions and perspectives.

CHAPTER 2

Objectives

The major goal of this thesis is to provide formal results about selected topics in aperiodically time-dependent dynamical systems. First, we have addressed the issue of providing a theoretical background for Lagrangian descriptors, a novel tool that has recently been used for the geometrical description of the solutions of time-dependent dynamical systems in multiple applications. Secondly, in the context of the Lozi Map, we rigorously prove the presence of a chaotic invariant set for the autonomous and nonautonomous version as well as exploring discrete Lagrangian descriptors (DLD) performance in this context.

The specific objectives in this thesis are as follows:

1. **To provide a formal framework for Lagrangian descriptors in the discrete and continuous cases.**

   As stated above, LDs are used as an alternative technique to uncover the phase space of a dynamical system. Considering a general time-dependent vector field on $\mathbb{R}^n$

   $$\frac{d\mathbf{x}}{dt} = v(\mathbf{x}, t), \quad \mathbf{x} \in \mathbb{R}^{\mathbf{n}}, t \in \mathbb{R} \tag{2.1}$$

   where $v(\mathbf{x}, t)$ is C^r $(r \geq 1)$ in space and continuous in time are required for existence of unique solutions and textcolorredits/their linearization for a sufficient time interval $[t^* - \tau, t^* + \tau]$ (Arnold, 1973; Coddington and Levinson, 1955). The first Lagrangian descriptor M was defined in Mendoza and Mancho (2010) as the Euclidean arc length of the curve defined by the trajectory of (2.1) passing through a point x^* at time $t = t^*$:

   $$M(x^*, t^*) = \int_{t^*-\tau}^{t^*+\tau} \sqrt{\sum_{i=1}^{n} \left(\frac{dx_i(t)}{dt} \right)^2} dt = \int_{t^*-\tau}^{t^*+\tau} ||v(\mathbf{x}(t), t)|| dt, \tag{2.2}$$

   where $\mathbf{x}(t) = (x_1(t), x_2(t), ..., x_n(t))$. Later in Mancho *et al.* (2013) different positive integrands instead of the modulus of the velocity were used, such as the modulus of the velocity raised to different powers, the modulus of the acceleration, the modulus of the derivative of the acceleration, etc. Mancho *et al.* (2013) discuss whether the integration of positive quantities supports the heuristic argument that a Lagrangian descriptor computed in this way will change abruptly at the boundaries of regions comprising trajectories with qualitatively different evolutions, since this is exactly what the stable and unstable manifolds separate. For a small integration period τ, the structure of M is smooth, but for long integration periods τ sharp features appear aligned with the invariant manifolds of the hyperbolic trajectories in the system described by Eq. (2.1). Our goal is to provide a formal framework to this phenomenology for which numerical evidence has been described. In order to proceed in an accessible

manner, we start by setting the problem in the context of discrete dynamical systems (section 3.1). In this setting, let $\{x_n, y_n\}_{n=-N}^{n=N}, N \in \mathbb{N}$ denote an orbit generated by a two dimensional map. We introduce a new definition for a DLD which preserves the property of accumulating positive quantities along trajectories, but with a structure that facilitates explicit calculations for formal proofs. Let us consider:

$$MD_p = \sum_{i=-N}^{N-1} |x_{i+1} - x_i|^p + |y_{i+1} - y_i|^p, \quad p \leq 1. \tag{2.3}$$

Here we use different 'p-norms'. Additionally, we proceed with a similar strategy for providing formal results in the continuous case (Section 3.2). We define the continuous Lagrangian descriptor (CLD)

$$M_p(x_0, t^*, \tau) = \int_{t^*-\tau}^{t^*+\tau} \sum_{i=1}^{n} |\dot{x}_i(t; x_0)|^p \, dt. \tag{2.4}$$

The condition $p \leq 1$ in (2.3) and (2.4) is essential in order to obtain nondifferentiability through points belonging to invariant manifolds, as shown in Section 3.1 and in Section 3.2.

Moreover, Section 3.2 discusses the objectivity (frame-invariance) property in the context of LDs and the ability of LDs to provide the correct description of phase space structures in different frames, as well as a general consideration of the objectivity property requirement. Finally, a link of LDs with the ergodic partition theory is provided.

2. **Rigorous proof and conditions for the existence of invariant chaotic sets in the autonomous and nonaoutonomous Lozi Map. Usage of Lagrangian descriptors to visualize the chaotic saddle of the Lozi map.**

Sufficient conditions for the existence of a chaotic saddle for autonomous (Moser, 1973) and nonautonomous systems (Balibrea-Iniesta *et al.*, 2015) are proved in Section 3.3. The strategy to reach this goal is based on the verification of the Conley-Moser conditions, which have been previously adapted to the nonautonomous case. We verify these conditions to the autonomous and nonautonomous Lozi map and we show that for some parameters we can prove the existence of this chaotic behavior.

Finally, we apply discrete Lagrangian descriptors to the Lozi map, thereby obtaining the chaotic saddle for some parameters.

CHAPTER 3

Results

The result of this thesis are the publication of three articles that have been published in different journals.

The first article, "Lagrangian descriptors for two dimensional, area preserving, autonomous and nonautonomous maps", is written jointly with F. Balibrea and my two advisors A. M. Mancho and S. Wiggins. It is published in *Communications in Nonlinear Science and Numerical Simulation* **27** (1-3) (2015) 40–51. This article provides a theoretical framework for Lagrangian descriptors in the context of discrete time dynamical systems for specific settings. We focus our results in four main cases: a hyperbolic saddle point for linear autonomous map, a hyperbolic saddle point for a nonlinear autonomous map, a hyperbolic saddle point for a linear nonautonomous map and a hyperbolic saddle point for a nonlinear nonautonomous map. All the considered maps are area preserving. Finally we illustrate the ability of this tool to capture the "chaotic saddle" of the Hénon map.

The second article, "A theoretical framework for Lagrangian descriptors", is written jointly with F. Balibrea-Iniesta, V. J. García-Garrido, and my two advisors A. M. Mancho and S. Wiggins. It is published in *International Journal of Bifurcation and Chaos* **27**, 1730001 (2017). We provide a theoretical framework for Lagrangian descriptors in the context of continuous time dynamical systems. Specifically we provide formal results in four different cases: a hyperbolic saddle point for linear autonomous systems, a hyperbolic saddle point for nonlinear autonomous systems, a hyperbolic saddle point for linear nonautonomous systems and a hyperbolic saddle point for nonlinear nonautonomous systems. Furthermore we discuss rigorous results that show the ability of this tool for revealing invariant sets such as n-tori. These results are just a simple extension of the ergodic partition theory (Mezic and Wiggins, 1999) and are illustrated in two examples: the harmonic oscillator and the 3D ABC flow. Finally, a discussion on the requirement of the objectivity (frame-invariance) property for tools designed to reveal phase space structures is presented.

The third one, "The Chaotic Saddle in the Lozi Map, Autonomous and Nonautonomous Versions" is written jointly with F. Balibrea-Iniesta and my two advisors A. M. Mancho and S. Wiggins. It is published in *International Journal of Bifurcation and Chaos* **25** (2015) 1550184-1-18. We study the orientation and area preserving version of the Lozi map. We apply the Conley-Moser conditions to its autonomous and nonautonomous version to proof the existence of a chaotic saddle. Finally, we show the structure of this nonautonomous chaotic saddle as parameters are varied.

3.1. Lagrangian Descriptors for Two Dimensional, Area Preserving, Autonomous and Nonautonomous Maps

Coauthors: Francisco Balibrea, Stephen Wiggins, Ana M. Mancho

Abstract: In this paper we generalize the method of Lagrangian descriptors to two dimensional, area preserving, autonomous and nonautonomous discrete time dynamical systems. We consider four generic model problems – a hyperbolic saddle point for a linear, area-preserving autonomous map, a hyperbolic saddle point for a nonlinear, area-preserving autonomous map, a hyperbolic saddle point for linear, area-preserving nonautonomous map, and a hyperbolic saddle point for nonlinear, area-preserving nonautonomous map. The discrete time setting allows us to evaluate the expression for the Lagrangian descriptors explicitly for a certain class of norms. This enables us to provide a rigorous setting for the notion that the "singular sets" of the Lagrangian descriptors correspond to the stable and unstable manifolds of hyperbolic invariant sets, as well as to understand how this depends upon the particular norms that are used. Finally we analyze, from the computational point of view, the performance of this tool for general nonlinear maps, by computing the "chaotic saddle" for autonomous and nonautonomous versions of the Hénon map.

Reference: C. Lopesino, F. Balibrea, S. Wiggins, A. M. Mancho. Lagrangian Descriptors for Two Dimensional, Area Preserving, Autonomous and Nonautonomous Maps. Commun Nonlinear Sci Numer Simulat **27** (1-3) (2015) 40–51.

Commun Nonlinear Sci Numer Simulat 27 (2015) 40–51

Contents lists available at ScienceDirect

Commun Nonlinear Sci Numer Simulat

journal homepage: www.elsevier.com/locate/cnsns

Lagrangian descriptors for two dimensional, area preserving, autonomous and nonautonomous maps

Carlos Lopesino [a], Francisco Balibrea [a], Stephen Wiggins [b,*], Ana M. Mancho [a]

[a] Instituto de Ciencias Matemáticas, CSIC-UAM-UC3M-UCM, C/ Nicolás Cabrera 15, Campus Cantoblanco UAM, 28049 Madrid, Spain
[b] School of Mathematics, University of Bristol, Bristol BS8 1TW, United Kingdom

ARTICLE INFO

Article history:
Received 7 December 2014
Received in revised form 25 February 2015
Accepted 28 February 2015
Available online 6 March 2015

Keywords:
Lagrangian descriptor
Chaotic saddle
Autonomous map
Nonautonomous map

ABSTRACT

In this paper we generalize the method of Lagrangian descriptors to two dimensional, area preserving, autonomous and nonautonomous discrete time dynamical systems. We consider four generic model problems – a hyperbolic saddle point for a linear, area-preserving autonomous map, a hyperbolic saddle point for a nonlinear, area-preserving autonomous map, a hyperbolic saddle point for linear, area-preserving nonautonomous map, and a hyperbolic saddle point for nonlinear, area-preserving nonautonomous map. The discrete time setting allows us to evaluate the expression for the Lagrangian descriptors explicitly for a certain class of norms. This enables us to provide a rigorous setting for the notion that the "singular sets" of the Lagrangian descriptors correspond to the stable and unstable manifolds of hyperbolic invariant sets, as well as to understand how this depends upon the particular norms that are used. Finally we analyze, from the computational point of view, the performance of this tool for general nonlinear maps, by computing the "chaotic saddle" for autonomous and nonautonomous versions of the Hénon map.

1. Introduction

Lagrangian descriptors (also referred to in the literature as the "*M* function") were first introduced as a tool for finding hyperbolic trajectories in [16]. In this paper the notion of *distinguished trajectory* was introduced as a generalization of the well-known idea of distinguished *hyperbolic* trajectory. The numerical computation of distinguished trajectories was discussed in some detail, and applications to known benchmark examples, as well as to geophysical fluid flows defined as data sets were also given. Later [18] showed that it could be used to reveal Lagrangian invariant structures in realistic fluid flows. In particular, a geophysical data set in the region of the Kuroshio current was analyzed and it was shown that Lagrangian descriptors could be used to reveal the Lagrangian skeleton of the flow, i.e. hyperbolic and elliptic regions, as well as the invariant manifolds that delineate these regions. A deeper study of the Lagrangian transport issue associated with the Kuroshio using Lagrangian descriptors is given in [19]. Advantages of the method over finite time Lyapunov exponents (FTLE) and finite size Lyapunov exponents (FSLE) were also discussed.

Since then Lagrangian descriptors have been further developed and their ability to reveal phase space structures in dynamical systems more generally has been confirmed. In particular, Lagrangian descriptors are used in [4] to reveal the Lagrangian structures that define transport routes across the Antarctic polar vortex. Further studies of transport issues related to the Antarctic polar vortex using Lagrangian descriptors are given in [5] where vortex Rossby wave breaking is

* Corresponding author.

http://dx.doi.org/10.1016/j.cnsns.2015.02.022
1007-5704/

related to Lagrangian structures. In [25] Lagrangian descriptors are used to study the influence of coherent structures on the saturation of a nonlinear dynamo. In [21] Lagrangian descriptors are used to analyze the influence of Lagrangian structure on the transport of buoys in the Gulf stream and in a region of the Gulf of Mexico relevant to the Deepwater Horizon oil spill. In [17] a detailed analysis of the behavior of Lagrangian descriptors is provided in terms of benchmark problems, new Lagrangian descriptors are introduced, extension of Lagrangian descriptors to 3D flows is given (using the time dependent Hills spherical vortex as a benchmark problem), and a detailed analysis and discussion of the computational performance (with a comparison with FTLE) is presented.

Lagrangian descriptors are based on the integration, for a finite time, along trajectories of an intrinsic bounded, positive geometrical and/or physical property of the trajectory itself, such as the norm of the velocity, acceleration, or curvature. Hyperbolic structures are revealed as singular features of the contours of the Lagrangian descriptors, but the sharpness of these singular features depends on the particular norm chosen. These issues were explored in [17], and further examined in this paper.

All of the work thus far on Lagrangian descriptors has been in the continuous time setting. In this article we generalize the method of Lagrangian descriptors to the discrete time setting of two dimensional area preserving maps, both autonomous and nonautonomous, and provide theoretical support for their performance.

This paper is organized as follows. In Section 2 we defined discrete Lagrangian descriptors. We then consider four examples. In Section 2.1 we consider a linear autonomous area preserving map have a hyperbolic saddle point at the origin, in 2.2 we consider a nonlinear autonomous area preserving map have a hyperbolic saddle point at the origin, in 2.3 we consider a linear nonautonomous area preserving map have a hyperbolic saddle trajectory at the origin, and in 2.4 we consider a nonlinear nonautonomous area preserving map have a hyperbolic trajectory at the origin. For each example we show that the Lagrangian descriptors reveal the stable and unstable manifolds by being singular on the manifolds. The notion of "being singular" is made precise in Theorem 1. In Section 3 we explore further the method beyond the analytical examples. We use discrete Lagrangian descriptors to computationally reveal the chaotic saddle of the Hénon map, and in Section 4 we consider a nonautonomous version of the Hénon map. In Section 5 we summarize the conclusions and suggest future directions for this work.

2. Lagrangian descriptors for maps

Let

$$\{x_n, y_n\}_{n=-N}^{n=N}, \quad N \in \mathbb{N}, \tag{1}$$

denote an orbit of length $2N+1$ generated by a two dimensional map. At this point it does not matter whether or not the map is autonomous or nonautonomous. The method of Lagrangian descriptors applies to orbits in general, regardless of the type of dynamics that generate the orbit.

The first Lagrangian descriptor (also known as the "M function") for continuous time systems was based on computing the arclength of trajectories for a finite time [16]. Extending this idea to maps is straightforward, and the corresponding discrete Lagrangian descriptor (DLD) is given by:

$$MD_2 = \sum_{i=-N}^{N-1} \sqrt{(x_{i+1} - x_i)^2 + (y_{i+1} - y_i)^2}. \tag{2}$$

In analogy with the work on continuous time Lagrangian descriptors in [17], we consider different norms for the discretized arclength as follows:

$$MD_p = \sum_{i=-N}^{N-1} \sqrt[p]{|x_{i+1} - x_i|^p + |y_{i+1} - y_i|^p}, \quad p > 1, \tag{3}$$

and

$$MD_p = \sum_{i=-N}^{N-1} |x_{i+1} - x_i|^p + |y_{i+1} - y_i|^p, \quad p \leqslant 1. \tag{4}$$

Considering the space of orbits as a sequence space, (3) and (4) are the ℓ^p norms of an orbit.

Henceforth, we will consider only the case $p \leqslant 1$ since the proofs are more simple in this case. Now we will explore these definitions in the context of some easily understood, but generic, examples.

2.1. Example 1: a hyperbolic saddle point for linear, area-preserving autonomous maps

2.1.1. Linear saddle point

Consider the following linear, area-preserving autonomous map:

$$\begin{cases} x_{n+1} = & \lambda x_n, \\ y_{n+1} = & \frac{1}{\lambda} y_n, \end{cases} \tag{5}$$

where we will take $\lambda > 1$. Note that this map is area-preserving, but area-preservation was not used in the definition of the DLD's above.

Now we will compute (4) for this example. Towards this end, we introduce the notation

$$MD_p = MD_p^+ + MD_p^-$$

where

$$MD_p^+ = \sum_{i=0}^{N-1} |x_{i+1} - x_i|^p + |y_{i+1} - y_i|^p,$$

and

$$MD_p^- = \sum_{i=-1}^{-N} |x_{i+1} - x_i|^p + |y_{i+1} - y_i|^p.$$

We begin by computing MD_p^+. The computation of MD_p^- is completely analogous, and therefore we will not provide the details. We have:

$$\begin{aligned} MD_p^+ &= \sum_{i=0}^{N-1} |x_{i+1} - x_i|^p + |y_{i+1} - y_i|^p = |x_1 - x_0|^p + |y_1 - y_0|^p + \cdots + |x_N - x_{N-1}|^p + |y_N - y_{N-1}|^p \\ &= |\lambda x_0 - x_0|^p + |1/\lambda y_0 - y_0|^p + \cdots + |\lambda^N x_0 - \lambda^{N-1} x_0|^p + |1/\lambda^N y_0 - 1/\lambda^{N-1} y_0|^p \\ &= |x_0|^p |\lambda - 1|^p \left(1 + \lambda^p + \cdots + \lambda^{(N-1)p}\right) + |y_0|^p |1/\lambda - 1|^p \left(1 + 1/\lambda^p + \cdots + 1/\lambda^{(N-1)p}\right) \\ &= |x_0|^p |\lambda - 1|^p \left(\frac{\lambda^{Np} - 1}{\lambda^p - 1}\right) + |y_0|^p |1/\lambda - 1|^p \left(\frac{1/\lambda^{Np} - 1}{1/\lambda^p - 1}\right) \end{aligned}$$

where in the last step we have used that the sums are geometric with rates λ^p and $1/\lambda^p$, respectively. By completely analogous calculations we obtain MD_p^- as:

$$MD_p^- = |x_0|^p |1/\lambda - 1|^p \left(\frac{1/\lambda^{Np} - 1}{1/\lambda^p - 1}\right) + |y_0|^p |\lambda - 1|^p \left(\frac{\lambda^{Np} - 1}{\lambda^p - 1}\right).$$

Putting the two terms together, we obtain:

$$MD_p = MD_p^+ + MD_p^- = \left(|x_0|^p + |y_0|^p\right) \left(|\lambda - 1|^p \left(\frac{\lambda^{Np} - 1}{\lambda^p - 1}\right) + |1/\lambda - 1|^p \left(\frac{1/\lambda^{Np} - 1}{1/\lambda^p - 1}\right) \right) = (|x_0|^p + |y_0|^p) f(\lambda, p, N), \tag{6}$$

where λ, p and N are fixed.

Extensive numerical simulations in a variety of examples (cf. [16,18,20,4,19,17,21]) have shown that "singular features" of Lagrangian descriptors correspond to stable and unstable manifolds of hyperbolic trajectories. We can make this statement rigorous and precise in the context of this example.

Theorem 1. *Consider a vertical line perpendicular to the unstable manifold of the origin. In particular, consider an arbitrary point $x = \bar{x}$ and a line parallel to the y axis passing through this point. Then the derivative of $MD_p, p < 1$, along this line becomes unbounded on the unstable manifold of the origin.*

Similarly, consider a horizontal line perpendicular to the stable manifold of the origin. In particular, consider an arbitrary point $y = \bar{y}$ and a line parallel to the x axis passing through this point. Then the derivative of $MD_p, p < 1$, along this line becomes unbounded on the stable manifold of the origin.

Proof. This is a simple calculation using (6) and the fact that $p < 1$. This is illustrated in Fig. 1. □

2.1.2. Linear rotated saddle point

In the example studied in the previous section the DLD is singular along the stable and unstable manifolds for any iteration n. However, the results discussed in [18,17] for the continuous time case show that the manifolds are observed for τ "sufficiently large", which is related to a large number of iterations in the discrete time case. We explore further these connections by studying the case of the rotated saddle point. In order to establish a direct link to the continuous time case, we consider the limits of small and large numbers of iterations, and $\lambda \approx 1$.

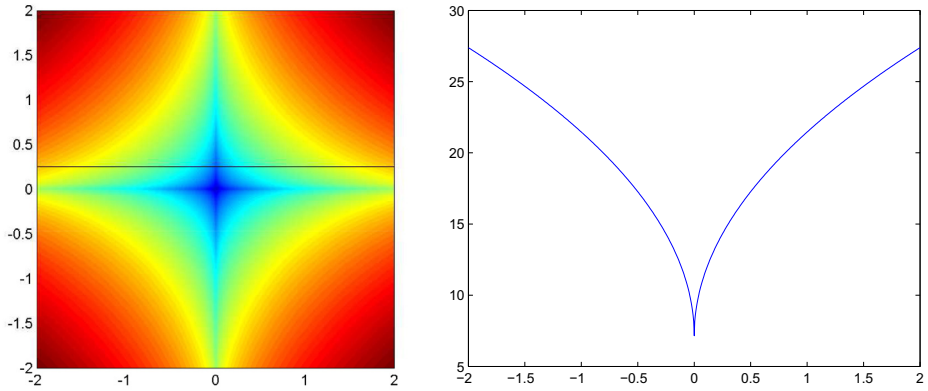

Fig. 1. The left-hand panel shows contours of MD_p for $p = 0.5, N = 20$ and $\lambda = 1.1$, with a grid point spacing of 0.005. The horizontal black line is at $y = 0.25$. The right-hand panel shows the graph of MD_p along this horizontal black line, which illustrates the singular nature of the derivative of MD_p on the stable manifold across the line $x = 0$.

We have the following discrete dynamical system:

$$F(x,y) = A\begin{pmatrix} x \\ \\ y \end{pmatrix} \tag{7}$$

where

$$A = \begin{pmatrix} \frac{1}{\lambda}+\lambda & \frac{1}{\lambda}-\lambda \\ \\ \frac{1}{\lambda}-\lambda & \frac{1}{\lambda}+\lambda \end{pmatrix} = \frac{1}{2\lambda}\begin{pmatrix} 1+\lambda^2 & 1-\lambda^2 \\ \\ 1-\lambda^2 & 1+\lambda^2 \end{pmatrix} \tag{8}$$

in our case with $\lambda > 1$. It is easy to see that the stable and the unstable manifolds are given by the vectors $(1,1)$ and $(1,-1)$ respectively. We want to compute $A^i - A^{i-i}$ in order to get the expressions of the DLD:

$$MD_p = \sum_{i=-N}^{N-1} |x_{i+1} - x_i|^p + |y_{i+1} - y_i|^p \tag{9}$$

and to find where the 'singularities' are produced and why.

We know that A can be diagonalized so there exist D and T such that

$$D = T^{-1} \cdot A \cdot T \tag{10}$$

where D is a diagonal matrix. Therefore we got the next expression

$$D^i = T^{-1} \cdot A^i \cdot T, \quad \text{for every } i.$$

which is equivalent to

$$A^i = T \cdot D^i \cdot T^{-1}, \quad \text{for every } i. \tag{11}$$

It is clear that the matrix T is

$$T = \begin{pmatrix} 1 & 1 \\ -1 & 1 \end{pmatrix} \tag{12}$$

and therefore

$$T^{-1} = \frac{1}{2}\begin{pmatrix} 1 & -1 \\ 1 & 1 \end{pmatrix}$$

We can check Eq. (10),

$$D = \frac{1}{4\lambda}\begin{pmatrix} 1 & -1 \\ 1 & 1 \end{pmatrix}\begin{pmatrix} 1+\lambda^2 & 1-\lambda^2 \\ 1-\lambda^2 & 1+\lambda^2 \end{pmatrix}\begin{pmatrix} 1 & 1 \\ -1 & 1 \end{pmatrix} = \begin{pmatrix} \lambda & 0 \\ 0 & \frac{1}{\lambda} \end{pmatrix} \tag{13}$$

So we can guess now how is A^i using Eq. (11),

$$A^i = \frac{1}{2}\begin{pmatrix} 1 & 1 \\ -1 & 1 \end{pmatrix}\begin{pmatrix} \lambda^i & 0 \\ 0 & \frac{1}{\lambda^i} \end{pmatrix}\begin{pmatrix} 1 & -1 \\ 1 & 1 \end{pmatrix} = \frac{1}{\lambda^i}\begin{pmatrix} 1+\lambda^{2i} & 1-\lambda^{2i} \\ 1-\lambda^{2i} & 1+\lambda^{2i} \end{pmatrix} \tag{14}$$

Therefore

$$A^i - A^{i-1} = \frac{1}{\lambda^i}\begin{pmatrix} \lambda^{2i} - \lambda^{2i-1} - \lambda + 1 & -\lambda^{2i} + \lambda^{2i-1} - \lambda + 1 \\ -\lambda^{2i} + \lambda^{2i-1} - \lambda + 1 & \lambda^{2i} - \lambda^{2i-1} - \lambda + 1 \end{pmatrix} \tag{15}$$

Now we are going to study the analytical expression of the stable and unstable manifold. For that purpose we will develop only MD_p^+ expression (MD_p^- is analogous). So we have to keep in mind the expression for MD_p^+ that is

$$MD_p^+ = \sum_{i=0}^{N-1} |x_{i+1} - x_i|^p + |y_{i+1} - y_i|^p \tag{16}$$

therefore using Eq. (15) for $N \geqslant 1$

$$\begin{aligned} MD_p^+ = \sum_{i=0}^{N-1} & \frac{1}{\lambda^{(i+1)p}} \left| (\lambda^{2(i+1)} - \lambda^{2(i+1)-1} - \lambda + 1)x_0 + (-\lambda^{2(i+1)} + \lambda^{2(i+1)-1} - \lambda + 1)y_0 \right|^p \\ & + \frac{1}{\lambda^{(i+1)p}} \left| (-\lambda^{2(i+1)} + \lambda^{2(i+1)-1} - \lambda + 1)x_0 + (\lambda^{2(i+1)} - \lambda^{2(i+1)-1} - \lambda + 1)y_0 \right|^p \end{aligned} \tag{17}$$

Each term on this sum has singularities along two different lines. In particular, for each i and λ, we have the two singular lines

$$y_0 = \frac{\lambda^{2(i+1)} - \lambda^{2(i+1)-1} - \lambda + 1}{\lambda^{2(i+1)} - \lambda^{2(i+1)-1} + \lambda - 1} x_0 = m(\lambda, i) x_0 \tag{18}$$

and

$$y_0 = \frac{1}{m(\lambda, n)} x_0 \tag{19}$$

where $m(\lambda, i)$ and $\frac{1}{m(\lambda,i)}$ are, respectively, the slopes of the singular lines. If we fix $\lambda = \lambda_0$ and we increase the number of iterations, we can see the evolution of the singular features to the limit shown in Fig. 2

$$\lim_{i \to \infty} m(\lambda_0, i) = 1 \tag{20}$$

This convergence is reached rapidly and, for example, for $\lambda = 1.1$ it is noticeable from $i = 20$ onwards. Thus at large i most of the terms in the summation (17) contribute with the same slope, i.e., (20), Therefore the contributions of terms in the summation (17) with small i are small and make little impact in the global sum (17). If i is small, the number of terms contributing to the DLD is small, and each term is a C^0 function with discontinuities along *different* lines. Since all terms contribute the same to the total pattern, no particular feature is highlighted (see Fig. 2(b) and (c)).

The limit $\lambda \approx 1$ is closely related to the Lagrangian Descriptors defined for the continuous time case. This can be seen by considering the limit and noting that λ quantifies the separation of points as they are iterated and relating this to the arclength integral for the linear saddle point discussed in [17].

For any $i = n_0$ fixed, it is possible to find a λ in the limit close to 1 that makes the slope m close to the limit value:

$$\lim_{\lambda \to 1} m(\lambda, n_0) = 0 \tag{21}$$

In this case, Eqs. (18) and (19) tend to $y = 0$ and $x = 0$, respectively. The approach to this limit can be observed in the sequence of images shown Fig. 2 and the DLD derivative along the line $y = 0.25$ shown in Fig. 3.

2.2. Example 2: a hyperbolic saddle point for nonlinear, area-preserving autonomous maps

We will analyze this case using a theorem of [23]. Moser's theorem applies to analytic, area preserving maps in a neighborhood of a hyperbolic fixed point. We will discuss how the assumptions of analyticity and area preservation can be removed later on, but for now we proceed with these assumptions.

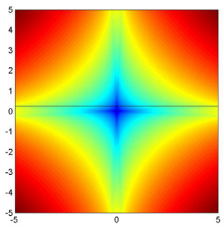

(a) DLD $\lambda = 1.1$ and $i = 1$

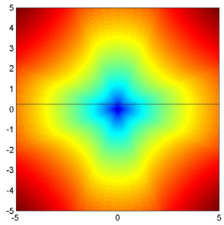

(b) DLD $\lambda = 1.1$ and $i = 5$

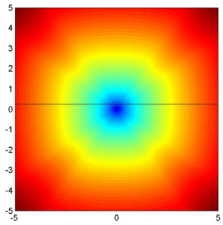

(c) DLD $\lambda = 1.1$ and $i = 10$

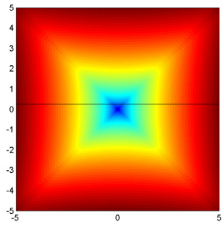

(d) DLD $\lambda = 1.1$ and $i = 20$

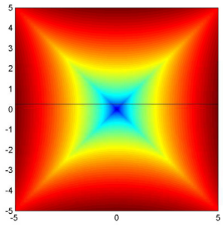

(e) DLD $\lambda = 1.1$ and $i = 30$

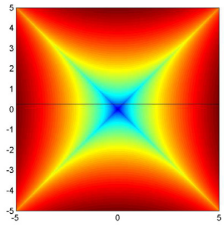

(f) DLD $\lambda = 1.1$ and $i = 100$

Fig. 2. DLD for different values of λ and iterations i.

We consider an analytic, area-preserving map in a neighborhood of $x = y = 0$ of the form:

$$\begin{cases} x_{n+1} = f(x_n, y_n) = \lambda x_n + \cdots \\ y_{n+1} = g(x_n, y_n) = \lambda^{-1} y_n + \cdots \end{cases} \tag{22}$$

where $\lambda > 1$ and "$\cdots$" represent nonlinear terms that obey the area-preserving constraint. Moser's Theorem states that there exists a real analytic, area preserving change of variables of the following form:

$$\begin{aligned} x &= x(\xi, \eta), \\ y &= y(\xi, \eta), \end{aligned} \tag{23}$$

with inverse

$$\begin{aligned} \xi &= \xi(x, y), \\ \eta &= \eta(x, y), \end{aligned} \tag{24}$$

such that in these new coordinates (22) has the following *normal form*:

$$\begin{cases} \xi_{n+1} &= U(\xi_n \eta_n)\xi_n \\ \eta_{n+1} &= U^{-1}(\xi_n \eta_n)\eta_n \end{cases} \tag{25}$$

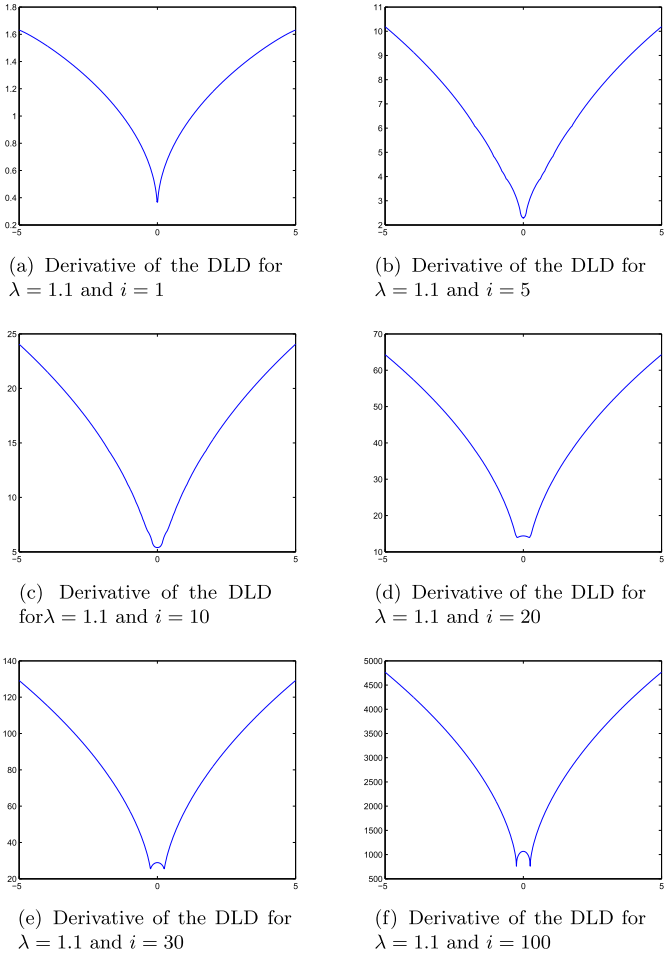

(a) Derivative of the DLD for $\lambda = 1.1$ and $i = 1$

(b) Derivative of the DLD for $\lambda = 1.1$ and $i = 5$

(c) Derivative of the DLD for$\lambda = 1.1$ and $i = 10$

(d) Derivative of the DLD for $\lambda = 1.1$ and $i = 20$

(e) Derivative of the DLD for $\lambda = 1.1$ and $i = 30$

(f) Derivative of the DLD for $\lambda = 1.1$ and $i = 100$

Fig. 3. Derivative of the DLD along the line $y = 0.25$ for different values of λ and iterations i.

where $U(\xi\eta)$ is a power series in the product $\xi\eta$ of the form $U_0 + U_2\xi\eta + \cdots$, with $U_0 = \lambda$, which converges in a neighborhood of the hyperbolic point. Note that it follows from the form of (25) that $U(\cdot)$ is constant on orbits of (25), i.e. $U(\xi_{i+1}\eta_{i+1}) = U(\xi_i\eta_i) = U,\ \forall i$.

The form of (25) implies that the same computation described in Section 2.1 applies. Therefore for MD_p^+ we have:

$$\begin{aligned} MD_p^+ &= \sum_{i=0}^{N-1} |\xi_{i+1} - \xi_i|^p + |\eta_{i+1} - \eta_i|^p = \sum_{i=0}^{N-1} |\xi_i|^p |U(\xi_i\eta_i) - 1|^p + |\eta_i|^p |U^{-1}(\xi_i\eta_i) - 1|^p = \sum_{i=0}^{N-1} |\xi_i|^p |U - 1|^p + |\eta_i|^p |U^{-1} - 1|^p \\ &= |\xi_0|^p |U - 1|^p \left(1 + |U|^p + \cdots + |U|^{(N-1)p}\right) + |\eta_0|^p |U^{-1} - 1|^p \left(1 + |U^{-1}|^p + \cdots + |U^{-1}|^{(N-1)p}\right) \\ &= |\xi_0|^p |U - 1|^p \left|\frac{U^{Np} - 1}{U^p - 1}\right| + |\eta_0|^p |U^{-1} - 1|^p \left|\frac{1/U^{Np} - 1}{1/U^p - 1}\right|. \end{aligned}$$

MD_p^- is computed analogously, and therefore $MD_p = MD_p^+ + MD_p^-$ is given by:

$$MD_p = (|\xi_0|^p + |\eta_0|^p)\left(|U - 1|^p \left|\frac{U^{Np} - 1}{U^p - 1}\right| + |U^{-1} - 1|^p \left|\frac{1/U^{Np} - 1}{1/U^p - 1}\right|\right),$$

In this expression U is constant along trajectories, *i.e.*, $U(\xi_0\eta_0) = U(\xi_i\eta_i) = U,\ \forall i$. But in general, different initial conditions (ξ_0, η_0) do not belong to the same trajectory, thus U depends on (ξ_0, η_0). More succinctly we express this as:

$$MD_p = (|\xi_0|^p + |\eta_0|^p) f(U(\xi_0, \eta_0), p, N) \tag{26}$$

This expression has the same form as (6), except for the dependence of the function f on $U(\xi_0, \eta_0)$. We note that U is analytical and thus it is a smooth function. Therefore Theorem 1 still applies because the first derivative is infinite due to the first factor in expression (26). We can conclude that the derivative of MD_p transverse to the stable manifold is singular on the manifold and the derivative of MD_p transverse to the unstable manifold is singular on the manifold. However, this is a statement that is true in the $\xi - \eta$ normal form coordinates. In practice we will compute the Lagrangian descriptor in the original x—y coordinates and therefore we would like to conclude that the "singular sets" of the Lagrangian descriptor in the x—y coordinates correspond to the stable and unstable manifolds of the hyperbolic fixed point. We will now show that this is the case. We will carry out the argument for the stable manifold. The argument for the unstable manifold is completely analogous.

First, using (23), in the x—y coordinates the stable manifold of the origin is given by the curve $(x(0,\eta), y(0,\eta))$. Here η is viewed as a parameter for this parametric representation of the stable manifold in the original x—y coordinates. A vector perpendicular to this curve at any point on the curve is given by $\left(-\frac{dy}{d\eta}(0,\eta), \frac{dx}{d\eta}(0,\eta)\right)$. Now we compute the rate of change of $MD_p = MD_p(x,y)$ in this direction and consider its behavior on the stable manifold of the origin.This is given by the directional derivative of $MD_p(x,y)$ in this direction evaluated on the stable manifold:

$$\left(\frac{\partial MD_p}{\partial x}(x(0,\eta), y(0,\eta)), \frac{\partial MD_p}{\partial y}(x(0,\eta), y(0,\eta))\right) \cdot \left(-\frac{dy}{d\eta}(0,\eta), \frac{dx}{d\eta}(0,\eta)\right), \tag{27}$$

where the derivatives are evaluated on $(x(0,\eta), y(0,\eta))$, but we will omit this explicitly for the sake of a less cumbersome notation. Next we will use the chain rule to express partial derivatives with respect to x and y in terms of ξ and η as follows:

$$\begin{aligned} \frac{\partial MD_p}{\partial x} &= \frac{\partial MD_p}{\partial \xi}\frac{\partial \xi}{\partial x} + \frac{\partial MD_p}{\partial \eta}\frac{\partial \eta}{\partial x}, \\ \frac{\partial MD_p}{\partial y} &= \frac{\partial MD_p}{\partial \xi}\frac{\partial \xi}{\partial y} + \frac{\partial MD_p}{\partial \eta}\frac{\partial \eta}{\partial y}. \end{aligned} \tag{28}$$

Substituting (28) into (27) gives:

$$-\left(\frac{\partial MD_p}{\partial \xi}\frac{\partial \xi}{\partial x} + \frac{\partial MD_p}{\partial \eta}\frac{\partial \eta}{\partial x}\right)\frac{dy}{d\eta} + \left(\frac{\partial MD_p}{\partial \xi}\frac{\partial \xi}{\partial y} + \frac{\partial MD_p}{\partial \eta}\frac{\partial \eta}{\partial y}\right)\frac{dx}{d\eta}. \tag{29}$$

Now it follows from the argument given in Theorem 1 that $\frac{\partial MD_p}{\partial \xi}$ is not differentiable on the stable manifold ($\xi = 0$ for $p < 1$). Hence (26) is not differentiable in a direction transverse to the stable manifold at a point on the stable manifold in the $x - y$ coordinates.

2.3. Example 3: a hyperbolic saddle point for linear, area-preserving nonautonomous maps

In this section we will consider the nonautonomous analog of example 1 in Section 2.1. Namely, we will consider a linear, area preserving nonautonomous map having a hyperbolic trajectory at the origin. The map that we consider has the following form:

$$\begin{cases} x_{n+1} = \lambda_n x_n \\ y_{n+1} = \frac{1}{\lambda_n} y_n \end{cases}$$

where $\lambda_n > 1,\ \forall n$. Note that $x = y = 0$ is a hyperbolic trajectory with stable manifold given by $x = 0$ and unstable manifold given by $y = 0$ *for all n*.

We will only compute MD_p^+ since the computation of MD_p^- is analogous. Hence, for MD_p^+ we have:

$$\begin{aligned} MD_p^+ &= \sum_{i=0}^{N-1} |x_{i+1} - x_i|^p + |y_{i+1} - y_i|^p = \sum_{i=0}^{N-1} |x_i|^p |\lambda_i - 1|^p + |y_i|^p |1/\lambda_i - 1|^p \\ &= |x_0|^p \left(|\lambda_0 - 1|^p + |\lambda_0|^p |\lambda_1 - 1|^p + \cdots + |\lambda_0 \cdots \lambda_{N-2}|^p |\lambda_{N-1} - 1|^p\right) \\ &\quad + |y_0|^p \left(|1/\lambda_0 - 1|^p + |1/\lambda_0|^p |1/\lambda_1 - 1|^p + \cdots + |1/\lambda_0 \cdots 1/\lambda_{N-2}|^p |1/\lambda_{N-1} - 1|^p\right) \\ &= |x_0|^p \left(|\lambda_0 - 1|^p + \sum_{i=1}^{N-1} \left(\prod_{j=0}^{i-1} |\lambda_j|^p\right) |\lambda_i - 1|^p\right) + |y_0|^p \left(|1/\lambda_0 - 1|^p + \sum_{i=1}^{N-1} \left(\prod_{j=0}^{i-1} |1/\lambda_j|^p\right) |1/\lambda_i - 1|^p\right) \end{aligned}$$

A similar calculation gives:

$$MD_p^- = |x_0|^p \left(|1 - 1/\lambda_{-1}|^p + \sum_{i=-2}^{-N} \left(\prod_{j=-1}^{i+1} |1/\lambda_j|^p \right) |1 - 1/\lambda_i|^p \right) + |y_0|^p \left(|1 - \lambda_{-1}|^p + \sum_{i=-2}^{-N} \left(\prod_{j=-1}^{i+1} |\lambda_j|^p \right) |1 - \lambda_i|^p \right).$$

Combining these two expressions gives:

$$MD_p = |x_0|^p f(\Lambda, p, N) + |y_0|^p g(\Lambda^*, p, N) \tag{30}$$

where

$$\Lambda = (\lambda_0, \lambda_1, \ldots, \lambda_{N-1}, 1/\lambda_{-1}, 1/\lambda_{-2}, \ldots, 1/\lambda_{-N})$$

and

$$\Lambda^* = (1/\lambda_0, 1/\lambda_1, \ldots, 1/\lambda_{N-1}, \lambda_{-1}, \lambda_{-2}, \ldots, \lambda_{-N}).$$

Now (30) has the same functional form as (6). So for $p < 1$ the same argument as given in Theorem 1 holds. Therefore, along a line transverse to the stable manifold (i.e. $x = 0$) MD_p is not differentiable at the point on this line that intersects the stable manifold. The analogous statement holds for the unstable manifold.

2.4. Example 4: a hyperbolic saddle point for a nonlinear, area preserving nonautonomous map

We now consider a two dimensional nonlinear area-preserving nonautonomous map having the following form:

$$\begin{aligned} x_{n+1} &= \lambda_n x_n + f_n(x_n, y_n), \\ y_{n+1} &= \lambda_n^{-1} y_n + g_n(x_n, y_n), \quad (x_n, y_n) \in \mathbb{R}^2, \ \forall n, \end{aligned} \tag{31}$$

where $\lambda_n > 1, \ \forall n$ with $f_n(0,0) = g_n(0,0) = 0, \ \forall n$. We assume that $f_n(\cdot,\cdot)$ and $g_n(\cdot,\cdot)$ are real valued nonlinear functions (i.e. of order quadratic or higher), they are at least C^1, and they satisfy the constraints that the nonlinear map defined by (31) is area preserving.

Since the origin is a hyperbolic trajectory it follows that it has (one dimensional) stable and unstable manifolds [14,3,15]. We will apply the method of discrete Lagrangian descriptors to (31) and show that the stable and unstable manifolds of the origin correspond to the "singular features" of MD_p ($p < 1$), in the sense described in Theorem 1. Our method of proof will be similar in spirit to how we showed the result for nonlinear autonomous maps by using Moser's theorem. Unfortunately, there is no analog of Moser's theorem for nonlinear, nonautonomous area preserving two dimensional maps. Nevertheless, we will still use a "change of variables", or "conjugation" result that is a nonautonomous map version of the Hartman–Grobman theorem due to [2].

The classical Hartman–Grobman [11,10,12,7,8] theorem applies to autonomous maps in a neighborhood of a hyperbolic fixed point. The result states that there exists a homeomorphism, defined in a neighborhood of the fixed point, which conjugates the map to its linear part. Stated another way, the homeomorphism provides a new set of coordinates where the map is given by its linear part in the new coordinates. There are two issues that we must immediately face in order for this approach to work as it did for the linear and nonlinear autonomous maps. One is the generalization of the Hartman–Grobman theorem to the setting on nonautonomous maps (this is dealt with in [2]) and the other is the smoothness of the conjugation ("change of coordinates") since a derivative is required in the application of the chain rule (see (28)).

In general, the conjugacy provided by the Hartman–Grobman theorem is not differentiable (see [22] for examples). However, there has been much work in determining conditions under which the conjugacy is at least C^1, see, e.g., [28,9]. Moreover, Hartman has proven [10] that in two dimensions, a C^2 diffeomorphism having a hyperbolic saddle can be linearized with a C^1 conjugacy (see also [26]). We also point out that differentiability is a property defined pointwise, and the nondifferentiability of the conjugacy typically fails to hold at the fixed point (see the examples in [22]) and we are not interested in differentiability at the fixed point, but at points along the stable and unstable manifolds of the fixed point. The conjugacy is differentiable at these points, as is described in the lecture notes of Rauch entitled "Conjugacy" available at http://www.math.lsa.umich.edu/∼rauch/courses.html. This result also follows from the rectification theorem for ordinary differential equations [1] which says that, away from points where the vector field vanishes, the vector field is conjugate to "rectilinear flow", and this conjugacy is as smooth as the vector field. Note that this result is valid for both autonomous and nonautonomous vector fields.

So setting aside the smoothness issues, we will give a brief discussion of the set-up of [2] for the nonautonomous Hartman–Grobman theorem. They consider that the phase space is given by a Banach space, denoted X (for us X is $\mathbb{R}^2$). The dynamics is described by a sequence of maps on X:

$$F_n(v) = A_n v + f_n(v), \quad v \in X, \ n \in \mathbb{Z}. \tag{32}$$

Precise assumptions on A_n and $f_n(v)$ are given in [2]. In particular A_n is a hyperbolic operator, which for us is:

$$A_n = \begin{pmatrix} \lambda_n & 0 \\ 0 & \lambda_n^{-1} \end{pmatrix} \tag{33}$$

and where $f_n(v)$ is "small", in some sense, e.g. $f_n(0) = 0$ with $f_n(v)$ satisfying a Lipschitz condition. Our $f_n(v)$ will be at least C^1 and satisfy the condition for the map (31) to be area preserving.

For each $n \in \mathbb{Z}$ construct a homeomorphism, $h_n(\cdot)$ that conjugates (32) to its linear part, i.e.,

$$A_n \circ h_n = h_{n+1} \circ F_n, \tag{34}$$

or, expressing this in a diagram for the full dynamics (following [2]) we have:

$$\begin{array}{ccccccccc} & & F_{n-1} & & F_n & & F_{n+1} & & \\ \longrightarrow & X & \longrightarrow & X & \longrightarrow & X & \longrightarrow & X & \longrightarrow \\ & \downarrow h_{n-1} & & \downarrow h_n & & \downarrow h_{n+1} & & \downarrow h_{n+2} & \\ & & A_{n-1} & & A_n & & A_{n+1} & & \\ \longrightarrow & X & \longrightarrow & X & \longrightarrow & X & \longrightarrow & X & \longrightarrow \end{array} \tag{35}$$

In Section 2.3 we proved that the discrete Lagrangian descriptor for the linear, area preserving nonautonomous map is singular along the stable and unstable manifolds of the hyperbolic trajectory at the origin, i.e. $x = 0$ and $y = 0$, respectively. Note that the discrete Lagrangian descriptor is only a function of the initial condition, (x_0, y_0). Hence we can use the change of coordinates $h_0(\cdot)$ and the argument given in Section 2.2 to conclude that the discrete Lagrangian descriptor for the nonlinear nonautonomous area preserving map (31) is singular along the stable and unstable manifolds.

3. Application to the chaotic saddle of the Hénon map

We now illustrate the method of discrete Lagrangian descriptors for autonomous, area preserving nonlinear maps by applying it to the Hénon map [13]:

$$H(x, y) = (A + By - x^2, x). \tag{36}$$

The map is area preserving for $|B| = 1$ and is orientation-preserving if $B < 0$. Moreover, it follows from work in [6] that for values of A larger than

$$A_2 = (5 + 2\sqrt{5})(1 + |B|)^2/4, \tag{37}$$

the Hénon map has a hyperbolic invariant Cantor set which is topologically conjugate to a Bernoulli shift on two symbols, i.e. it has a *chaotic saddle*. We will use the method of discrete Lagrangian descriptors to visualize this chaotic saddle.

We consider $B = -1$, which after substituting this value into (37), gives $A_2 = 5 + 2\sqrt{5} \approx 9.47$, and therefore we choose $A = 9.5$, which satisfies the chaos condition. With these choices of parameters we have $H(x, y) = (9.5 - y - x^2, x)$. Applying the method of discrete Lagrangian descriptors to this map gives the structures shown in Fig. 4, where the chaotic saddle is the set that appears as dark blue. This method, in contrast to other techniques for computing chaotic saddles (see for instance [24]), has the advantage that it simultaneously provides insight into the manifold structure associated with the chaotic saddle.

4. Application to the chaotic saddle of a nonautonomous Hénon map

We now illustrate the method of discrete Lagrangian descriptors for nonautonomous, area preserving maps by applying it to a nonautonomous version of the Hénon map. In particular, in (36) we take;

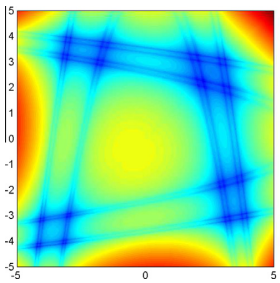

Fig. 4. Computation of the chaotic saddle of the Hénon map for $A = 9.5$, $B = -1$, after $N = 5$ iterations and $p = 0.05$.

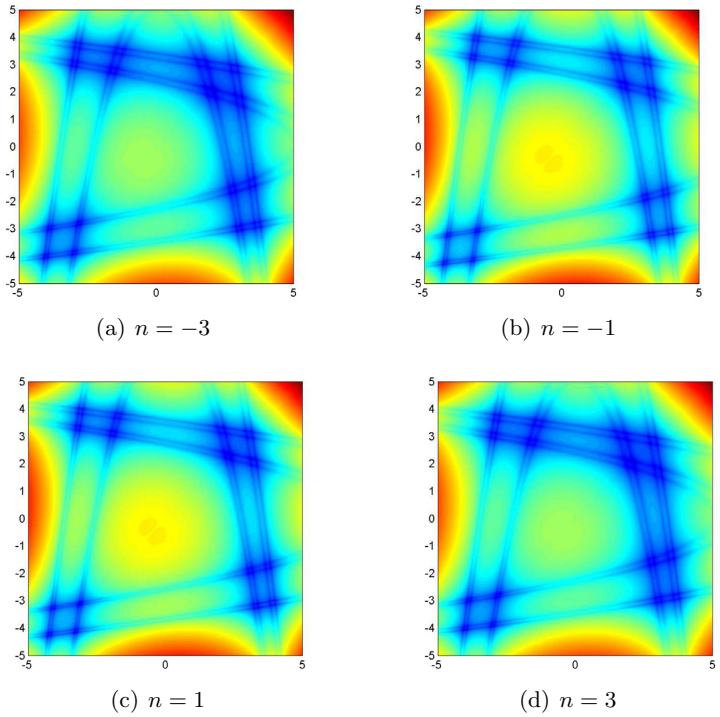

(a) $n = -3$ (b) $n = -1$

(c) $n = 1$ (d) $n = 3$

Fig. 5. Computation of the chaotic saddle of the nonautonomous Hénon map for $A = 9.5 + \epsilon\cos(n)$, $B = -1$, after $N = 5$ iterations and $p = 0.05$. The output is shown for four different times.

$$B = -1, \quad A = 9.5 + \epsilon\cos(n). \tag{38}$$

For ϵ "small", this is a nonautonomous perturbation of the situation considered in Section 3, so that we would expect to have a structure similar to that shown in Fig. 4, but slightly varying with n, i.e. a nonautonomous chaotic saddle (see [27]).

The discrete Lagrangian descriptor method provides us with a numerical tool to explore this question. Fig. 5 illustrates the phase space structure at different times for the nonautonomous Hénon map. Clearly the output is similar to that shown in Fig. 4, but varying with respect to n.

5. Summary and conclusions

In this paper we have generalized the notion of Lagrangian descriptors, originally developed for continuous time dynamical systems, to autonomous and nonautonomous maps. We have restricted our discussion to two dimensional, area preserving maps, but with additional work it should be possible to remove these restrictions.

In the discrete time setting explicit expressions for the Lagrangian descriptors were derived, and for the ℓ^p norm, $p < 1$, we proved a theorem that gave rigorous meaning to the statement that "singular sets" of the Lagrangian descriptors correspond to the stable and unstable manifolds of hyperbolic invariant sets.

Acknowledgments

The research of AMM is supported by the MINECO under Grant MTM2011-26696. The research of SW is supported by ONR Grant No. N00014-01-1-0769. We acknowledge support from MINECO: ICMAT Severo Ochoa project SEV-2011-0087.

References

[1] Arnold VI. Ordinary differential equations. MIT Press; 1973.
[2] Barreira L, Valls C. A Grobman–Hartman theorem for nonuniformly hyperbolic dynamics. J Differ Equ 2006;228:285–310.
[3] de Blasi FS, Schinas J. On the stable manifold theorem for discrete time dependent processes in banach spaces. Bull London Math Soc 1973;5:275–82.

[4] de la Cámara A, Mancho AM, Ide K, Serrano E, Mechoso C. Routes of transport across the Antarctic polar vortex in the southern spring. J Atmos Sci 2012;69(2):753–67.
[5] de la Cámara A, Mechoso C, Mancho AM, Serrano E, Ide K. Quasi-horizontal transport within the antarctic polar night vortex: Rossby wave breaking evidence and lagrangian structures. J Atmos Sci 2013;70:2982–3001.
[6] Devaney R, Nitecki Z. Shift automorphisms in the Hénon mapping. Commun Math Phys 1979;67:137–79.
[7] Grobman DM. Homeomorphisms of systems of differential equations. Doklady Akad Nauk SSSR 1959;128:880–1.
[8] Grobman DM. Topological classification of neighborhoods of a singularity in n-space. Mat Sbornik 1962;56(98):77–94.
[9] Guysinsky M, Hasselblatt B, Rayskin V. Differentiability of the Hartman–Grobman linearization. Discrete Contin Dyn Syst 2003;9(4):979–84.
[10] Hartman P. A lemma in the theory of structural stability of differential equations. Proc Am Math Soc 1960;11:610–20.
[11] Hartman P. On local homeomorphisms of Euclidean spaces. Boletín de la Sociedad Matemática Mexicana 1960;5:220–41.
[12] Hartman P. On the local linearization of differential equations. Proc Am Math Soc 1963;14:568–73.
[13] Hénon M. A two-dimensional mapping with a strange attractor. Commun Math Phys 1976;50:69–77.
[14] Irwin MC. Hyperbolic time dependent processes. Bull London Math Soc 1973;5:209–17.
[15] Katok A, Hasselblatt B. Introduction to the modern theory of dynamical systems. Cambridge: Cambridge University Press; 1995.
[16] Madrid JAJ, Mancho AM. Distinguished trajectories in time dependent vector fields. Chaos 2009;19:013111.
[17] Mancho AM, Wiggins S, Curbelo J, Mendoza C. Lagrangian descriptors: a method for revealing phase space structures of general time dependent dynamical systems. Commun Nonlinear Sci Numer Simul 2013;18(12):3530–57.
[18] Mendoza C, Mancho AM. The hidden geometry of ocean flows. Phys Rev Lett 2010;105(3):038501.
[19] Mendoza C, Mancho AM. The Lagrangian description of ocean flows: a case study of the Kuroshio current. Nonlinear Proc Geophys 2012;19(4):449–72.
[20] Mendoza C, Mancho AM, Rio M-H. The turnstile mechanism across the Kuroshio current: analysis of dynamics in altimeter velocity fields. Nonlinear Proc Geophys 2010;17(2):103–11.
[21] Mendoza C, Mancho AM, Wiggins S. Lagrangian descriptors and the assessment of the predictive capacity of oceanic data sets. Nonlinear Proc Geophys 2014;21:677–89.
[22] Meyer KR. Counter-examples in dynamical systems via normal form theory. SIAM Rev 1986;28(1):41–51.
[23] Moser J. The analytic invariants of an area-preserving mapping near a hyperbolic fixed point. Commun Pure Appl Math 1956;9:673–92.
[24] Nusse H, Yorke JA. A procedure for finding numerical trajectories on chaotic saddles. Physica D 1989;36:137–56.
[25] Rempel EL, Chian AC-L, Brandenburg A, Munoz PR, Shadden SC. Coherent structures and the saturation of a nonlinear dynamo. J Fluid Mech 2013;729:309–29.
[26] Stowe D. Linearization in two dimensions. J Differ Equ 1986;63:183–226.
[27] Wiggins S. Chaos in the dynamics generated by sequences of maps, with applications to chaotic advection in flows with aperiodic time dependence. Z Angew Math Phys (ZAMP) 1999;50:585–616.
[28] van Strien S. Smooth linearization of hyperbolic fixed points without resonance. J Differ Equ 1990;85(1):66–90.

3.2. A theoretical framework for Lagrangian descriptors

Coauthors: Francisco Balibrea-Iniesta, Stephen Wiggins, Ana M. Mancho

Abstract: This paper provides a theoretical background for Lagrangian Descriptors (LDs). The goal of achieving rigorous proofs that justify the ability of LDs to detect invariant manifolds is simplified by introducing an alternative definition for LDs. The definition is stated for n-dimensional systems with general time dependence, however we rigorously prove that this method reveals the stable and unstable manifolds of hyperbolic points in four particular 2D cases: a hyperbolic saddle point for linear autonomous systems, a hyperbolic saddle point for nonlinear autonomous systems, a hyperbolic saddle point for linear nonautonomous systems and a hyperbolic saddle point for nonlinear nonautonomous systems. We also discuss further rigorous results which show the ability of LDs to highlight additional invariants sets, such as n-tori. These results are just a simple extension of the ergodic partition theory which we illustrate by applying this methodology to well-known examples, such as the planar field of the harmonic oscillator and the 3D ABC flow. Finally, we provide a thorough discussion on the requirement of the objectivity (frame-invariance) property for tools designed to reveal phase space structures and their implications for Lagrangian descriptors.

Reference: C. Lopesino, F. Balibrea-Iniesta, V. J. García-Garrido, S. Wiggins, A. M. Mancho. A theoretical framework for Lagrangian descriptors. International Journal of Bifurcation and Chaos **27**, 1730001 (2017).

Feature Articles

International Journal of Bifurcation and Chaos, Vol. 27, No. 1 (2017) 1730001 (25 pages)

DOI: 10.1142/S0218127417300014

A Theoretical Framework for Lagrangian Descriptors

C. Lopesino*, F. Balibrea-Iniesta*, V. J. García-Garrido*,
S. Wiggins† and A. M. Mancho*
*Instituto de Ciencias Matemáticas, CSIC-UAM-UC3M-UCM,
C/Nicolás Cabrera 15, Campus Cantoblanco UAM,
28049 Madrid, Spain
†School of Mathematics, University of Bristol,
Bristol BS8 1TW, UK

Received September 21, 2016

This paper provides a theoretical background for Lagrangian Descriptors (LDs). The goal of achieving rigorous proofs that justify the ability of LDs to detect invariant manifolds is simplified by introducing an alternative definition for LDs. The definition is stated for n-dimensional systems with general time dependence, however we rigorously prove that this method reveals the stable and unstable manifolds of hyperbolic points in four particular 2D cases: a hyperbolic saddle point for linear autonomous systems, a hyperbolic saddle point for nonlinear autonomous systems, a hyperbolic saddle point for linear nonautonomous systems and a hyperbolic saddle point for nonlinear nonautonomous systems. We also discuss further rigorous results which show the ability of LDs to highlight additional invariants sets, such as n-tori. These results are just a simple extension of the ergodic partition theory which we illustrate by applying this methodology to well-known examples, such as the planar field of the harmonic oscillator and the 3D ABC flow. Finally, we provide a thorough discussion on the requirement of the objectivity (frame-invariance) property for tools designed to reveal phase space structures and their implications for Lagrangian descriptors.

Keywords: Lagrangian descriptors; hyperbolic trajectories; stable and unstable manifolds; n-tori; invariant sets.

1. Introduction

Lagrangian descriptors were first introduced in the literature by Madrid and Mancho [2009] in the form of a function, denoted M, that was used to provide a definition for *distinguished trajectories*. The mathematical construction of distinguished trajectories generalized the notion of *distinguished hyperbolic trajectory*, first discussed in [Ide *et al.*, 2002], by including also trajectories with an elliptic type of stability. Distinguished trajectories were highlighted by special minima of the function M referred to as *limit coordinates*.

In the past few years the applicability of the concept of Lagrangian Descriptor has been extended and has become a method for detecting invariant manifolds of hyperbolic trajectories [Mendoza & Mancho, 2010]. Invariant manifolds were highlighted by "singular features" of both the function M and some of its generalizations (see [Mendoza & Mancho, 2012; Mancho *et al.*, 2013]). Since these early papers, numerous applications of Lagrangian descriptors have been given, e.g. in [de la Cámara *et al.*, 2012], where they were used in the context of atmospheric sciences to reveal the Lagrangian structures that define transport routes across the Antarctic polar vortex. This work was extended in [de la Cámara *et al.*, 2013], where LDs were applied to analyze the Lagrangian structures

associated with Rossby wave breaking. In the field of magnetohydrodynamics, Lagrangian descriptors have also been shown to be useful for studying the influence of coherent structures on the saturation of a nonlinear dynamo in [Rempel *et al.*, 2013]. There are also several applications in oceanography. In [Mendoza *et al.*, 2014], LDs were used to analyze transport in a region of the Gulf of Mexico relevant to the Deepwater Horizon oil spill. García-Garrido *et al.* [2015] have applied this tool to analyze the search strategy for debris from the missing MH370 flight followed by the Australian Maritime Authorities, and recently García-Garrido *et al.* [2016] have studied the role played by LDs in the management of the Oleg Naydenov oil spill that took place in the south of Gran Canaria. All these works are related to various aspects of fluid dynamics. However, Lagrangian descriptors can be applied to the general study of the phase space structure of dynamical systems in different contexts. This has recently been illustrated in several applications of the tool to fundamental problems in chemical reaction dynamics. In particular, it has been applied to a study of chemical reactions under external time-dependent driving in [Craven & Hernandez, 2015], a study of phase space structure and reaction dynamics for a class of "barrierless reactions" in [Junginger & Hernandez, 2016], and to a study of the isomerization dynamics of ketene in [Craven & Hernandez, 2016].

The ability of LDs to reveal invariant manifolds has been established in the references above from a phenomenological and numerical point of view, however a rigorous framework is missing in these works. Recently Lopesino *et al.* [2015] have provided rigorous proofs in the framework of discrete maps, where it is precisely defined what is meant by the phrase "singular features". One of the goals of this article is to extend those results to continuous time dynamical systems. In order to simplify the demonstrations, this paper provides a new way of constructing Lagrangian descriptors in the same spirit as in [Lopesino *et al.*, 2015]. The idea is based on considering the p-norm of each velocity component, instead of the p-norm of the modulus of the velocity. This idea follows the heuristic argument discussed by [Mancho *et al.*, 2013] of integrating positive quantities along particle trajectories, and the positive quantity is such that it results in tractable proofs. The choice allows us to mathematically prove that the stable and unstable manifolds of hyperbolic trajectories in the selected examples are detected as singular features of the Lagrangian descriptor. As in [Lopesino *et al.*, 2015], we are able to make the notion of "singular feature" mathematically precise.

This paper discusses further rigorous results found in the literature on the ergodic partition theory. These are based on the evaluation of averages along trajectories for obtaining invariant sets (cf. [Mezić & Wiggins, 1999; Susuki & Mezić, 2009]). We show that LDs are directly related to these findings and thus they also capture coherent structures described as n-tori. To illustrate the full potential of this technique, we apply it to the well-known ABC flow. Finally, we discuss the issue of objectivity and how phase space geometry behaves under coordinate transformations. In this context we show, with some examples from the literature, how outputs of LDs in different frames consistently reproduce phase portraits.

This paper is organized as follows. In Sec. 2, a theoretical mathematical background for Lagrangian descriptors is developed, which is based on providing an alternative definition of LDs, and we discuss a variety of Hamiltonian examples that are variations of the linear saddle. Section 3 presents some results on non-Hamiltonian systems. In Sec. 4, we illustrate the link between Lagrangian descriptors and the ergodic partition theory in the linear elliptic case. Section 5 is devoted to the application of LDs to a well-known 3D example, the ABC flow, providing evidence of the effectiveness of LDs in the detection of both invariant manifolds and invariant tori in 3D flows by means of, respectively, singular features and contours of converged averages. Section 6 offers a detailed discussion of the objectivity (frame-invariance) property in the context of LDs and the ability of LDs to provide the correct description of phase space structures in different frames, as well as a general consideration of the objectivity property requirement for tools in relation to their capability for revealing Lagrangian structures in phase space. Finally, in Sec. 7 we present the conclusions.

2. Rigorous Results for Lagrangian Descriptors

In this section, we provide some rigorous results allowing us to establish a theoretical framework for Lagrangian descriptors. In order to achieve this goal

we propose an alternative definition of LDs for n-dimensional vector fields with arbitrary time dependence, following the ideas developed in [Lopesino *et al.*, 2015] for the discrete time setting. We consider the general time-dependent vector field,

$$\frac{d\mathbf{x}}{dt} = \mathbf{v}(\mathbf{x}, t), \quad \mathbf{x} \in \mathbb{R}^n, \ t \in \mathbb{R} \tag{1}$$

where $\mathbf{v}(\mathbf{x}, t) \in C^r$ $(r \geq 1)$ in $\mathbf{x}$ and continuous in time. The definition of LDs depends on the initial condition $\mathbf{x}_0 = \mathbf{x}(t_0)$, on the time interval $[t_0 - \tau, t_0 + \tau]$, and takes the form,

$$M_p(\mathbf{x}_0, t_0, \tau) = \int_{t_0-\tau}^{t_0+\tau} \sum_{i=1}^{n} |\dot{x}_i(t; \mathbf{x}_0)|^p dt \tag{2}$$

where $p \in (0, 1]$ and $\tau \in \mathbb{R}^+$ are freely chosen parameters, and the overdot symbol represents the derivative with respect to time.

2.1. *The autonomous saddle point*

The first example that we analyze is the Hamiltonian linear saddle point. The velocity field is given by:

$$\begin{cases} \dot{x} = \lambda x \\ \dot{y} = -\lambda y \end{cases}, \quad \lambda > 0. \tag{3}$$

For an initial condition (x_0, y_0), the unique solution of this system is:

$$\begin{cases} x(t, x_0) = x_0 e^{\lambda t} \\ y(t, y_0) = y_0 e^{-\lambda t} \end{cases}, \quad \lambda > 0. \tag{4}$$

For this example, the origin $(0, 0)$ is a hyperbolic fixed point with stable and unstable manifolds:

$$W^s(0, 0) = \{(x, y) \in \mathbb{R}^2 \,|\, x = 0, y \neq 0\}, \tag{5}$$

$$W^u(0, 0) = \{(x, y) \in \mathbb{R}^2 \,|\, y = 0, x \neq 0\}. \tag{6}$$

For simplicity we assume, without loss of generality, that $t_0 = 0$ (this is possible for autonomous systems) and we apply (2) to (3) to obtain:

$$\begin{aligned} &M_p((x_0, y_0), t_0, \tau) \\ &\quad = \int_{-\tau}^{\tau} |\lambda x_0 e^{\lambda t}|^p + |-\lambda y_0 e^{-\lambda t}|^p dt \\ &\quad = (|x_0|^p + |y_0|^p) \frac{\lambda^{p-1}(e^{\lambda p \tau} - e^{-\lambda p \tau})}{p} \\ &\quad = 2(|x_0|^p + |y_0|^p) \frac{\lambda^{p-1} \sinh(\lambda p \tau)}{p}. \end{aligned} \tag{7}$$

This expression allows us to conclude the following theorem, which is proven exactly in the same way as Theorem 1 in [Lopesino *et al.*, 2015].

Theorem 1. *Consider a vertical line perpendicular to the unstable manifold of the origin. Then the derivative of M_p, $p \leq 1$, along this line does not exist on the unstable manifold of the origin.*

Similarly, consider a horizontal line perpendicular to the stable manifold of the origin. Then the derivative of M_p, $p \leq 1$ along this line does not exist on the stable manifold of the origin.

This theorem is graphically illustrated in Fig. 1. Note that this result holds *for any* finite value of τ, i.e. $M_p((x_0, y_0), t_0, \tau) < \infty$ possesses, *for any* finite τ, singularities along the stable and unstable manifolds. The definition of this singularity is made precise as follows:

Definition 2.1. Given τ and p, an orientable surface ϕ with normal vector $\mathbf{n}$ is said to be a singular feature of $M_p(\cdot, t_0, \tau)$, if for every $\mathbf{x}_0 \in \phi$ the normal derivative $\frac{\partial M_p}{\partial \mathbf{n}}(\mathbf{x}_0, t_0, \tau)$ does not exist.

A recent article by Ruiz-Herrera [2016] deals with a similar setting and argues about the impossibility of defining this derivative in the limit $\tau \to \infty$ due to the unbounded character of M_p in this limit. These arguments do not apply to our case as this limit of τ is not considered in our construction.

Remark 2.1. We emphasize that the term $|\cdot|^p + |\cdot|^p$, $p \leq 1$, at the end of expression (7), whose arguments (denoted by "$\cdot$") vanish on the stable and unstable manifolds, is the essential "structural feature" of M_p that gives rise to the "singular nature" (i.e. unboundedness or discontinuity in the derivative) of the LD along the stable and unstable manifolds of the hyperbolic trajectory. This feature will appear explicitly in M_p for the benchmark examples to follow.

2.2. *The rotated saddle point*

In the previous example, Lagrangian descriptors were shown to be singular along the stable and unstable manifolds of the hyperbolic fixed point at the origin for any finite value of τ. However for the examples given in [Mendoza & Mancho, 2010] and [Mancho *et al.*, 2013], it was shown that a sufficiently large τ was required in order to obtain "sharp" images/figures on/over the manifolds. In the next example we illustrate this particular role

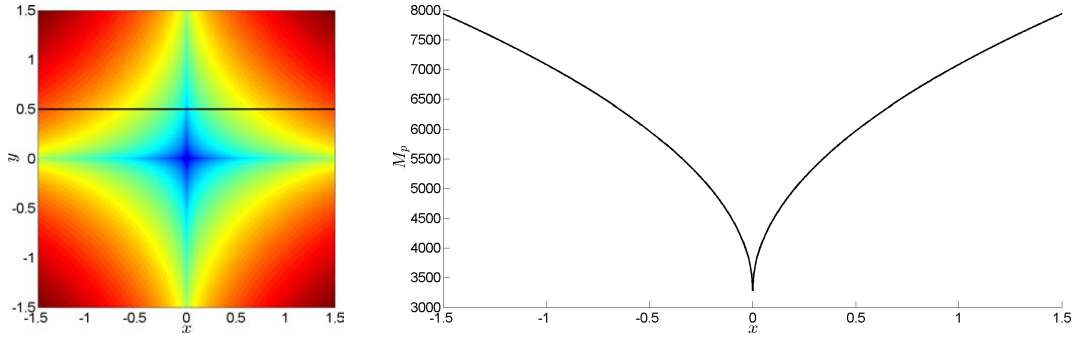

(a) (b)

Fig. 1. (a) Shows contours of $M_{p=0.5}$ for system (3) with $\tau = 15$ and $\lambda = 1$. The contours of M_p are computed on a grid with spacing 0.005 and the integration time step of the vector field is chosen to be 0.1. The horizontal black line is at $y = 0.5$ and (b) shows the graph of M_p along this line, which illustrates the singular nature of the derivative of M_p on the stable manifold $\{x = 0\}$.

of τ by considering the same example of the previous section, but rotated 45°. The autonomous system corresponding to the 45° rotated saddle has the form:

$$\begin{cases} \dot{x} = y \\ \dot{y} = x. \end{cases} \tag{8}$$

The solution of this system yields,

$$\begin{cases} x(t) = x_0 \cosh t + y_0 \sinh t \\ y(t) = x_0 \sinh t + y_0 \cosh t, \end{cases} \tag{9}$$

or equivalently,

$$\begin{cases} x(t) = ae^t + be^{-t} \\ y(t) = ae^t - be^{-t}, \end{cases} \tag{10}$$

where

$$a = \frac{x_0 + y_0}{2}, \quad b = \frac{x_0 - y_0}{2}. \tag{11}$$

Note that $a = 0$ corresponds to the stable manifold and $b = 0$ corresponds to the unstable manifold.

The function M_p for this example takes the form:

$$M_p((x_0, y_0), t_0, \tau) = \int_{-\tau}^{\tau} |ae^t - be^{-t}|^p + |ae^t + be^{-t}|^p dt. \tag{12}$$

In this example, it is not possible to compute analytically the integrals which define M_p. However, we are able to compute approximations of M_p that are sufficiently accurate to enable the understanding of the relationship between singularities of M_p and the stable and unstable manifolds for both small and large τ limits.

First we study the behavior of M_p in order to show where the singularities of the derivative of M_p appear for small $\tau = \tau_0$. The Taylor expansions of $\sinh t$ and $\cosh t$ are:

$$\begin{aligned} \sinh t &= t + \frac{t^3}{3!} + \frac{t^5}{5!} + \cdots, \\ \cosh t &= 1 + \frac{t^2}{2!} + \frac{t^4}{4!} + \cdots. \end{aligned} \tag{13}$$

Using (9) and the Taylor expansion of $M_p((x_0, y_0), t_0, \tau_0)$ at $\tau_0 = 0$,

$$\begin{aligned} &M_p((x_0, y_0), t_0, \tau_0) \\ &\quad = M_p((x_0, y_0), t_0, 0) + \frac{\partial M_p((x_0, y_0), t_0, 0)}{\partial \tau_0} \tau_0 \\ &\qquad + O(\tau_0^2) \\ &\quad = 0 + (|x_0 \sinh \tau_0 + y_0 \cosh \tau_0|^p \\ &\qquad + |x_0 \cosh \tau_0 + y_0 \sinh \tau_0|^p)_{\tau_0 = 0} \tau_0 \\ &\qquad + (|x_0 \sinh(-\tau_0) + y_0 \cosh(-\tau_0)|^p \\ &\qquad + |x_0 \cosh(-\tau_0) + y_0 \sinh(-\tau_0)|^p)_{\tau_0 = 0} \tau_0 \\ &\qquad + O(\tau_0^2) \\ &\quad \sim 2(|y_0|^p + |x_0|^p)\tau_0 \end{aligned} \tag{14}$$

where in the last step we have used that $\sinh \tau_0 = -\sinh(-\tau_0) = 0$, and that $\cosh \tau_0 = \cosh(-\tau_0) = 1$. Therefore the singularities of the derivative of M_p

appear on the lines $x = 0$ and $y = 0$ for small τ, which are not the stable and unstable manifolds of the origin.

Now we consider the case of large values of τ, and fixed τ_0. In order to analyze this case we divide the integral into three parts,

$$\begin{aligned} &M_p((x_0, y_0), t_0, \tau) \\ &\quad = M_p((x_0, y_0), t_0, \tau_0) + \int_{\tau_0}^{\tau} |\dot{x}(t)|^p + |\dot{y}(t)|^p dt \\ &\qquad + \int_{-\tau}^{-\tau_0} |\dot{x}(t)|^p + |\dot{y}(t)|^p dt. \end{aligned} \tag{15}$$

Since τ_0 is fixed and τ is large enough, we can expand the last part of (15) to yield,

$$\begin{aligned} &\int_{\tau_0}^{\tau} |\dot{x}(t)|^p + |\dot{y}(t)|^p dt \\ &\quad = \int_{\tau_0}^{\tau} |ae^t - be^{-t}|^p + |ae^t + be^{-t}|^p dt \\ &\quad = 2\int_{\tau_0}^{\tau} |ae^t|^p + O\left(\frac{|b|}{|a|^{1-p}} e^{2t-p}\right) dt. \end{aligned} \tag{16}$$

Analogously, for the range of negative values we obtain,

$$\begin{aligned} &\int_{-\tau}^{-\tau_0} |\dot{x}(t)|^p + |\dot{y}(t)|^p dt \\ &\quad = \int_{-\tau}^{-\tau_0} |ae^t - be^{-t}|^p + |ae^t + be^{-t}|^p dt \\ &\quad = 2\int_{-\tau}^{-\tau_0} |be^{-t}|^p + O\left(\frac{|a|}{|b|^{1-p}} e^{-2t+p}\right) dt. \end{aligned} \tag{17}$$

Using the fact that $\tau \gg \tau_0 > 0$, it is clear that the leading order terms of (16) and (17) after the integration are given by

$$2\frac{|a|^p}{p} e^{\tau p} \quad \text{and} \quad 2\frac{|b|^p}{p} e^{\tau p} \tag{18}$$

respectively. Consequently,

$$\begin{aligned} &M((x_0, y_0), t_0, \tau) \\ &\quad = M((x_0, y_0), t_0, \tau_0) \\ &\qquad + \int_{\tau_0}^{\tau} |ae^t - be^{-t}|^p + |ae^t + be^{-t}|^p dt \\ &\qquad + \int_{-\tau}^{-\tau_0} |ae^t - be^{-t}|^p + |ae^t + be^{-t}|^p dt \\ &\quad = 2(|x_0|^p + |y_0|^p)\tau_0 + \frac{2^{1-p} e^{\tau p}}{p} \\ &\qquad \cdot (|x_0 + y_0|^p + |x_0 - y_0|^p) + B. \end{aligned} \tag{19}$$

In (20), B depends on τ_0 and lower order terms in τ. The singularities previously discussed, observed for small enough τ along the horizontal and vertical axes, are still present in the first term, although the weight of this term makes it negligible when compared to the second term. For large τ, (20) depicts the singular features of M_p over/at the lines $\{y = -x\}$ (the stable manifold) and $\{y = x\}$ (the unstable manifold). The evolution of the contours of M_p and its singularities can be seen in Figs. 2 and 3, respectively, as we increase the integration time parameter τ. It is clear from these figures that the longer we integrate the system (increasing τ) the closer we get to patterns that enhance the diagonal structure. For very small τ, the major contribution of M_p comes from the first term in (20), while for intermediate τ values the contribution of B is the dominant one, although we do not know its explicit expression. Finally, for very large τ, the dominant term in (20) is the second one. We remark that Figs. 2 and 3 show that the very large τ required for the singular features of M_p to be visibly aligned along the stable and unstable manifolds, is achieved already at $\tau = 5$, i.e. a *finite* τ value at which of course $M_p < \infty$. The recent article by Ruiz-Herrera [2016] argues, for a similar setting, that the presence of terms such as the first one in Eq. (20) does not allow that M_p highlights invariant manifolds by means of singular features. Our discussion here however confirms the ability of M_p to highlight invariant manifolds aligned in different directions by means of singular features defined as in 2.1.

2.3. *The autonomous nonlinear saddle point*

In this section, we treat the autonomous nonlinear saddle point by using a theorem by [Moser, 1956]. Moser's theorem applies to analytic two-dimensional symplectic maps having a hyperbolic fixed point or, similarly, to two-dimensional time-periodic Hamiltonian vector fields having a hyperbolic periodic orbit (which can be reduced to the former case considering a Poincaré map). In this case, we are considering the flow of an autonomous Hamiltonian system, which is a one-parameter

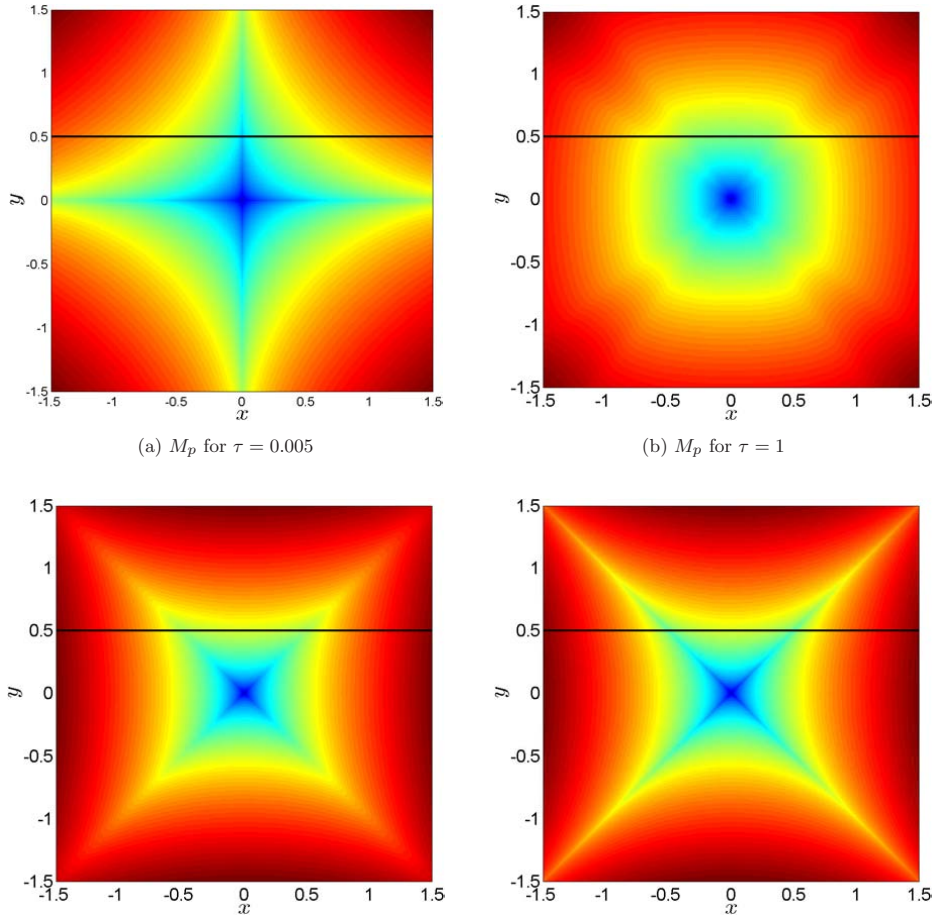

(a) M_p for $\tau = 0.005$

(b) M_p for $\tau = 1$

(c) M_p for $\tau = 2.5$

(d) M_p for $\tau = 5$

Fig. 2. M_p function for $p = 0.5$ and using different values of τ. For this example, the integration time step and grid spacing are 0.005. The black line is defined at $y = 0.5$ and is used in Fig. 3.

family of symplectic maps, and therefore Moser's theorem applies.

We consider a two-dimensional autonomous analytic Hamiltonian vector field of the form,

$$\begin{cases} \dot{x} = H_y(x, y), \\ \dot{y} = -H_x(x, y), \end{cases} \tag{21}$$

having a hyperbolic fixed point at the origin. Moser's theorem proves the existence of an area-preserving change of variables,

$$\begin{cases} x = x(\xi, \eta) \\ y = y(\xi, \eta) \end{cases} \tag{22}$$

with inverse,

$$\begin{cases} \xi = \xi(x, y) \\ \eta = \eta(x, y) \end{cases} \tag{23}$$

by which the system (21) is transformed into the following normal form,

$$\begin{cases} \dot{\xi} = F_\eta \\ \dot{\eta} = -F_\xi \end{cases} \tag{24}$$

where $F = F(\xi\eta) = a_0\xi\eta + a_1(\xi\eta)^2 + \cdots$ depends only on the product $\xi\eta$ and $a_0 \equiv \lambda \in \mathbb{R}$, $\lambda \neq 0$ (onwards it will be taken that $\lambda > 0$). It is

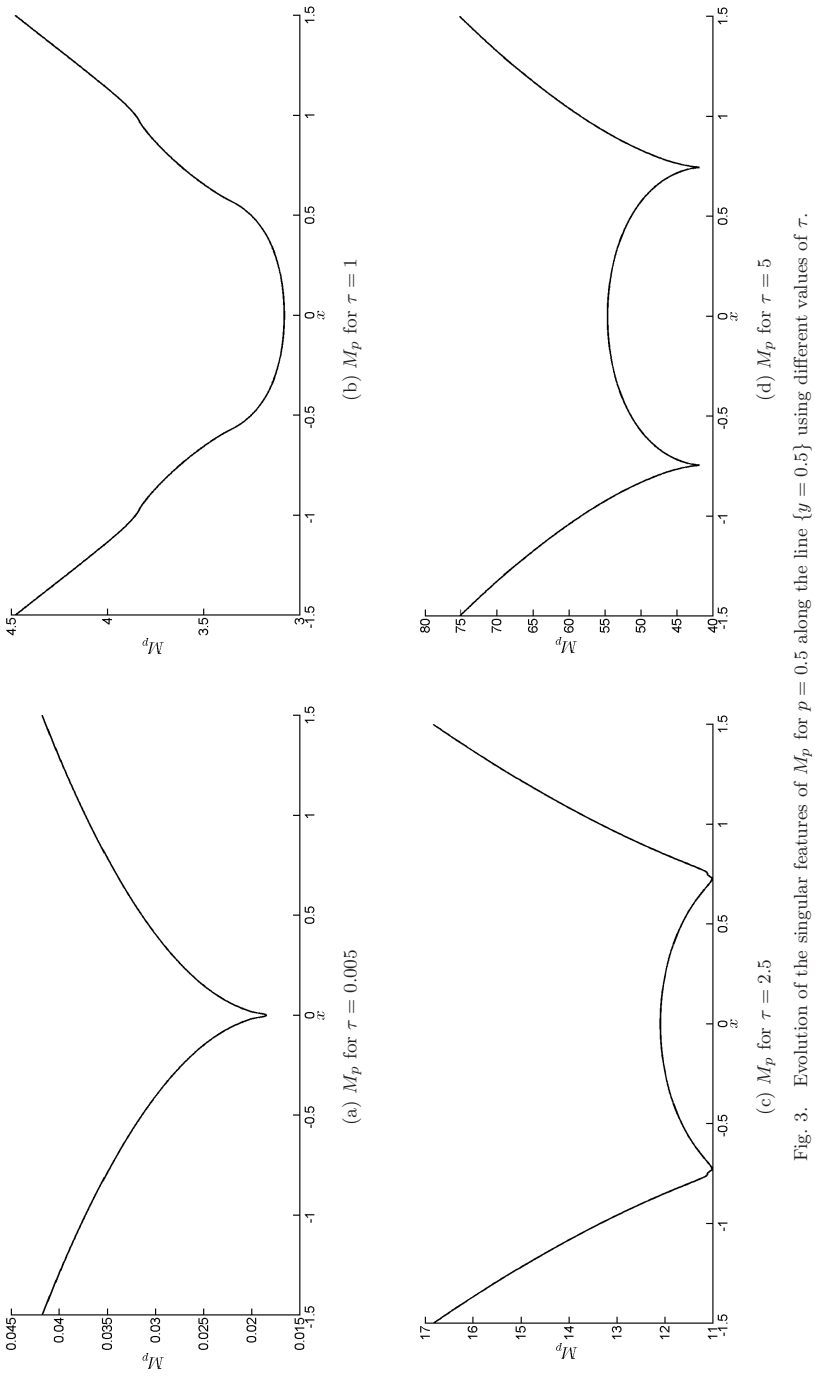

(a) M_p for $\tau = 0.005$

(b) M_p for $\tau = 1$

(c) M_p for $\tau = 2.5$

(d) M_p for $\tau = 5$

Fig. 3. Evolution of the singular features of M_p for $p = 0.5$ along the line $\{y = 0.5\}$ using different values of τ.

straightforward to verify that $\frac{d}{dt}(\xi\eta) = 0$, or equivalently, $\xi_0\eta_0 = \xi\eta$. Moreover, if we define $\frac{dF}{dz}(z) = F'(z)$, with $z \equiv \xi\eta$ then (24) takes the form,

$$\begin{cases} \dot{\xi} = F'\xi \\ \dot{\eta} = -F'\eta \end{cases} \tag{25}$$

where $F' = F'(\xi_0\eta_0)$ is constant on trajectories. This last system is easily integrated and its solutions are given by the expressions,

$$\begin{cases} \xi = \xi_0 e^{F't} \\ \eta = \eta_0 e^{-F't}. \end{cases} \tag{26}$$

Applying the descriptor M_p to this system (and setting $t_0 = 0$ since it is autonomous) we obtain,

$$\begin{aligned} &M_p((\xi_0, \eta_0), t_0, \tau) \\ &\quad = \int_{-\tau}^{\tau} |\xi_0 e^{F't} F'|^p + |\eta_0 e^{-F't} F'|^p dt \\ &\quad = 2(|\xi_0|^p + |\eta_0|^p) \frac{|F'|^p}{pF'} \sinh(pF'\tau). \end{aligned} \tag{27}$$

As we can see above, the derivative of M_p has singularities through the stable $\{\xi = 0\}$ and unstable $\{\eta = 0\}$ manifolds in the ξ–η coordinates, i.e. the directional derivatives of M_p across $\xi = 0$ and $\eta = 0$ do not exist on the manifolds.

In order to complete this example, there are two technical points that we must address. From (27) we observe that there might be possible singularities in the case when F' vanishes. However, recall that F' is,

$$\frac{dF}{dz} = \lambda + 2a_1 z + 3a_2 z^2 \cdots, \tag{28}$$

where $z \equiv \xi\eta$. For a sufficiently small neighborhood of the origin (no larger than the domain of validity of the normal form) the term λ is the dominant term in the series, and therefore F' is not zero.

We have shown that M_p is singular on the stable and unstable manifolds in the ξ–η coordinates. However, the system (21) was originally expressed in the x–y coordinates. Now we show that M_p is singular on the stable and unstable manifolds in these coordinates. We will carry out the proof for the stable manifold. The proof for the unstable manifold is completely analogous.

For this purpose we use expression (22) and that the stable manifold is given by $\xi = 0$ to obtain the following parametrization for the stable manifold in the x–y coordinates,

$$\eta \in \mathbb{R} \mapsto (x(0, \eta), y(0, \eta)) \in \mathbb{R}^2, \tag{29}$$

where $(\frac{\partial x}{\partial \eta}(0, \eta), \frac{\partial y}{\partial \eta}(0, \eta))$ is the tangent vector of this curve at every point $(x(0, \eta), y(0, \eta))$. Additionally, since the Jacobian of the transformation (22) is nonzero,

$$J(\xi, \eta) = \frac{\partial x}{\partial \xi}\frac{\partial y}{\partial \eta}(\xi, \eta) - \frac{\partial y}{\partial \xi}\frac{\partial x}{\partial \eta}(\xi, \eta) \neq 0 \quad \text{for all } (\xi, \eta) \in \mathbb{R}^2, \tag{30}$$

the pair of vectors

$$\left\{ \left(\frac{\partial x}{\partial \xi}(0, \eta), \frac{\partial y}{\partial \xi}(0, \eta) \right), \left(\frac{\partial x}{\partial \eta}(0, \eta), \frac{\partial y}{\partial \eta}(0, \eta) \right) \right\}_{\eta \in \mathbb{R}} \tag{31}$$

cannot be parallel, and thus they form a basis of $\mathbb{R}^2$ at every point $(x(0, \eta), y(0, \eta))$ of the stable manifold. Since the change of variables (22) is analytic, one can construct a family of unit normal vectors $\{\mathbf{n}(\eta)\}_{\eta \in \mathbb{R}}$ to the stable manifold (29) which can be expressed as follows,

$$\mathbf{n}(\eta) = a(\eta) \begin{pmatrix} \frac{\partial x}{\partial \xi}(0, \eta) \\ \frac{\partial y}{\partial \xi}(0, \eta) \end{pmatrix} + b(\eta) \begin{pmatrix} \frac{\partial x}{\partial \eta}(0, \eta) \\ \frac{\partial y}{\partial \eta}(0, \eta) \end{pmatrix} \tag{32}$$

where $a, b \in C^0(\mathbb{R})$ are two scalar functions. Here $a(\eta) \neq 0$, $\forall\, \eta \in \mathbb{R}$, since, by definition, every normal vector is perpendicular to the tangent vector at every single point of a C^1-curve, and thus must have a nonzero component along a vector which is not parallel to the tangent direction. On the other hand, the Jacobian of the transformation only confirms that the vectors (31) are not parallel, but not that they are perpendicular. For this reason $b(\eta)$ can take values different from zero.

Now the directional derivative of M_p in the direction $\mathbf{n}(\eta)$ is given by,

$$\begin{aligned} &\left(\frac{\partial M_p}{\partial x}(x(0, \eta), y(0, \eta)), \frac{\partial M_p}{\partial y}(x(0, \eta), y(0, \eta)) \right) \cdot \mathbf{n}(\eta) \\ &\quad = a(\eta) \left[\frac{\partial M_p}{\partial x}(x(0, \eta), y(0, \eta)) \frac{\partial x}{\partial \xi}(0, \eta) \right. \end{aligned}$$

$$+\frac{\partial M_p}{\partial y}(x(0,\eta),y(0,\eta))\frac{\partial y}{\partial \xi}(0,\eta)\Big]$$
$$+b(\eta)\left[\frac{\partial M_p}{\partial x}(x(0,\eta),y(0,\eta))\frac{\partial x}{\partial \eta}(0,\eta)\right.$$
$$\left.+\frac{\partial M_p}{\partial y}(x(0,\eta),y(0,\eta))\frac{\partial y}{\partial \eta}(0,\eta)\right]$$
$$=a(\eta)\frac{\partial M_p}{\partial \xi}(0,\eta)+b(\eta)\frac{\partial M_p}{\partial \eta}(0,\eta),\quad \forall\,\eta\in\mathbb{R}. \tag{33}$$

Since $a(\eta)$ cannot be equal to zero, this derivative is unbounded in the direction of the normal vector $\mathbf{n}(\eta)$ for $p\in(0,1)$ or has a discontinuity for $p=1$. In both cases, we are speaking in terms of the nondifferentiability of function M_p, therefore displaying a singular feature over the manifolds expressed in the x–y coordinates. Indeed its directional derivative is bounded and continuous only when evaluated with respect to the tangent vector direction.

2.4. *The nonautonomous linear saddle point*

In this section, we consider the nonautonomous linear saddle point. Given a function $f\in C^1(t_0-\tau, t_0+\tau)$, and $f(t)>0$ for every $t\in[t_0-\tau,t_0+\tau]$, we define the following vector field,

$$\begin{cases}\dot{x}=f(t)x,\\ \dot{y}=-f(t)y.\end{cases} \tag{34}$$

For any initial condition $(x(t_0),y(t_0))=(x_0,y_0)$, the solution of (34) is given by,

$$\begin{cases}x(t,x_0)=x_0e^{F(t)}\\ y(t,y_0)=y_0e^{-F(t)}\end{cases} \tag{35}$$

where $F(t)=\int_0^t f(s)ds$. This system has a stationary hyperbolic trajectory at the origin, with stable manifold given by $W^s(0,0)=\{(x,y):x=0,y\neq 0\}$ and unstable manifold given by $W^u(0,0)=\{(x,y):x\neq 0,y=0\}$. The Lagrangian descriptor defined in (2) for this system takes the form,

$$M_p((x_0,y_0),t_0,\tau)$$
$$=\int_{t_0-\tau}^{t_0+\tau}|x_0e^{F(t)}f(t)|^p+|-y_0e^{-F(t)}f(t)|^pdt$$
$$=|x_0|^pA(t)+|y_0|^pB(t) \tag{36}$$

where

$$A(t)=\int_{t_0-\tau}^{t_0+\tau}|e^{F(t)}f(t)|^pdt,$$
$$B(t)=\int_{t_0-\tau}^{t_0+\tau}|e^{-F(t)}f(t)|^pdt \tag{37}$$

are functions that do not depend on x_0 and y_0. Consequently, (36) has the same functional form as (7) and we can apply the same argument as given in Theorem 1 to obtain nondifferentiability of M_p along any line transverse to the stable manifold $W^s(0,0)$ for $p\leq 1$. Similarly we obtain nondifferentiability of M_p along any line transverse to the unstable manifold $W^u(0,0)$.

2.5. *The nonautonomous nonlinear saddle point*

We now consider a nonautonomous nonlinear system having a hyperbolic saddle trajectory at the origin. Let $f\in C^1(t_0-\tau,t_0+\tau)$, and $f(t)>0$ for every $t\in[t_0-\tau,t_0+\tau]$. Our system has the form,

$$\begin{cases}\dot{x}=f(t)x+g_1(t,x,y)\\ \dot{y}=-f(t)y+g_2(t,x,y),\end{cases} \tag{38}$$

where $g_1,g_2:\mathbb{R}\times\mathbb{R}^2\to\mathbb{R}$ with $g_1(t,0,0)=g_2(t,0,0)=0$, $\forall\,t$. We suppose that g_1,g_2 are real valued nonlinear functions and their order is quadratic or higher in (x,y), with $g_1,g_2\in C^1$ satisfying the conditions that make (38) Hamiltonian. It is straightforward to verify that $(x,y)=(0,0)$ is a hyperbolic trajectory. For hyperbolic trajectories in nonautonomous vector fields, their corresponding stable and unstable manifolds are, respectively, tangent to the stable and unstable subspaces of the linear approximation at the hyperbolic trajectory [Coddington & Levinson, 1955; Irwin, 1973; de Blasi & Schinas, 1973; Katok & Hasselblatt, 1995; Fenichel, 1991]. We will show that the Lagrangian descriptor detects the manifolds in this example in the same manner as for the earlier examples in this paper.

The strategy for demonstrating this fact is exactly the same as the one used to show that the structure of the Lagrangian descriptor for the linear autonomous saddle (discussed in Sec. 2.1) coincides with the structure for the autonomous nonlinear saddle point (discussed in Sec. 2.3). A differentiable, invertible change of coordinates was made (given by [Moser, 1956]), in such a way that effectively transformed the autonomous nonlinear saddle

point into the form of the autonomous linear saddle point. Then it was obvious that the results for the autonomous linear saddle point, in the transformed coordinates, carried over the autonomous nonlinear saddle point directly. A final argument showing that the singularities of the Lagrangian descriptor for the nonlinear autonomous saddle point in the transformed coordinates were also present in the original coordinates completed the argument.

A similar strategy is carried out in the nonautonomous case, but it is not as straightforward as in the autonomous case. There has been a recent extension of Moser's theorem to the nonautonomous case [Fortunati & Wiggins, 2016], but the requirements on the time dependence are too stringent for all the applications that we will consider, and therefore we will not utilize this result in our arguments for this example. Another approach is to utilize a result like the Hartman–Grobman theorem [Hartman, 1960a, 1960b, 1963; Grobman, 1959, 1962] for nonautonomous systems. Recently this result has been generalized to nonautonomous systems in [Barreira & Valls, 2006]. However, an issue with these "linearization theorems" is that the linearization transformations are not differentiable on the hyperbolic trajectory. This situation has been discussed in detail in [Lopesino *et al.*, 2015] where it is argued that, for our purpose, this situation is essentially of a technical nature and does not prevent our use of such results to reach the desired conclusion.

3. Non-Hamiltonian Systems

In this section, we consider some issues related to the interpretation of the output of Lagrangian descriptors when they are applied to non-Hamiltonian systems.

As an example, we consider the following non-Hamiltonian system:

$$\begin{cases} \dot{x} = \lambda x \\ \dot{y} = -\mu y \end{cases}, \quad \mu, \lambda > 0 \quad \text{and} \quad \mu \neq \lambda \tag{39}$$

for which the exact solution takes the expression,

$$\begin{cases} x(t) = x_0 e^{\lambda t} \\ y(t) = y_0 e^{-\mu t}. \end{cases} \tag{40}$$

In this case the origin is a hyperbolic fixed point with stable and unstable manifolds as in the example described in Sec. 2.1,

$$\begin{aligned} W^s(0,0) &= \{(x,y) \in \mathbb{R}^2 \,|\, x = 0, y \neq 0\}, \\ W^u(0,0) &= \{(x,y) \in \mathbb{R}^2 \,|\, y = 0, x \neq 0\}. \end{aligned} \tag{41}$$

For the dynamical system (39) at $t_0 = 0$, $M_p((x_0,y_0),t_0,\tau)$ is explicitly computed as:

$$\begin{aligned} &M_p((x_0,y_0),t_0,\tau) \\ &\quad = \int_{-\tau}^{\tau} |\lambda x_0 e^{\lambda t}|^p + |-\mu y_0 e^{-\mu t}|^p dt \\ &\quad = \lambda^{p-1}|x_0|^p \frac{(e^{\lambda p\tau} - e^{-\lambda p\tau})}{p} \\ &\qquad + \mu^{p-1}|y_0|^p \frac{(e^{\mu p\tau} - e^{-\mu p\tau})}{p}. \end{aligned} \tag{42}$$

From the form of the LD it is easy to see that nondifferentiability of the directional derivatives on the stable and unstable manifolds follows from the same argument given in Theorem 1. The singularities in expression (42) satisfy Definition 2.1, which in turn is stated in the spirit of the phenomenology described in [Mendoza & Mancho, 2010; Mancho *et al.*, 2013]. Therefore it is useful to point out here that the term "singularities" does *not* refer to any property of the contour lines of M_p, as incorrectly asserted in [Ruiz-Herrera, 2015a]. Based on this misinterpretation, Ruiz-Herrera [2015b] has claimed that (39) is a "counter-example" to the method of Lagrangian descriptors. This is an incorrect statement as demonstrated by (42).

This implies that care should be taken when trying to visualize the singular features of (42) as in Definition 2.1 from contour plots of M_p itself. Observe that given a fixed p and a sufficiently large τ, the terms in expression (42) can take values which can differ by orders of magnitude. Figure 4(a) illustrates this point by showing the contours of M_p with $p = 0.5$ and $\tau = 15$, for the values $\lambda = 2$ and $\mu = 1$. In this case the first term in (42) is much greater than the second, and thus the effect of the latter goes unnoticed in the figure. Still, the presence of the singularities can also be highlighted by plotting the partial derivatives of M_p, as illustrated in Fig. 5. Using the quotient of the two terms in expression (42), where each term in the quotient evaluates M_p on each manifold, we obtain an idea of their different contribution.

$$\frac{M_p((x_0,0),0,\tau)}{M_p((0,y_0),0,\tau)} = \left(\frac{\lambda}{\mu}\right)^{p-1} \frac{|x_0|^p}{|y_0|^p} \frac{e^{2p\tau\lambda} - 1}{e^{2p\tau\mu} - 1} e^{p\tau(\mu-\lambda)}.$$

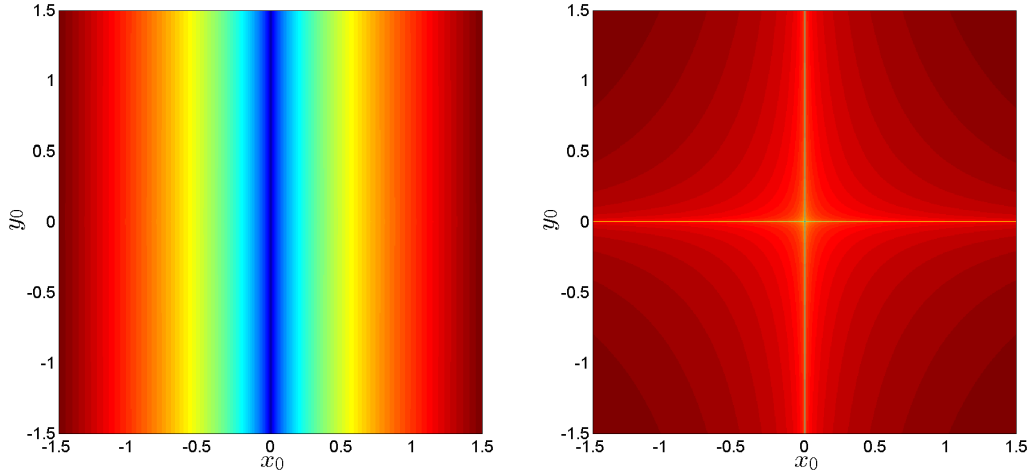

(a) (b)

Fig. 4. Contour plots of Lagrangian descriptors computed for system (39) with $\lambda = 2$ and $\mu = 1$: (a) M_p for $p = 0.5$ and $\tau = 15$ and (b) M_p for $p = 1/\tau$ and $\tau = 15$.

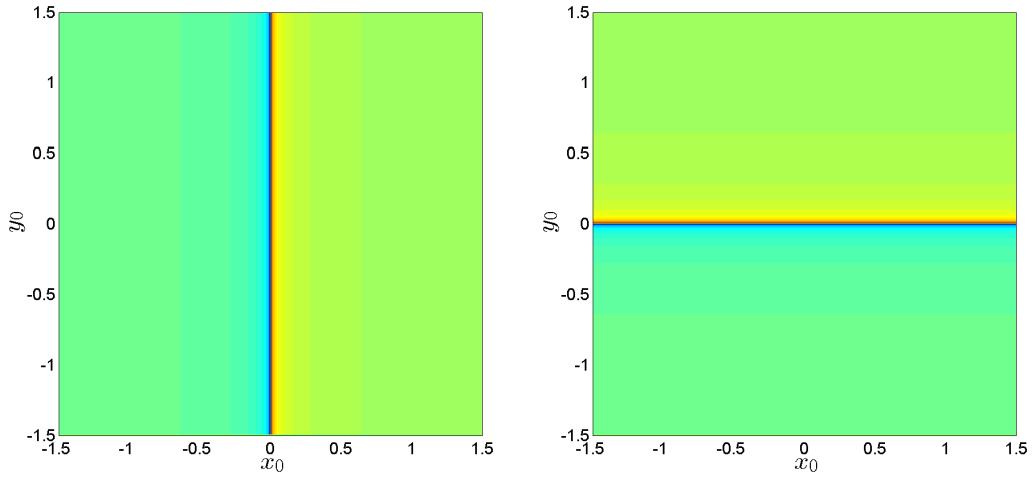

(a) (b)

Fig. 5. Lagrangian descriptors applied to the system (39) with $\lambda = 2$ and $\mu = 1$: (a) Contours of $\frac{\partial M_p}{\partial x_0}$ using $p = 0.5$ and $\tau = 15$ and (b) contours of $\frac{\partial M_p}{\partial y_0}$ using $p = 0.5$ and $\tau = 15$.

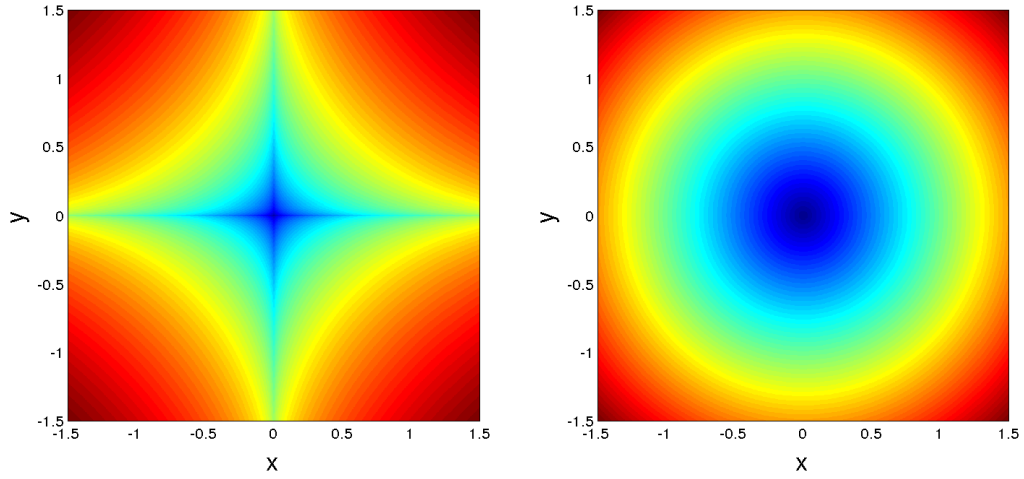

Fig. 6. Panel (a) shows contours of M_p for $p = 0.5$ and panel (b) shows contours of M function. Both are obtained for system (45) for $\tau = 15$.

In particular, for large τ we have

$$\frac{M_p((x_0,0),0,\tau)}{M_p((0,y_0),0,\tau)} = \left(\frac{\lambda}{\mu}\right)^{p-1} \frac{|x_0|^p}{|y_0|^p} e^{p\tau(\lambda-\mu)}. \quad (43)$$

Observe that a good visualization of both manifolds in the same plot can be obtained from the contours if the exponential in (43) is kept of order $\mathcal{O}(1)$ [see Fig. 4(b)]. This is achieved for $p\tau(\lambda-\mu) \approx 1$, that is,

$$p = \frac{1}{\tau(\lambda-\mu)}. \quad (44)$$

We consider next another non-Hamiltonian system,

$$\begin{cases} \dot{x} = -x, \\ \dot{y} = -y. \end{cases} \quad (45)$$

This system has a global attractor at the origin. Furthermore, we can analytically compute Lagrangian descriptors for this example. In the case of the M_p function, we have

$$M_p((x_0,y_0),0,\tau) = \int_{-\tau}^{\tau} |x_0 e^{-t}|^p + |y_0 e^{-t}|^p dt$$
$$= (|x_0|^p + |y_0|^p)\frac{e^{-p\tau} + e^{p\tau}}{p} \quad (46)$$

where the singularities are located on the axes $x = 0$ and $y = 0$, as is observed in Fig. 6(a). Certainly these lines correspond to stable manifolds of the fixed point, however any line passing through the origin is a stable manifold of it, because in fact the whole plane is a stable manifold. In this case one could ask to what extent it is useful highlighting just two lines of the whole plane.

In addition, this observed feature at representing the M_p function for the global attractor is no longer reproduced when computing original M function as in [Madrid and Mancho, 2009]. We then obtain

$$M((x_0,y_0),0,\tau) = \int_{-\tau}^{\tau} \sqrt{x_0^2 e^{-2t} + y_0^2 e^{-2t}}\, dt$$
$$= 2\sqrt{x_0^2 + y_0^2}\sinh(\tau). \quad (47)$$

In this case M does not highlight any singular feature, except for the fixed point at the origin, and therefore the entire stable manifold is not associated with singular feature, as can be seen in Fig. 6(b).

4. Lagrangian Descriptors and the Ergodic Partition Theory

This section illustrates, by using a very simple example, the link between Lagrangian descriptors and previous rigorous results on the ergodic partition theory [Mezić & Wiggins, 1999; Susuki & Mezić, 2009].

We consider the dynamical system:

$$\begin{cases} \dot{x} = y, \\ \dot{y} = -x, \end{cases} \tag{48}$$

where the origin is an elliptic fixed point. This system can be expressed in action-angle variables (ρ, θ) as follows,

$$\begin{cases} \dot{\rho} = \dfrac{\partial H}{\partial \theta} = 0 \\ \dot{\theta} = -\dfrac{\partial H}{\partial \rho} = -1 \end{cases}, \quad \rho \in [0, \infty), \quad \theta \in [0, 2\pi) \tag{49}$$

where $x = \rho \cos\theta$ and $y = \rho \sin\theta$. The Hamiltonian expressed in action-angle variables is $H(\rho, \theta) = \rho$. From these expressions it is clear that ($\rho = \rho_0$, $\theta(t) = -t + \theta_0$) are solutions to the system (49) which correspond to invariant 1-tori. In summary, the phase plane of system (56) is foliated by invariant sets consisting of concentric circles. The autonomous system (56) does not have hyperbolic fixed points nor their invariant manifolds, thus the ideas based on "singular features" of M_p explained in the preceding sections are not directly applicable here. However it is interesting to realize that the described results of LDs are complementary to other previous results in the literature, which we explain next, that rigorously justify the ability of LDs to highlight Lagrangian coherent structures characterized by invariant n-tori.

The definition of M_p given in (2) is the sum of n quantities representing the integration along trajectories of the functions $|\dot{x}_i|^p$, where $i \in \{1, \ldots, n\}$. These quantities, up to a factor $1/(2\tau)$, are the time averages along trajectories of the given functions. Analogously, the original definition of LDs given by [Mendoza & Mancho, 2010; Mancho *et al.*, 2013] based on the Euclidean arc length is obtained by integrating the modulus of the velocity along trajectories, i.e.

$$M(\mathbf{x}_0, t_0, \tau) = \int_{t_0-\tau}^{t_0+\tau} \|\mathbf{v}(\mathbf{x}(t; \mathbf{x}_0), t)\| dt. \tag{50}$$

Again, M is the average along trajectories of the function $\|\mathbf{v}\|$ up to a factor $1/(2\tau)$. The role of averages of functions along trajectories for obtaining invariant sets is discussed in works by [Mezić & Wiggins, 1999; Susuki & Mezić, 2009]. There, the Birkhoff ergodic theorem is used. This theorem states that in the limit $\tau \to \infty$, averages of functions along trajectories of dynamical systems which preserve smooth measures and are defined on compact sets do exist. Level sets of these limit functions are invariant sets. However, we note that the Birkhoff ergodic theorem has *not* been generalized to the case of aperiodically time-dependent vector fields.

We examine these ideas in the case of M_p for the example (56). First, we remark that Hamiltonian dynamical systems preserve smooth measures as they are volume preserving. We show next that the limit of the time average can be analytically calculated for this system using $p = 1$. Considering the solutions of (56), $M_{p=1}$ is

$$\begin{aligned} &M_{p=1}(\mathbf{x}_0, 0, \tau) \\ &\quad = \rho_0 \int_{-\tau}^{\tau} |\sin(-t + \theta_0)| + |\cos(-t + \theta_0)| dt \\ &\quad = \rho_0 \int_{-\tau+\theta_0}^{\theta_0} |\sin(s)| + |\cos(s)| ds \\ &\qquad + \rho_0 \int_{\theta_0}^{\tau+\theta_0} |\sin(s)| + |\cos(s)| ds. \end{aligned} \tag{51}$$

Now we can write $\tau = N\pi + q$ with $q \in [0, \pi)$ and calculate one of the integrals of (51) as,

$$\begin{aligned} &\int_{\theta_0}^{\theta_0+\tau} |\sin s| ds \\ &\quad = \int_{\theta_0}^{\theta_0+N\pi+q} |\sin s| ds \\ &\quad = \int_{\theta_0}^{\theta_0+N\pi} |\sin s| ds + \int_{\theta_0+N\pi}^{\theta_0+N\pi+q} |\sin s| ds \\ &\quad = N \int_{\theta_0}^{\theta_0+\pi} |\sin s| ds + \int_{\theta_0}^{\theta_0+q} |\sin s| ds \\ &\quad = 2N + \int_{\theta_0}^{\theta_0+q} |\sin s| ds. \end{aligned}$$

Analogously for the other terms we obtain,

$$\int_{\theta_0}^{\theta_0+\tau} |\cos s| ds = 2N + \int_{\theta_0}^{\theta_0+q} |\cos s| ds,$$

$$\int_{-\tau+\theta_0}^{\theta_0} |\sin s| ds = 2N + \int_{\theta_0-q}^{\theta_0} |\sin s| ds,$$

$$\int_{-\tau+\theta_0}^{\theta_0} |\cos s| ds = 2N + \int_{\theta_0-q}^{\theta_0} |\cos s| ds.$$

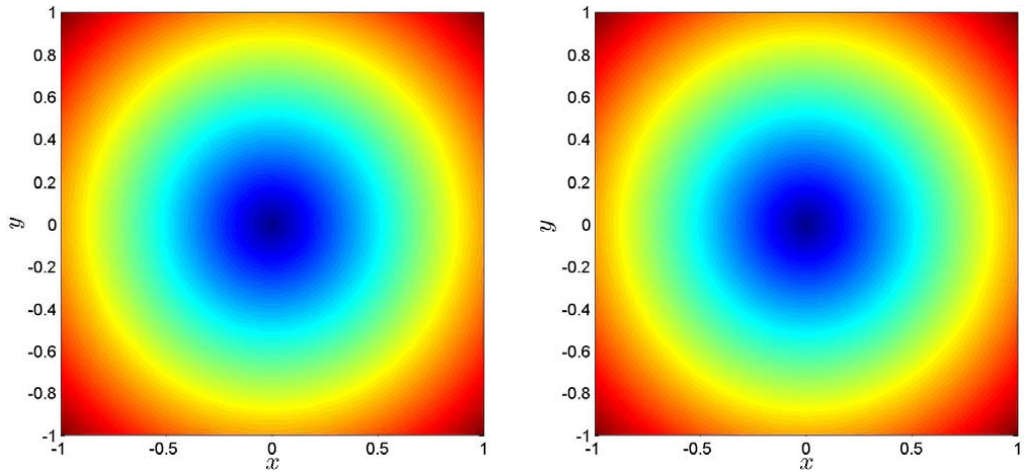

(a) (b)

Fig. 7. Phase space of (56) calculated with: (a) M for $\tau = 10$ and (b) M_1 for $\tau = 10$.

Consequently the time average of $M_{p=1}$ is the limit

$$\begin{aligned}\lim_{\tau\to\infty}\frac{1}{2\tau}M_1(\mathbf{x}_0,0,\tau)&\\ =\lim_{N\to\infty}\frac{8N\rho_0}{2(N\pi+q)}+\frac{\rho_0}{2(N\pi+q)}&\\ \times\int_{\theta_0-q}^{\theta_0+q}|\cos s|+|\sin s|ds&\\ =\frac{4\rho_0}{\pi}=\frac{4}{\pi}\sqrt{x_0^2+y_0^2}.&\end{aligned}\tag{52}$$

In order to prove that the time average of M_p also converges for $0 < p < 1$, we can use that

$$\begin{aligned}0\le\frac{1}{2\tau}M_p(\mathbf{x}_0,0,\tau)&\\ =\frac{1}{2\tau}\rho_0^p\int_{-\tau}^{\tau}|\sin(-t+\theta_0)|^p+|\cos(-t+\theta_0)|^p dt&\\ \le\frac{1}{2\tau}\rho_0^p\int_{-\tau}^{\tau}(1+1)dt=2\rho_0^p,\quad\forall\, p\in(0,1].&\end{aligned}$$

Since $\frac{1}{2\tau}M_p(\mathbf{x}_0,0,\tau)$ is an increasing function of τ and it is bounded by a constant value, then $\frac{1}{2\tau}M_p(\mathbf{x}_0,0,\tau)$ also converges when $\tau\to\infty$.

Results for M are also easily obtained, given that arc length is $M = 2\tau\rho$. In order to obtain the limit of the time average here, it is not necessary to go up to very large τ, since the time average is a constant function in τ (i.e. $\frac{1}{2\tau}M = \rho$), and thus the convergence is obtained for any finite τ. We note that contour lines of both M_p and M are the same as their averages. The important point for those level sets to be invariant sets is that they have to be taken once the convergence of the average is reached. In the case of M_p a sufficiently large τ is required and in the case of M any τ is valid. In both cases the invariant sets are just the concentric circles given by the 1-tori (see Fig. 7). Further averages of functions to complete an ergodic partition as described by [Mezić & Wiggins, 1999; Susuki & Mezić, 2009], are not required for this particular example, as the circles are already minimal invariant sets.

As a final remark we note that despite the similarity between Figs. 7(a) and 6(b), the interpretation of LDs is completely different in each case. The link between contour lines of M and invariant sets requires a measure preserving dynamical system defined on a compact set, and this is clearly not the case for system (45) represented in Fig. 6(b).

5. Lagrangian Descriptors and 3D Flows

Visualizing flow structures in three dimensions is of much interest, but achieving success requires overcoming numerous difficulties. Probably the fundamental issue is that it is difficult to "organize" the data from an ensemble of trajectories in such a way as to "reveal" geometrical structures. In this context, LDs were applied to study the transport

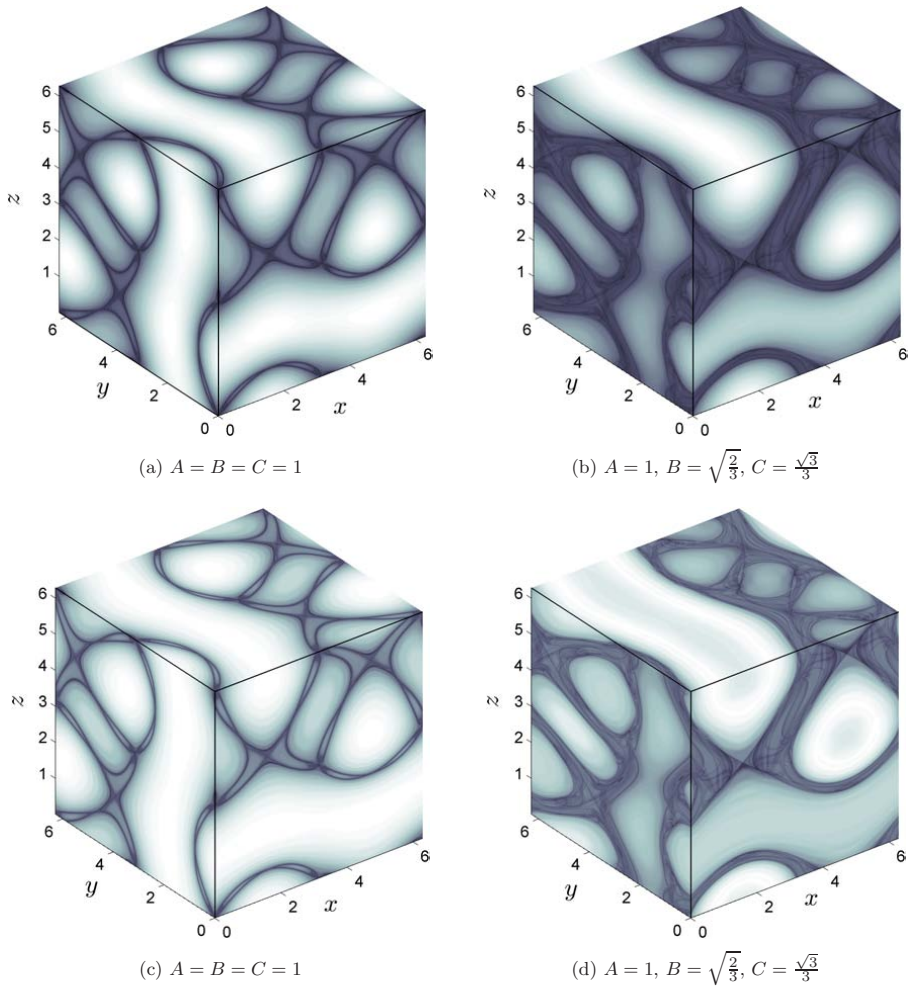

(a) $A = B = C = 1$ (b) $A = 1$, $B = \sqrt{\frac{2}{3}}$, $C = \frac{\sqrt{3}}{3}$

(c) $A = B = C = 1$ (d) $A = 1$, $B = \sqrt{\frac{2}{3}}$, $C = \frac{\sqrt{3}}{3}$

Fig. 8. (a) and (b) Contours of M for the ABC flow with $\tau = 30$; (c) and (d) contours of M_1 for the ABC flow with $\tau = 30$.

in the three-dimensional unsteady Hill's spherical vortex in [Mancho *et al.*, 2013]. The method of Lagrangian descriptors was successful in this study in that it revealed both invariant manifolds of hyperbolic trajectories and invariant sets related to n-tori solutions.

A brief review on the background and issues associated with the dynamical systems approach to transport in three dimensions was given in [Wiggins, 2010]. A collection of representative references of the dynamical systems approach to Lagrangian transport in three dimensions, that should not be interpreted as an exhaustive review of this topic, are: [MacKay, 1994; Mezić & Wiggins, 1994; Fountain *et al.*, 1998; Sotiropoulos *et al.*, 2001; Xu & Homsy, 2007; Mullowney *et al.*, 2005; Green *et al.*, 2007; Branicki & Wiggins, 2009; Pouransari *et al.*, 2010; Levnajić & Mezić, 2010; Lester *et al.*, 2012; Smith *et al.*, 2012, 2014; McIlhany *et al.*, 2015; Smith *et al.*, 2016].

We illustrate the ability of LDs to visualize three-dimensional flows by analyzing the well known Arnold–Beltrami–Childress (ABC) flow [Arnold, 1965; Arnold & Korkina, 1983; Dombre *et al.*, 1986]. This flow models prototypes of fast dynamos in magnetohydrodynamics (cf. [Arnold &

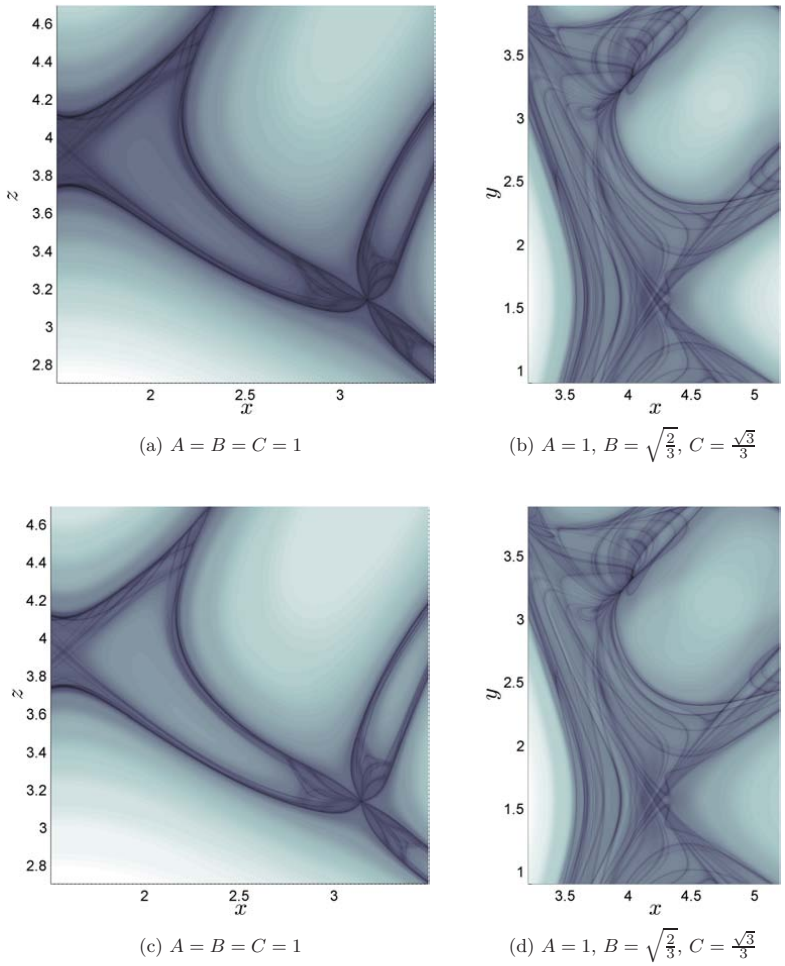

(a) $A = B = C = 1$ (b) $A = 1$, $B = \sqrt{\frac{2}{3}}$, $C = \frac{\sqrt{3}}{3}$

(c) $A = B = C = 1$ (d) $A = 1$, $B = \sqrt{\frac{2}{3}}$, $C = \frac{\sqrt{3}}{3}$

Fig. 9. Contours of LDs with $\tau = 30$: (a) Zoom of M on the plane $\{y = 0\}$, (b) zoom of M on the plane $\{z = 0\}$, (c) zoom of M_1 on the plane $\{y = 0\}$ and (d) zoom of M_1 on the plane $\{z = 0\}$.

Korkina, 1983; Galloway, 2012]) and it is also a steady solution of Euler's equations for inviscid fluid flows (see [Childress, 1966]).

The equations for fluid particle trajectories of the ABC flow are given by,

$$\begin{cases} \dot{x} = A\sin z + C\cos y, \\ \dot{y} = B\sin x + A\cos z, \quad x, y, z \in [0, 2\pi], \\ \dot{z} = C\sin y + B\cos x, \end{cases} \tag{53}$$

where A, B, and C are parameters to be chosen shortly. The ABC flow is one of the first flows for which the existence of chaotic particle paths was demonstrated (cf. [Arnold, 1965]). Subsequently, there have been numerous studies of the flow structure of the ABC flow from the dynamical systems point of view, e.g. [Dombre *et al.*, 1986; Haller, 2001; Sulman *et al.*, 2013]. Here we show that both the very intricate manifold structures and the coherent structures of the ABC flow can be visualized with Lagrangian descriptors. In order to illustrate this we choose two sets of parameter values,

$$A = B = C = 1, \quad A = 1, \quad B = \sqrt{\frac{2}{3}}, \quad C = \frac{\sqrt{3}}{3}.$$

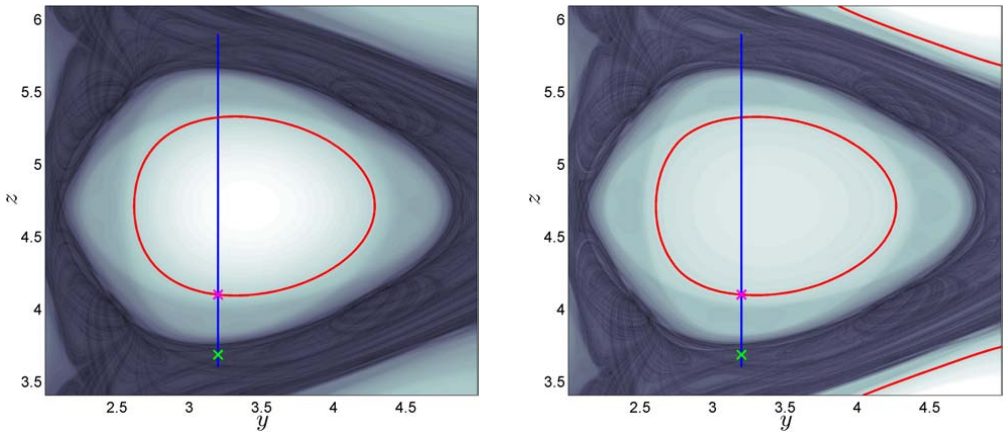

(a) (b)

Fig. 10. (a) M function on an elliptic region located on the plane $\{x = 0\}$ for $\tau = 75$ (value for which convergence inside the elliptic region is ensured) and (b) M_1 function on an elliptic region located on the plane $\{x = 0\}$ for $\tau = 100$ (value for which convergence inside the elliptic region is ensured). In both panels the blue line represents the line of initial conditions considered for the time average analysis, the magenta cross is an initial condition inside the elliptic region and the green cross an initial condition located in a chaotic region. Also, we display in red color the contours corresponding to the magenta initial condition after the time average has converged.

Figure 8 shows the results obtained with M and M_1 for these parameter values. The figure shows both coherent structures and the complicated tangle of repeatedly intersecting stable and unstable manifolds of hyperbolic trajectories along heteroclinic orbits. This chaotic tangle provides the "geometric template" for the chaotic mixing mechanism of particles, which is visible from Fig. 9.

In addition, we demonstrate next with this example the link of LDs to invariant sets. The results discussed in the previous section are applicable here as the ABC flow is incompressible and consequently preserves an invariant measure. In order to analyze the detection of KAM tori by means of LDs for the ABC flow we will focus on the system with parameters $A = 1$, $B = \sqrt{2}/\sqrt{3}$, $C = \sqrt{3}/3$. In

(a)

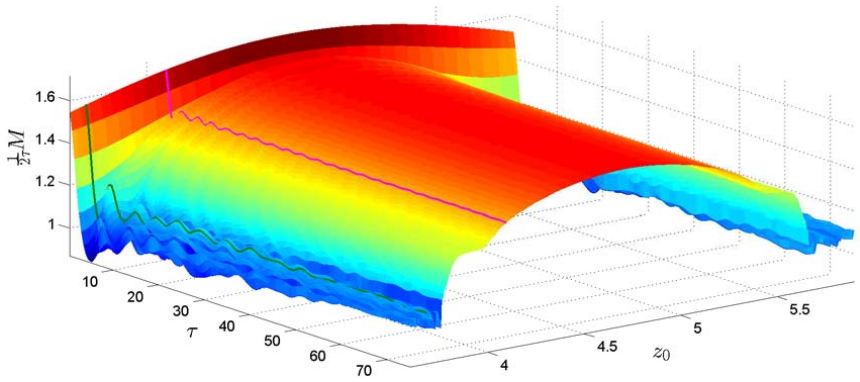

Fig. 11. (a) Time average evolution of M in the range $\tau \in (0, 75]$ for the line of initial conditions (54) and (b) time average evolution of the pink and green initial conditions depicted in Fig. 10.

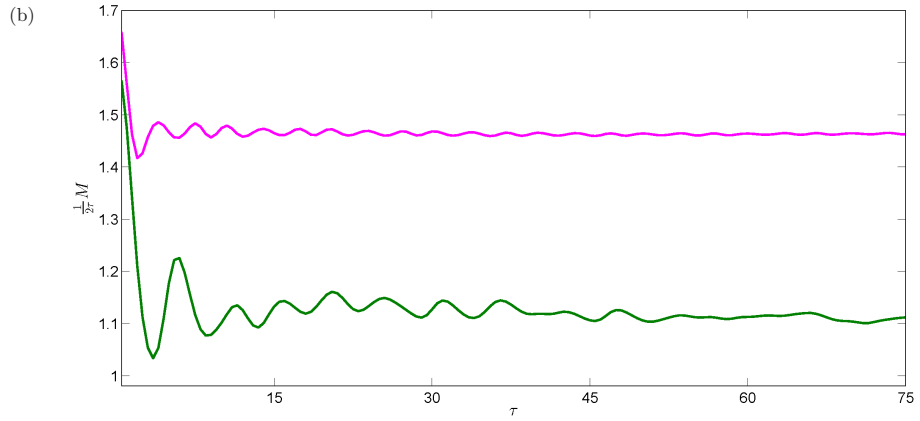

Fig. 11. (*Continued*)

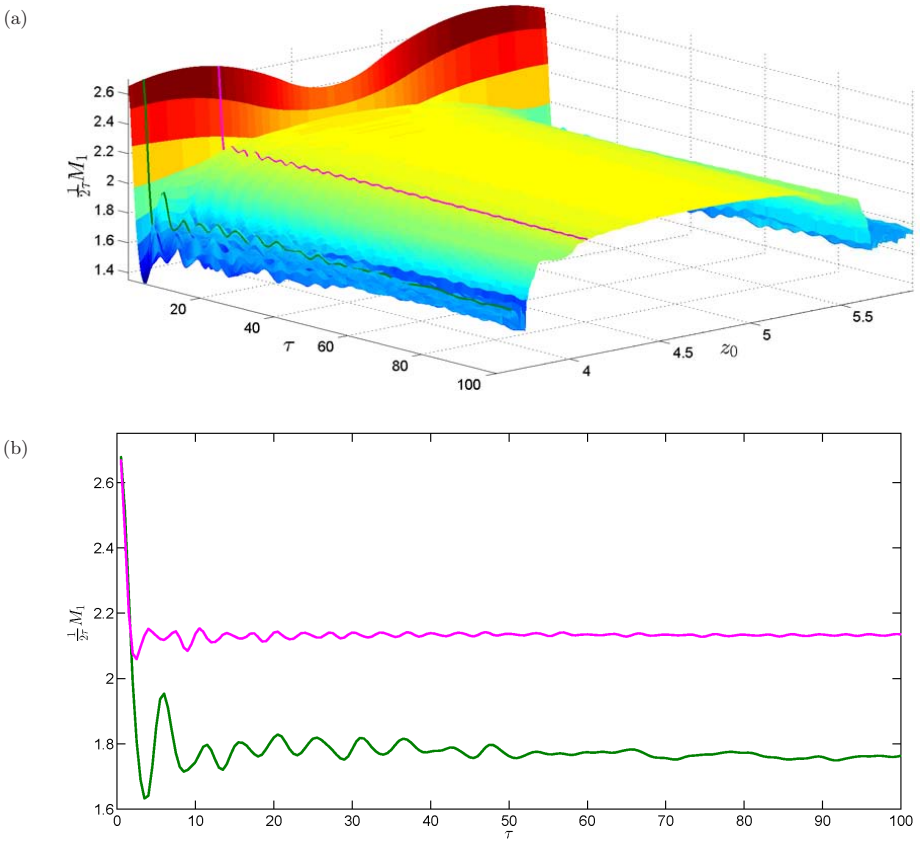

Fig. 12. (a) Time average evolution of M_1 in the range $\tau \in (0, 100]$ for the line of initial conditions (54) and (b) time average evolution of the pink and green initial conditions depicted in Fig. 10.

particular, we consider a line of initial conditions,

$$\mathbf{x}_0 = (0, 3.2, z_0), \quad z_0 \in [3.6, 5.9] \tag{54}$$

which crosses an elliptic region of phase space as shown in Fig. 10 in blue. For these initial conditions we study the convergence of the time averages of M and M_p so the invariant sets present in the elliptic regions of the phase portrait for the ABC flow can be recovered from the contours of LDs contained in these regions. Figures 11 and 12 show the evolution of the time averages of $M/(2\tau)$ and $M_1/(2\tau)$ respectively. Observe also that their convergence at two particular initial conditions, one inside the elliptic region (marked with a magenta cross) and one inside the chaotic tangle regime (green cross), have been highlighted (see Figs. 10–12). These figures emphasize how at initial conditions inside elliptic regions, the time averages $M/(2\tau)$ and $M_1/(2\tau)$ reach convergence for sufficiently large τ, meanwhile for initial conditions located in hyperbolic regions, $M/(2\tau)$ and $M_1/(2\tau)$ do not seem to converge for that time period (see Figs. 11–13). Thus contour lines of M and M_p at the τ values where convergence is met are in 1-1 correspondence to invariant set. Thus contrary to what is stated in [Farazmand & Haller, 2016], LDs distinguish coherent structures which are invariant and this is backed by specific mathematical results. Similar results to

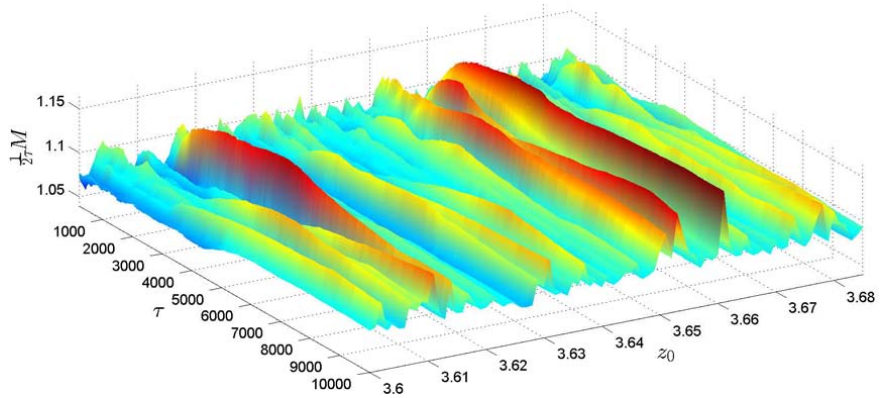

(a)

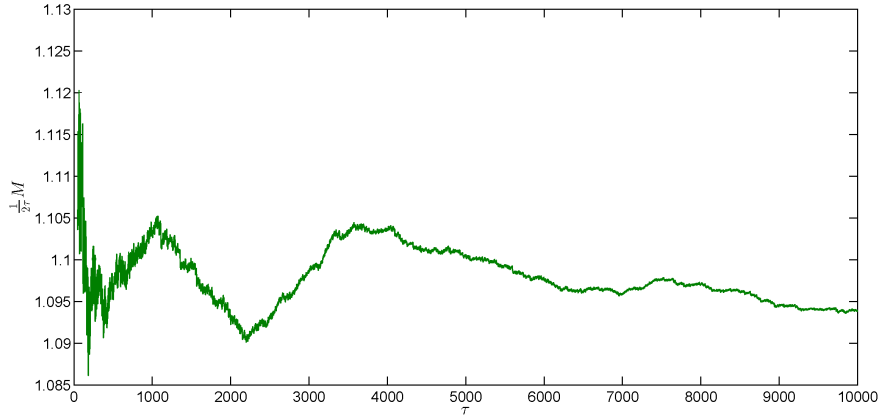

(b)

Fig. 13. (a) Time average evolution of M in the range $\tau \in (0, 10\,000]$ for a subset of the line (54) in the chaotic region and (b) time average evolution of green initial condition in the range $\tau \in (0, 10\,000]$.

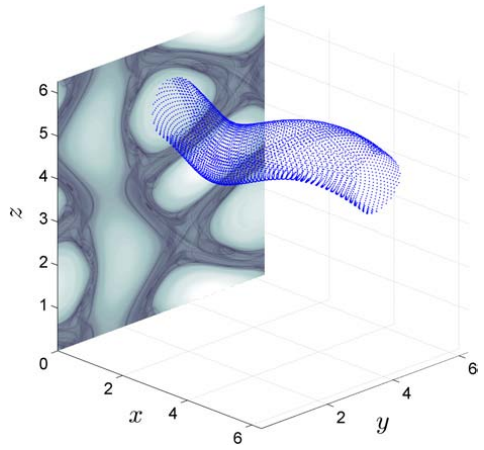

Fig. 14. Trajectory of an initial condition inside the elliptic region which displays the associated invariant set.

the ones discussed here are found in [Budišić & Mezić, 2012]. We remark that the decomposition achieved by the LD is not minimal in the domain $x, y, z \in [0, 2\pi]$. As an example, this is observed from the red level sets displayed in the top and bottom right corners in Fig. 10(b), which would correspond to invariant sets disconnected from the one inside the elliptic region. Figure 14 shows the integration of a trajectory starting from the initial condition $(0, 3.2, 4.1)$, marked with a magenta cross on one of the contour lines obtained from the time-average convergence (see Fig. 10), confirming the invariant and minimal character of the level set restricted to the elliptic region.

6. Objectivity and Phase Space Structure

The utility of LDs for revealing phase space structure has been questioned in the literature [Haller, 2015] as a result of them not having the property of objectivity. Briefly, a scalar valued and time-dependent, function is said to be *objective* if it is invariant under Galilean coordinate transformations. In other words, the pointwise values of a function are the same at points that are transformed under a Galilean transformation, for each value of the time variable, see, e.g. [Truesdell & Noll, 2004; Haller *et al.*, 2016]. Other accepted definitions for objectivity are given in the literature in terms of consistency between frames [Mendoza & Mancho, 2012; Peacock *et al.*, 2015] but in this section we base our discussion on the objectivity definition given above as it is the one considered when debating LDs performance. Certainly in physics many scalar valued functions describing physical quantities, such as energy, or the magnitude of angular momentum, should be invariant under Galilean transformations. But this is *not* a property that is desirable for any tool designed to reveal phase space structure since phase space structure may not be invariant under Galilean coordinate transformations. We demonstrate this in the following example.

We consider the simplest possible dynamical system on the plane, the zero vector field:

$$\dot{\mathbf{x}} = 0, \quad \text{where } \mathbf{x} \in \mathbb{R}^2. \tag{55}$$

This represents a system at rest. We apply a Galilean transformation to this vector field, i.e. a rotation $\underline{\mathbf{x}} = R(t)^T\mathbf{x}$, where $R(t)^T$ denotes the transpose of the orthogonal matrix with angular speed $\omega = 1$:

$$R(t) = \begin{pmatrix} \cos t & -\sin t \\ \sin t & \cos t \end{pmatrix}.$$

In this rotating frame, (55) takes the form:

$$\begin{cases} \dot{\underline{x}} = \underline{y} \\ \dot{\underline{y}} = -\underline{x}. \end{cases} \tag{56}$$

The phase portrait of (55) consists entirely of fixed points. The phase portrait of (56), which represents a particular case of an harmonic oscillator, consists of a one-parameter family of invariant circles (see [Arnold, 1973, pp. 44–45]). Clearly the phase space structure of these two dynamical systems is different, and as the LDs can be analytically computed for both dynamical systems, this fact is verified explicitly.

The arclength based LD, denoted by M, measures the arclength of a trajectory through an initial condition in both forward and backward time, for a specified time. For (55) this is identically zero since every point is a fixed point, and therefore the arclength of every trajectory is zero, regardless of the time for which it is computed. As for (56), we recall results in Sec. 4 where it was shown that $M = (2\tau)\rho$ for this example. The contours of M are the same as the contours of the Hamiltonian $H = \rho$, and therefore the contours of M are in 1-1 correspondence with the trajectories of (56). Therefore, M recovers the correct phase space structure

for both (55) and (56). Evidently, if M were objective, i.e. the same for each of these vector fields, it would not recover the phase space structure for each vector field.

It is instructive to consider what Lyapunov exponents, both finite and infinite time, would reveal for these examples. For (55) both the finite and infinite time Lyapunov exponents *for any* trajectory are zero. For (49) the infinite time Lyapunov exponents of every trajectory are zero and the value of the finite time Lyapunov exponents depend on the time interval over which they are computed. Therefore, we can make the following conclusions.

- While the infinite time Lyapunov exponents are objective, in the sense that they give the same values for (55) and (49), they fail to reveal the phase space structure for (49).
- Finite time Lyapunov exponents are *not* objective. Their values, and hence the phase space structure that they reveal, depend on the time interval over which they are computed. A discussion of this can be found in [Branicki & Wiggins, 2010; Mancho *et al.*, 2013].

We discuss next another example taken from [Haller, 2005, 2015; Wang, 2015] to show that LDs recover the correct phase space structure even when it is not evident in the instantaneous streamline phase portrait. We consider the following time-dependent dynamical system,

$$\dot{\mathbf{x}} = \begin{pmatrix} \sin 2\omega t & \omega + \cos 2\omega t \\ -\omega + \cos 2\omega t & -\sin 2\omega t \end{pmatrix} \mathbf{x}. \tag{57}$$

Figure 15(a) shows the instantaneous velocity fields and streamlines at $t = 0$ for this example with $\omega = 2$. They show a circulating pattern suggesting the presence of an eddy. However, the following coordinate transformation,

$$\mathbf{x} = R(t)^T \underline{\mathbf{x}}, \quad R(t) = \begin{pmatrix} \cos \omega t & -\sin \omega t \\ \sin \omega t & \cos \omega t \end{pmatrix}$$

where $R(t)^T$ is the transpose of $R(t)$, converts system (57) into a stationary saddle,

$$\begin{cases} \dot{\underline{x}} = \underline{y} \\ \dot{\underline{y}} = \underline{x}. \end{cases} \tag{58}$$

Hence (57), despite the structure revealed by the instantaneous streamline curves, is actually a rotating saddle point, i.e. a saddle point at the origin with rotating stable and unstable manifolds. Precisely this structure is revealed by the LD M_p, as it is illustrated in Fig. 16, which shows contours of

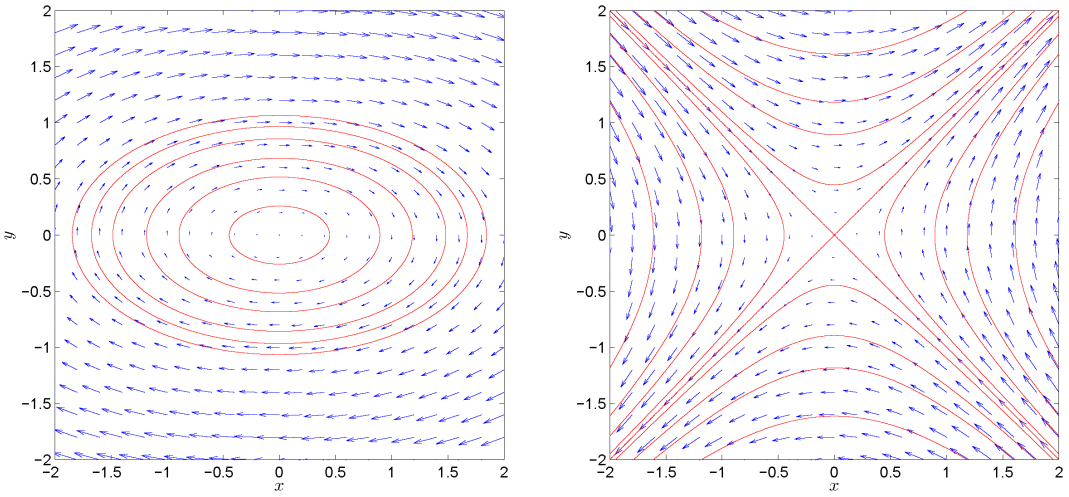

(a) (b)

Fig. 15. (a) Streamlines and velocity field for system (57) at $t = 0$ and (b) streamlines and velocity field for system (58) at $t = 0$.

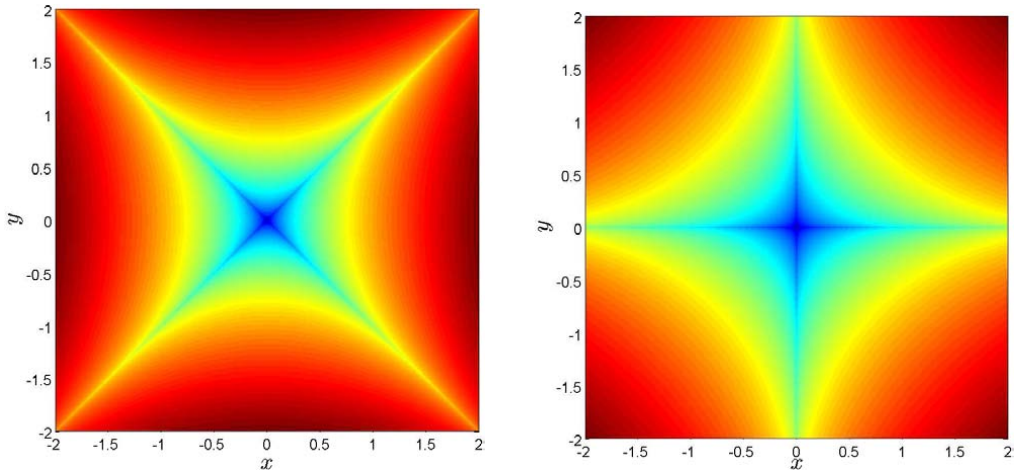

(a) (b)

Fig. 16. Contours of $M_{p=0.5}$ obtained for system (57) with $\tau = 10$ at successive times (a) $t = 0$ and (b) $t = \pi/8$.

$M_{p=0.5}$ at successive times $t = 0, \pi/8$. The contours clearly reveal the rotating saddle point structure.

In this example, M_p is clearly not objective since the pointwise values of M_p vary from (57) to (58). Nevertheless, it is clear that *if* M_p satisfied this criterion of objectivity, it would be the same for both systems and thus it would *not* distinguish between the phase space structure for each of these very different systems, providing an inconsistent description in both frames. Of course, the values of M_p at specific points of space certainly change with the reference frame, but the points at which M_p is singular, which are the features containing the Lagrangian information, are transformed with a smooth change of coordinates in the same manner in which the manifolds themselves are transformed. This was also illustrated for the rotating Duffing equation in [Mendoza & Mancho, 2012].

Moreover, with respect to the question of the requirement of objectivity in the context of techniques for revealing Lagrangian structure, it is instructive to note the following. Recently, in the context of fluid mechanics, a technique called Lagrangian-averaged vorticity deviation (LAVD) [Haller *et al.*, 2016] has been developed. This technique, by construction, has the property of being invariant under Galilean transformations. Consequently, it does not distinguish between the phase portraits of (55) and (56), as we now show.

The Lagrangian-averaged vorticity deviation is defined as follows,

$$\mathrm{LAVD}_{t_0}^{t_0+\tau}(\mathbf{x}_0) = \int_{t_0}^{t_0+\tau} |w(\mathbf{x}(\mathbf{x_0}, t_0, t), t) - \overline{w}(t)| dt \tag{59}$$

where the vorticity $w = \nabla \times \mathbf{v}$, is evaluated along the trajectory $\mathbf{x}(\mathbf{x_0}, t_0, t)$. In this expression $\overline{w}$ is the instantaneous spatial mean of the vorticity over $U(t)$:

$$\overline{w}(t) = \frac{\displaystyle\int_{U(t)} w(\mathbf{x}, t) dV}{\mathrm{vol}(U(t))}$$

where $U(t)$ is a domain invariant under the fluid flow and vol() denotes the volume. Let us evaluate LAVD for system (56). The vorticity is constant everywhere $w = -2$, in particular, also along the trajectories. On the other hand, let us consider the domain $U(t) = \{(x, y) \,|\, \sqrt{x^2 + y^2} \leq \rho_1\}$ which is invariant under the flow of system (56). In this case, it is easily found that:

$$\overline{w}(t) = \frac{-2 \displaystyle\int_{U(t)} dV}{\pi \rho_1^2} = -2$$

thus LAVD is constantly zero on the whole domain for (56). This is also clearly the case for (55) and

thus LAVD contour lines do not distinguish between these systems.

Finally, a reflection on the property of objectivity, understood as a property of functions which preserve pointwise values under a Galilean transformation, and when it may be required, is useful. From the point of view of distinguishing Lagrangian structures in velocity fields related by a Galilean coordinate transformation, our examples show that objectivity is *not* a desirable property for a method to detect phase space structures in different frames.

7. Conclusions

This paper provides a theoretical framework for Lagrangian descriptors. In particular, the issues surrounding the ability of LDs to detect invariant stable and unstable manifolds of hyperbolic points are stated and clarified. This is accomplished by precisely defining the notion of "singular feature" and rigorously proving the presence of these features aligned with invariant manifolds in four particular cases: a hyperbolic saddle point for linear autonomous systems, a hyperbolic saddle point for nonlinear autonomous systems, a hyperbolic saddle point for linear nonautonomous systems and a hyperbolic saddle point for nonlinear nonautonomous systems. In order to achieve this goal we have proposed a new way of constructing Lagrangian descriptors that keeps proofs simple.

We have also discussed well known rigorous results of the ergodic partition theory which are related to LDs. As a result we show the ability of LDs to highlight additional invariant sets, such as n-tori, by means of contour plots of converged averages.

We have presented the application of LDs to the 3D ABC flow, in which it is shown how LDs locate simultaneously invariant manifolds, that are distinguishable as singular features, and invariant tori, visible from contour lines. The ability of LDs to highlight both manifolds and coherent eddy-like or jet-like structures had been noted in the literature [de la Cámara *et al.*, 2012; Wiggins & Mancho, 2014; García-Garrido *et al.*, 2015], although in this paper it is linked to previously known rigorous results. We note however that these works dealt with aperiodic flows and there is no generalization of the Birkhoff ergodic theorem to the case of aperiodically time-dependent vector fields, which is required for the ergodic partition theory.

Finally, we have provided a discussion of the topic of objectivity in the context of Lagrangian descriptors. Specifically, we have analyzed their ability to provide the correct description of phase space structures under Galilean transformation, as well as showing that the requirement of the objectivity property in general for tools in order to reveal phase space structures is not a desirable property.

Acknowledgments

The research of C. Lopesino, F. Balibrea-Iniesta, V. J. García-Garrido and A. M. Mancho is supported by the MINECO under grant MTM2014-56392-R. The research of S. Wiggins is supported by ONR Grant No. N00014-01-1-0769. We acknowledge support from MINECO: ICMAT Severo Ochoa project SEV-2011-0087.

References

Arnold, V. I. [1965] "Sur la topologie des écoulements stationnaires des fluides parfaits," *C. R. Acad. Sci. Paris A* **261**, 17–20.

Arnold, V. I. [1973] *Ordinary Differential Equations* (MIT Press).

Arnold, V. I. & Korkina, E. I. [1983] "The growth of a magnetic field in the three-dimensional steady flow of an incompressible fluid," *Moskovskii Universitet Vestnik Seriia Matematika Mekhanika*, pp. 43–46.

Barreira, L. & Valls, C. [2006] "A Grobman–Hartman theorem for nonuniformly hyperbolic dynamics," *J. Diff. Eqs.* **228**, 285–310.

Branicki, M. & Wiggins, S. [2009] "An adaptive method for computing invariant manifolds in non-autonomous, three-dimensional dynamical systems," *Physica D* **238**, 1625–1657.

Branicki, M. & Wiggins, S. [2010] "Finite-time Lagrangian transport analysis: Stable and unstable manifolds of hyperbolic trajectories and finite-time Lyapunov exponents," *Nonlin. Process. Geophys.* **17**, 1–36.

Budišić, M. & Mezić, I. [2012] "Geometry of the ergodic quotient reveals coherent structures in flows," *Physica D* **241**, 1255–1269.

Childress, S. [1966] "Solutions of Euler's equations containing finite eddies," *Phys. Fluids* **9**, 860–872.

Coddington, E. A. & Levinson, N. [1955] *Theory of Ordinary Differential Equations* (McGraw-Hill, NY).

Craven, G. T. & Hernandez, R. [2015] "Lagrangian descriptors of thermalized transition states on time-varying energy surfaces," *Phys. Rev. Lett.* **115**, 148301.

Craven, G. T. & Hernandez, R. [2016] "Deconstructing field-induced ketene isomerization through Lagrangian descriptors," *Phys. Chem. Chem. Phys.* **18**, 4008.

de Blasi, F. S. & Schinas, J. [1973] "On the stable manifold theorem for discrete time dependent processes in Banach spaces," *Bull. London Math. Soc.* **5**, 275–282.

de la Cámara, A., Mancho, A. M., Ide, K., Serrano, E. & Mechoso, C. [2012] "Routes of transport across the Antarctic polar vortex in the southern spring," *J. Atmos. Sci.* **69**, 753–767.

de la Cámara, A., Mechoso, C. R., Serrano, E. & Ide, K. [2013] "Quasi-horizontal transport within the Antarctic polar night vortex: Rossby wave breaking evidence and Lagrangian structures," *J. Atmos. Sci.* **70**, 2982–3001.

Dombre, T., Frisch, U., Greene, J. M., Hénon, M., Mehr, A. & Soward, A. M. [1986] "Chaotic streamlines in the ABC flows," *J. Fluid Mech.* **167**, 353–391.

Farazmand, M. & Haller, G. [2016] "Polar rotation angle identifies elliptic islands in unsteady dynamical systems," *Physica D* **315**, 1–12.

Fenichel, N. [1991] "Hyperbolicity and exponential dichotomy for dynamical systems," *Dynamics Reported*, eds. Jones, C. K. R. T., Kirchgraber, U. & Walther, J. O., Vol. 5 (Springer-Verlag, Heidelberg, Berlin, NY), pp. 1–25.

Fortunati, A. & Wiggins, S. [2016] "Normal forms á la Moser for aperiodically time-dependent Hamiltonians in the vicinity of a hyperbolic equilibrium," *Discr. Contin. Dyn. Syst.-S* **9**, 1109–1118.

Fountain, G. O., Khakhar, D. V. & Ottino, J. M. [1998] "Visualization of three-dimensional chaos," *Science* **281**, 683–686.

Galloway, D. [2012] "ABC flows then and now," *Geophys. Astrophys. Fluid Dyn.* **106**, 450–467.

García-Garrido, V. J., Mancho, A. M., Wiggins, S. & Mendoza, C. [2015] "A dynamical systems approach to the surface search for debris associated with the disappearance of flight MH370," *Nonlin. Process. Geophys.* **22**, 701–712.

García-Garrido, V. J., Ramos, A., Mancho, A. M., Coca, J. & Wiggins, S. [2016] "A dynamical systems perspective for a real-time response to a marine oil spill," *Marine Pollut. Bull.* **112**, 201–210.

Green, M. A., Rowley, C. W. & Haller, G. [2007] "Detection of Lagrangian coherent structures in three-dimensional turbulence," *J. Fluid Mech.* **572**, 111–120.

Grobman, D. M. [1959] "Homeomorphisms of systems of differential equations," *Dokl. Akad. Nauk SSSR* **128**, 880–881.

Grobman, D. M. [1962] "Topological classification of neighborhoods of a singularity in n-space," *Mat. Sbornik* **56**, 77–94.

Haller, G. [2001] "Distinguished material surfaces and coherent structures in three-dimensional fluid flows," *Physica D* **149**, 248–277.

Haller, G. [2005] "An objective definition of a vortex," *J. Fluid Mech.* **525**, 1–26.

Haller, G. [2015] "Lagrangian coherent structures," *Ann. Rev. Fluid Mech.* **47**, 137–162.

Haller, G., Hadjighasem, A., Farazmand, M. & Huhn, F. [2016] "Defining coherent vortices objectively from the vorticity," *J. Fluid Mech.* **795**, 136–173.

Hartman, P. [1960a] "A lemma in the theory of structural stability of differential equations," *Proc. Amer. Math. Soc.* **11**, 610–620.

Hartman, P. [1960b] "On local homeomorphisms of Euclidean spaces," *Bol. Soc. Mat. Mexicana* **5**, 220–241.

Hartman, P. [1963] "On the local linearization of differential equations," *Proc. Amer. Math. Soc.* **14**, 568–573.

Ide, K., Small, D. & Wiggins, S. [2002] "Distinguished hyperbolic trajectories in time dependent fluid flows: Analytical and computational approach for velocity fields defined as data sets," *Nonlin. Process. Geophys.* **9**, 237–263.

Irwin, M. C. [1973] "Hyperbolic time dependent processes," *Bull. London Math. Soc.* **5**, 209–217.

Junginger, A. & Hernandez, R. [2016] "Uncovering the geometry of barrierless reactions using Lagrangian descriptors," *J. Phys. Chem. B* **120**, 1720.

Katok, A. & Hasselblatt, B. [1995] *Introduction to the Modern Theory of Dynamical Systems* (Cambridge University Press, Cambridge).

Lester, D., Smith, L. D., Metcalfe, G. & Rudman, M. [2012] "Beyond Hamiltonian: Chaotic advection in a three-dimensional volume preserving flow," *Proc. 9th Int. Conf. CFD in the Minerals and Process Industries*, http://www.cfd.com.au/cfd_conf12/PDFs/006LES.pdf.

Levnajić, Z. & Mezić, I. [2010] "Ergodic theory and visualization. I. Mesochronic plots for visualization of ergodic partition and invariant sets," *Chaos* **20**, 033114.

Lopesino, C., Balibrea, F., Wiggins, S. & Mancho, A. M. [2015] "Lagrangian descriptors for two dimensional, area preserving autonomous and nonautonomous maps," *Commun. Nonlin. Sci. Numer. Simul.* **27**, 40–51.

MacKay, R. S. [1994] "Transport in 3d volume-preserving flows," *J. Nonlin. Sci.* **4**, 329–354.

Madrid, J. A. J. & Mancho, A. M. [2009] "Distinguished trajectories in time dependent vector fields," *Chaos* **19**, 013111.

Mancho, A. M., Wiggins, S., Curbelo, J. & Mendoza, C. [2013] "Lagrangian descriptors: A method for revealing phase space structures of general time

dependent dynamical systems," *Commun. Nonlin. Sci. Numer. Simul.* **18**, 3530–3557.

McIlhany, K. L., Guth, S. & Wiggins, S. [2015] "Lagrangian and Eulerian analysis of transport and mixing in the three dimensional, time dependent Hill's spherical vortex," *Phys. Fluids* **27**, 063603.

Mendoza, C. & Mancho, A. M. [2010] "The hidden geometry of ocean flows," *Phys. Rev. Lett.* **105**, 038501.

Mendoza, C. & Mancho, A. M. [2012] "The Lagrangian description of ocean flows: A case study of the Kuroshio current," *Nonlin. Process. Geophys.* **19**, 449–472.

Mendoza, C., Mancho, A. M. & Wiggins, S. [2014] "Lagrangian descriptors and the assesment of the predictive capacity of oceanic data sets," *Nonlin. Process. Geophys.* **21**, 677–689.

Mezić, I. & Wiggins, S. [1994] "On the integrability and perturbation of three-dimensional fluid flows with symmetry," *J. Nonlin. Sci.* **4**, 157–194.

Mezić, I. & Wiggins, S. [1999] "A method for visualization of invariant sets of dynamical systems based on the ergodic partition," *Chaos* **9**, 213–218.

Moser, J. [1956] "The analytic invariants of an area-preserving mapping near a hyperbolic fixed point," *Commun. Pure Appl. Math.* **9**, 673–692.

Mullowney, P., Julien, K. & Meiss, J. [2005] "Blinking rolls: Chaotic advection in a three-dimensional flow with an invariant," *SIAM J. Appl. Dyn. Syst.* **4**, 159–186.

Peacock, T., Froyland, G. & Haller, G. [2015] "Objective detection of coherent structures," *Chaos* **25**, 087201.

Pouransari, Z., Speetjens, M. & Clercx, H. [2010] "Formation of coherent structures by fluid inertia in three-dimensional laminar flows," *J. Fluid Mech.* **654**, 5–34.

Rempel, E. L., Chian, A. C.-L., Brandenburg, A., Munuz, P. R. & Shadden, S. C. [2013] "Coherent structures and the saturation of a nonlinear dynamo," *J. Fluid Mech.* **729**, 309–329.

Ruiz-Herrera, A. [2015a] "Some examples related to the method of Lagrangian descriptors," *Chaos* **25**, 063112.

Ruiz-Herrera, A. [2015b] "Limitations of the method of Lagrangian descriptors in incompressible flows," available at http://arxiv.org/abs/1510.04838.

Ruiz-Herrera, A. [2016] "Performance of Lagrangian descriptors and their variants in incompressible flows," *Chaos* **26**, 103116.

Smith, L., Lester, D. & Metcalfe, G. [2012] "Chaotic advection in a three-dimensional volume preserving potential flow," *Proc. 18th AFMC*, http://www.afms.org.au/proceedings.html.

Smith, L., Rudman, M., Lester, D. & Metcalfe, G. [2014] "Coherent structures in a three-dimensional chaotic potential flow," *Proc. 19th AFMC*.

Smith, L. D., Rudman, M., Lester, D. R. & Metcalfe, G. [2016] "Bifurcations and degenerate periodic points in a 3D chaotic fluid flow," *Chaos* **26**, 053106.

Sotiropoulos, F., Ventikos, Y. & Lackey, T. C. [2001] "Chaotic advection in three-dimensional stationary vortex-breakdown bubbles: Šil'nikov's chaos and the devil's staircase," *J. Fluid Mech.* **444**, 257–297.

Sulman, M. H. M., Huntley, H. S., Lipphardt Jr., B. L. & Kirwan Jr., A. D. [2013] "Leaving flatland: Diagnostics for Lagrangian coherent structures in three-dimensional flows," *Physica D* **258**, 77–92.

Susuki, Y. & Mezić, I. [2009] "Ergodic partition of phase space in continuous dynamical systems," *Joint 48th IEEE Conf. Decision and Control and 28th Chinese Control Conf.*, pp. 7497–7502.

Truesdell, C. & Noll, W. [2004] *The Non-Linear Field Theories of Mechanics*, 3rd edition (Springer-Verlag, Berlin, Heidelberg, NY).

Wang, Y. [2015] "Identification and tracking of coherent Agulhas current rings," PhD thesis, University of Miami, http://scholarlyrepository.miami.edu/oa_dissertations/1528/.

Wiggins, S. [2010] "Coherent structures and chaotic advection in three dimensions," *J. Fluid Mech.* **654**, 1–4.

Wiggins, S. & Mancho, A. M. [2014] "Barriers to tranport in aperiodically time-dependent two dimensional velocity fields: Nekhoroshev's Theorem and 'Nearly Invariant' Tori," *Nonlin. Process. Geophys.* **21**, 165–185.

Xu, X. & Homsy, G. M. [2007] "Three-dimensional chaotic mixing inside drops driven by a transient electric field," *Phys. Fluids* **19**, 013102.

3.3. The Chaotic Saddle in the Lozi Map, Autonomous and Nonautonomous Versions

Coauthors: Francisco Balibrea-Iniesta, Stephen Wiggins, Ana M. Mancho

Abstract: In this paper, we prove the existence of a chaotic saddle for a piecewise-linear map of the plane, referred to as the Lozi map. We study the Lozi map in its orientation and area preserving version. First, we consider the autonomous version of the Lozi map to which we apply the Conley–Moser conditions to obtain the proof of a chaotic saddle. Then we generalize the Lozi map on a nonautonomous version and we prove that the first and the third Conley–Moser conditions are satisfied, which imply the existence of a chaotic saddle. Finally, we numerically demonstrate how the structure of this nonautonomous chaotic saddle varies as parameters are varied.

Reference: C. Lopesino, F. Balibrea-Iniesta, S. Wiggins, A. M. Mancho. The Chaotic Saddle in the Lozi Map, Autonomous and Nonautonomous Versions. International Journal of Bifurcation and Chaos **25** (2015) 1550184-1-18.

International Journal of Bifurcation and Chaos, Vol. 25, No. 13 (2015) 1550184 (18 pages)

DOI: 10.1142/S0218127415501849

The Chaotic Saddle in the Lozi Map, Autonomous and Nonautonomous Versions

Carlos Lopesino* and Francisco Balibrea-Iniesta†
Instituto de Ciencias Matemáticas,
CSIC-UAM-UC3M-UCM, C/Nicolás Cabrera 15,
Campus Cantoblanco UAM, 28049 Madrid, Spain
**carlos.lopesino@icmat.es*
†*francisco.balibrea@icmat.es*

Stephen Wiggins
School of Mathematics, University of Bristol,
BS8 1TW Bristol, UK
maxsw@bristol.ac.uk

Ana M. Mancho
Instituto de Ciencias Matemáticas,
CSIC-UAM-UC3M-UCM, C/Nicolás Cabrera 15,
Campus Cantoblanco UAM, 28049 Madrid, Spain
a.m.mancho@icmat.es

Received June 24, 2015

In this paper, we prove the existence of a chaotic saddle for a piecewise-linear map of the plane, referred to as the Lozi map. We study the Lozi map in its orientation and area preserving version. First, we consider the autonomous version of the Lozi map to which we apply the Conley–Moser conditions to obtain the proof of a chaotic saddle. Then we generalize the Lozi map on a nonautonomous version and we prove that the first and the third Conley–Moser conditions are satisfied, which imply the existence of a chaotic saddle. Finally, we numerically demonstrate how the structure of this nonautonomous chaotic saddle varies as parameters are varied.

Keywords: Chaotic saddle; autonomous dynamics; nonautonomous dynamics; Lozi map; Conley–Moser conditions.

1. Introduction

In this paper, we prove that the Lozi map [Lozi, 1978], as well as a nonautonomous generalization of the Lozi map, possesses a chaotic saddle, i.e. a hyperbolic invariant set on which the dynamics is topologically conjugate to a Bernoulli shift. Our construction uses the Conley–Moser conditions for autonomous maps as developed in [Moser, 1973] (see also [Wiggins, 2003]) and the nonautonomous Conley–Moser conditions as developed in [Wiggins, 1999] and [Balibrea-Iniesta *et al.*, 2015]. For earlier work in a similar spirit as the Conley–Moser conditions see [Alekseev, 1968a, 1968b, 1969].

Previously, the autonomous Conley–Moser conditions have been used by [Devaney & Nitecki, 1979] to show the existence of a chaotic invariant set for the Hénon map and by [Holmes, 1982] and [Chastaing *et al.*, 2015] to show the existence of a chaotic invariant set for the bouncing ball map.

While the development of the "dynamical systems approach to nonautonomous dynamics" is currently a topic of much interest in the pure

mathematics community, it is not a topic that is widely known in the applied dynamical systems community (especially the fundamental work that was done in the 1960's). An applied motivation for such work is an understanding from the dynamical systems point of view of fluid transport for aperiodically time dependent flows. Wiggins and Mancho [2014] completed a survey of the history of nonautonomous dynamics as well as its application to fluid transport. Earlier work on chaos in nonautonomous systems is described in [Lerman & Silnikov, 1992; Stoffer, 1988a, 1988b].

This paper is outlined as follows. In Sec. 2, we introduce the setup of the problem. The definitions and theorems given in this section make clear what we mean by the phrase chaotic invariant set for both autonomous and nonautonomous maps. In Secs. 3 and 4, we construct chaotic invariant sets (i.e. *chaotic saddles*) for both the autonomous and nonautonomous versions of the Lozi map, respectively. In Sec. 5, we show how these sets are detected using the Discrete Lagrangian Descriptor (see [Lopesino *et al.*, 2015]) for different parameter values, both in the autonomous and in the nonautonomous case. Finally, in Sec. 6 we summarize our results.

2. Setup and Geometry of the Problem

In this section, we recall the set-up for the autonomous Conley–Moser conditions that were introduced by [Moser, 1973] and the nonautonomous Conley–Moser conditions introduced in [Wiggins, 1999]. We follow the structure in [Wiggins, 2003] for our exposition, but with an inverse notation (that is, $f \equiv L^{-1}$ in the autonomous case and $f_n \equiv L_n^{-1}$ in the nonautonomous case, where we use the notation L in the autonomous case and L_n^{-1} in the nonautonomous case to denote the general form for the maps under consideration, rather than f and f_n, respectively, from the original references, since L is traditionally used to refer to the Lozi map).

2.1. *The autonomous Conley–Moser conditions*

We begin with the following two definitions.

Definition 2.1. A μ_v-vertical curve is the graph of a function $x = v(y)$ for which

$$-R \leq v(y) \leq R,$$
$$|v(y_1) - v(y_2)| \leq \mu_v |y_1 - y_2| \quad \text{for } -R \leq y_1,\ y_2 \leq R.$$

Similarly, a μ_h-horizontal curve is the graph of a function $y = h(x)$ for which

$$-R \leq h(x) \leq R,$$
$$|h(x_1) - h(x_2)| \leq \mu_h |x_1 - x_2| \quad \text{for } -R \leq x_1,\ x_2 \leq R.$$

Definition 2.2. Given two nonintersecting μ_v-vertical curves $v_1(y) < v_2(y)$, $y \in [-R, R]$, we define a μ_v-vertical strip as

$$V = \{(x, y) \in \mathbb{R}^2 \,|\, x \in [v_1(y), v_2(y)]; y \in [-R, R]\}.$$

Similarly, given two nonintersecting μ_h-horizontal curves $h_1(x) < h_2(x)$, $x \in [-R, R]$, we define a μ_h-horizontal strip as

$$H = \{(x, y) \in \mathbb{R}^2 \,|\, y \in [h_1(x), h_2(x)]; x \in [-R, R]\}.$$

The width of horizontal and vertical strips is defined as

$$d(H) = \max_{x \in [-R,R]} |h_2(x) - h_1(x)|,$$
$$d(V) = \max_{y \in [-R,R]} |v_2(y) - v_1(y)|.$$

Keeping these definitions in mind, we begin with the Conley–Moser conditions for the autonomous case. We consider a map

$$L : D \to \mathbb{R}^2,$$

where D is a square in $\mathbb{R}^2$, i.e.

$$D = \{(x, y) \in \mathbb{R}^2 \,|\, -R \leq x \leq R, -R \leq y \leq R\}.$$

Let

$$I = \{1, 2, \ldots, N\}, \quad (N \geq 2),$$

be an index set, and let

$$H_i, \quad i \in I$$

be a set of disjoint μ_h-horizontal strips and let

$$V_i, \quad i \in I$$

be a set of disjoint μ_v-vertical strips. Suppose that L satisfies the following two conditions.

Assumption 1. $0 \leq \mu_v, \mu_h < 1$ and L maps V_i homeomorphically onto H_i, $(L(V_i) = H_i)$ for $i \in I$. Moreover, the horizontal boundaries of V_i map to the horizontal boundaries of H_i and the vertical boundaries of V_i map to the vertical boundaries of H_i.

Assumption 2. Suppose H is a μ_h-horizontal strip contained in $\bigcup_{i\in I} H_i$. Then

$$L(H) \cup H_i \equiv \tilde{H}_i$$

is a μ_h-horizontal strip for every $i \in I$. Moreover,

$$d(\tilde{H}_i) \leq \nu_h d(H) \quad \text{for some } 0 < \nu_h < 1.$$

Similarly, suppose V is a μ_v-vertical strip contained in $\bigcup_{i\in I} V_i$. Then

$$L^{-1}(V) \cap V_i \equiv \tilde{V}_i$$

is a μ_v-vertical strip for every $i \in I$. Moreover,

$$d(\tilde{V}_i) \leq \nu_v d(V) \quad \text{for some } 0 < \nu_v < 1.$$

Then we have the following theorem.

Theorem 1. *Suppose L satisfies Assumptions 1 and 2. Then L has an invariant Cantor set, Λ, on which it is topologically conjugate to a full shift on N symbols, i.e. the following diagram commutes*

$$\begin{array}{ccc} \Lambda & \xrightarrow{L} & \Lambda \\ {\scriptstyle\phi}\downarrow & & \downarrow{\scriptstyle\phi} \\ \Sigma^N & \xrightarrow{\sigma} & \Sigma^N \end{array} \tag{1}$$

where ϕ is a homeomorphism mapping Λ onto Σ^N and σ denotes the shift map acting on a space of bi-infinite sequence of N symbols, denoted by Σ^N.

More details on the map σ and the space Σ^N can be found in [Wiggins, 2003], as well as in comments following (10).

2.2. *The nonautonomous Conley–Moser conditions*

Next, we describe the setting for the nonautonomous Conley–Moser conditions. These conditions were generalized by [Wiggins, 1999] but we are using the notation used in [Balibrea-Iniesta *et al.*, 2015], where a more detailed discussion of the definitions is given.

Definition 2.3. Let $D \subset \mathbb{R}^2$ denote a closed and bounded set. We define its projections as

$$D_x = \{x \in \mathbb{R} \text{ for which there exists a } y \in \mathbb{R} \text{ with } (x, y) \in D\}$$

$$D_y = \{y \in \mathbb{R} \text{ for which there exists a } x \in \mathbb{R} \text{ with } (x, y) \in D\}.$$

D_x and D_y represent the projections of D onto the x-axis and the y-axis, respectively. Let I_x be a closed interval contained in D_x and let I_y be a closed interval contained in D_y.

Definition 2.4. Let $0 \leq \mu_h < \infty$. A μ_h-horizontal curve, $\overline{H}$, is defined to be the graph of a function $h : I_x \to \mathbb{R}$ where h satisfies the following two conditions:

(1) The set $\overline{H} = \{(x, h(x)) \in \mathbb{R} \times \mathbb{R}$ such that $x \in I_x\}$ is contained in D.
(2) For every x_1, $x_2 \in I_x$, we have

$$|h(x_1) - h(x_2)| \leq \mu_h |x_1 - x_2|. \tag{2}$$

Similarly, let $0 \leq \mu_v < \infty$. A μ_v-vertical curve, $\overline{V}$, is defined to be the graph of a function $v : I_y \to \mathbb{R}$ where v satisfies the following two conditions:

(1) The set $\overline{V} = \{(v(y), y) \in \mathbb{R} \times \mathbb{R}$ such that $y \in I_y\}$ is contained in D.
(2) For every y_1, $y_2 \in I_y$, we have

$$|v(y_1) - v(y_2)| \leq \mu_v |y_1 - y_2|. \tag{3}$$

Now we can define two-dimensional strips by using these horizontal and vertical curves.

Definition 2.5. Given two nonintersecting μ_v-vertical curves $v_1(y) < v_2(y)$, $y \in I_y$, we define a μ_v vertical strip as

$$V = \{(x, y) \in \mathbb{R}^2 \text{ such that } x \in [v_1(y), v_2(y)]; y \in I_y\}.$$

Similarly, given two nonintersecting μ_h-horizontal curves $h_1(x) < h_2(x)$, $x \in I_x$, we define a μ_h horizontal strip as

$$H = \{(x, y) \in \mathbb{R}^2 \text{ such that } y \in [h_1(x), h_2(x)]; x \in I_x\}.$$

The width of horizontal and vertical strips is defined as

$$d(H) = \max_{x\in I_x} |h_2(x) - h_1(x)|,$$

$$d(V) = \max_{y\in I_y} |v_2(y) - v_1(y)|.$$

Additionally, we define horizontal and vertical boundaries of the strips.

Definition 2.6. The vertical boundary[1] of a μ_h-horizontal strip H is denoted $\partial_v H$ and is defined

[1]The symbol ∂ is the usual notation from topology denoting the boundary of a set. In this paper, we further refine this notion by referring to horizontal boundaries, ∂_h, and vertical boundaries, ∂_v.

as

$$\partial_v H = \{(x,y) \in H \text{ such that } x \in \partial I_x\}.$$

The horizontal boundary of a μ_h-horizontal strip H is denoted $\partial_h H$ and is defined as

$$\partial_h H \equiv \partial H - \partial_v H.$$

We can similarly find the boundaries of μ_v-vertical strips.

Now we need to define another kind of strip which will appear for the nonautonomous Conley–Moser conditions.

Definition 2.7. We say that H is a μ_h-horizontal strip contained in a μ_v-vertical strip V if the two μ_h-horizontal curves defining the vertical boundary of H are contained in V, with the remaining boundary components of H contained in $\partial_v V$.

The two μ_h-horizontal curves defining the horizontal boundary of H are referred to as the horizontal boundary of H, and the remaining boundary components are referred to as the vertical boundary of H. This is described in detail in the next definition.

Definition 2.8. Let $\tilde{H}$ be a μ_h-horizontal strip contained in a μ_v-vertical strip, V. We define the boundaries of $\tilde{H}$ as

$$\begin{aligned}\partial_v \tilde{H} &= \{(x,y) \in \partial \tilde{H} \text{ such that } (x,y) \in \partial_v H\} \\ &= \partial \tilde{H} \cap \partial_v H\end{aligned}$$

and

$$\partial_h \tilde{H} = \partial \tilde{H} - \partial_v \tilde{H}.$$

The boundaries of $\tilde{V}\mu_v$-vertical strip contained in $H\mu_h$-horizontal strip are defined analogously.

We will be interested in the behavior of μ_v-vertical strips under maps. We want to focus on the case when the image of a μ_v-vertical strip intersects its preimage.

Definition 2.9. Let V and $\tilde{V}$ be μ_v-vertical strips. $\tilde{V}$ is said to intersect V fully if $\tilde{V} \subset V$ and $\partial_h \tilde{V} \subset \partial_h V$.

Now we can state the main theorem for the nonautonomous case. Let $\{L_n, D_n\}_{n=-\infty}^{+\infty}$ be a sequence of maps with

$$\begin{aligned}&L_n : D_n \to D_{n+1}, \quad \forall\, n \in \mathbb{Z} \quad \text{and} \\ &L_n^{-1} : D_{n+1} \to D_n\end{aligned} \tag{4}$$

in case the corresponding inverse function exists.

We require that on each domain D_n there exists a finite collection of vertical strips $V_i^n \subset D_n$ ($\forall\, n \in \mathbb{Z}$ and $\forall\, i \in I = \{1, 2, \ldots, N\}$) which map into a finite collection of horizontal strips located in D_{n+1}:

$$H_i^{n+1} \subset D_{n+1} \quad \text{with } L_n(V_i^n) = H_i^{n+1}, \quad \forall\, n \in \mathbb{Z},\ \ i \in I. \tag{5}$$

We also need to define

$$\begin{aligned}H_{ij}^{n+1} &\equiv H_i^{n+1} \cap V_j^{n+1} \\ V_{ji}^n &\equiv L_n^{-1}(V_j^{n+1}) \cap V_i^n.\end{aligned} \tag{6}$$

Following this idea we introduce the definition of transition matrix associated to a sequence of maps $\{L_n, D_n\}_{n=-\infty}^{+\infty}$,

$A \equiv \{A^n\}_{n=-\infty}^{+\infty}$ is a sequence of matrices of dimension $N \times N$ such that

$$A_{ij}^n = \begin{cases} 1 & \text{if } L_n(V_i^n) \cap V_j^{n+1} \neq \emptyset \\ 0 & \text{otherwise} \end{cases} \quad \text{or equivalently}$$

$$A_{ij}^n = \begin{cases} 1 & \text{if } H_i^{n+1} \cap V_j^{n+1} = H_{ij}^{n+1} \neq \emptyset \\ 0 & \text{otherwise} \end{cases} \quad \forall\, i,j \in I \tag{7}$$

which will be needed for applying the Conley–Moser conditions to a given sequence of maps $\{L_n, D_n\}_{n=-\infty}^{+\infty}$ and then proving the existence of a chaotic invariant set.

Assumption 1. For all $i, j \in I$ such that $A_{ij}^n = 1$, H_{ij}^{n+1} is a μ_h-horizontal strip contained in V_j^{n+1} with $0 \leq \mu_v \mu_h < 1$. Moreover, L_n maps V_{ji}^n homeomorphically onto H_{ij}^{n+1} with $L_n^{-1}(\partial_h H_{ij}^{n+1}) \subset \partial_h V_i^n$.

Remark 2.1. The fact that every nonempty $H_{ij}^{n+1} \subset D_{n+1}$ is a μ_h-horizontal strip contained in V_j^{n+1} shows that the two μ_h-horizontal curves which form the boundary ($\partial_h L_n(V_i^n) = \partial_h H_i^{n+1}$) cut the horizontal boundary of V_i^{n+1} in exactly four points.

Furthermore, since L_n is one-to-one on $D_V^n \equiv \bigcup_{i=1}^N V_i^n$ then we can define an inverse function L_n^{-1} on $L_n(D_V^n) = \bigcup_{i=1}^N L_n(V_i^n) \equiv \bigcup_{i=1}^N H_i^{n+1}$.

And since L_n maps V_{ji}^n homeomorphically onto H_{ij}^{n+1} with $L_n^{-1}(\partial_h H_{ij}^{n+1}) \subset \partial_h V_i^n$ then L_n^{-1} maps H_{ij}^{n+1} homeomorphically onto V_{ji}^n ($\forall\, i,j \in I$) with

$$L_n(L_n^{-1}(\partial_h H_{ij}^{n+1})) = \partial_h H_{ij}^{n+1} \subset L_n(\partial_h V_i^n). \tag{8}$$

Assumption 2. Let V^{n+1} be a μ_v-vertical strip which intersects V_j^{n+1} fully. Then $L_n^{-1}(V^{n+1}) \cap V_i^n \equiv \tilde{V}_i^n$ is a μ_v-vertical strip intersecting V_i^n fully for all $i \in I$ such that $A_{ij}^n = 1$. Moreover,

$$d(\tilde{V}_i^n) \leq \nu_v d(V^{n+1}) \quad \text{for some } 0 < \nu_v < 1. \tag{9}$$

Similarly, let H^n be a μ_h-horizontal strip contained in V_i^n such that also $H^n \subset H_{ji}^n$ for some $i, j \in I$ with $A_{ji}^{n-1} = 1$. Then $L_n(H^n) \cap V_k^{n+1} \equiv \tilde{H}_k^{n+1}$ is a μ_h-horizontal strip contained in V_k^{n+1} for all $k \in I$ such that $A_{ik}^n = 1$. Moreover,

$$d(\tilde{H}_k^{n+1}) \leq \nu_h d(H^n) \quad \text{for some } 0 < \nu_h < 1. \tag{10}$$

We also need to adapt some definitions from symbolic dynamics. Let

$$s = (\cdots s_{n-k} \cdots s_{n-2} s_{n-1} \cdot s_n s_{n+1} \cdots s_{n+k} \cdots) \tag{11}$$

denote a bi-infinite sequence with $s_l \in I$ $(\forall\, l \in \mathbb{Z})$ where adjacent elements of the sequence satisfy the rule $A_{s_n s_{n+1}}^n = 1$, $\forall\, n \in \mathbb{Z}$.

We denote the set of all such symbol sequences by $\Sigma_{\{A^n\}}^N$. If σ denotes the shift map

$$\begin{aligned} \sigma(s) &= \sigma(\cdots s_{n-2} s_{n-1} \cdot s_n s_{n+1} \cdots) \\ &= (\cdots s_{n-2} s_{n-1} s_n \cdot s_{n+1} \cdots) \end{aligned} \tag{12}$$

on $\Sigma_{\{A^n\}}^N$, we define the "extended shift map" $\tilde{\sigma}$ on $\tilde{\Sigma} \equiv \Sigma_{\{A^n\}}^N \times \mathbb{Z}$ by

$$\tilde{\sigma}(s, n) = (\sigma(s), n + 1). \tag{13}$$

It is also defined as

$$f(x, y; n) = (L_n(x, y), n + 1).$$

We now can state the main theorem.

Theorem 2. *Suppose $\{L_n, D_n\}_{n=-\infty}^{+\infty}$ satisfies A1 and A2. There exists a sequence of sets $\Lambda_n \subset D_n$, with $L_n(\Lambda_n) = \Lambda_{n+1}$, such that the following diagram commutes*

$$\begin{array}{ccc} \Lambda_n \times \mathbb{Z} & \xrightarrow{\;f\;} & \Lambda_{n+1} \times \mathbb{Z} \\ {\scriptstyle\phi}\downarrow & & \downarrow{\scriptstyle\phi} \\ \Sigma_{\{A^n\}}^N \times \mathbb{Z} & \xrightarrow{\;\tilde{\sigma}\;} & \Sigma_{\{A^n\}}^N \times \mathbb{Z} \end{array} \tag{14}$$

where $\phi(x, y; n) \equiv (\phi_n(x, y), n)$ with $\phi_n(x, y)$ is a homeomorphism mapping Λ_n onto $\Sigma_{\{A^n\}}^N$.

Remark 2.2. We are referring to $\{\Lambda_n\}$ as an infinite sequence of chaotic invariant sets. Defining

$$\Lambda \equiv \bigcup_{n \in \mathbb{Z}} \Lambda_n,$$

then Λ contains an uncountable infinity of orbits where each orbit is unstable (of saddle type), and the dynamics on the invariant set exhibits sensitive dependence on initial conditions.

As we will see, it can be difficult to verify Assumption 2 in specific examples. For that reason we will define the third condition known as the "cone condition". Before stating this condition, we define the following

$$\mathcal{V}^n = \bigcup_{i,j \in I} V_{ij}^n \equiv \bigcup_{i,j \in I} V_i^n \cap L_n^{-1}(V_j^{n+1}), \tag{15}$$

$$\begin{aligned} \mathcal{H}^{n+1} &= \bigcup_{i,j \in I} H_{ji}^{n+1} \\ &\equiv \bigcup_{i,j \in I} V_j^{n+1} \cap L_n(V_i^n), \quad L_n(\mathcal{V}^n) = \mathcal{H}^{n+1} \end{aligned} \tag{16}$$

$$S_{\mathcal{K}}^s = \{(\xi_z, \eta_z) \in \mathbb{R}^2 \,|\, |\eta_z| \leq \mu_v |\xi_z|, z \in \mathcal{K}\} \tag{17}$$

$$S_{\mathcal{K}}^u = \{(\xi_z, \eta_z) \in \mathbb{R}^2 \,|\, |\xi_z| \leq \mu_h |\eta_z|, z \in \mathcal{K}\}, \tag{18}$$

with $\mathcal{K}$ being either $\mathcal{V}^n$ or $\mathcal{H}^{n+1}$.

Now we can state Assumption 3.

Assumption 3. The cone condition. $Df_n(S_{\mathcal{V}^n}^u) \subset S_{\mathcal{H}^{n+1}}^u$, $Df_n^{-1}(S_{\mathcal{H}^{n+1}}^s) \subset S_{\mathcal{V}^n}^s$.

Moreover, if $(\xi_{L_n(z_0^n)}, \eta_{L_n(z_0^n)}) \equiv DL_n(z_0^n) \cdot (\xi_{z_0^n}, \eta_{z_0^n}) \in S_{\mathcal{H}^{n+1}}^u$ then

$$|\eta_{L_n(z_0^n)}| \geq \left(\frac{1}{\mu}\right) |\eta_{z_0^n}|. \tag{19}$$

If $(\xi_{L_n^{-1}(z_0^{n+1})}, \eta_{L_n^{-1}(z_0^{n+1})}) \equiv DL_n^{-1}(z_0^{n+1}) \cdot (\xi_{z_0^{n+1}}, \eta_{z_0^{n+1}}) \in S_{\mathcal{V}^n}^s$ then

$$|\xi_{L_n^{-1}(z_0^{n+1})}| \geq \left(\frac{1}{\mu}\right) |\xi_{z_0^{n+1}}| \quad \text{for } \mu > 0. \tag{20}$$

We have the following theorem.

Theorem 3. *If nonautonomous A1 and A3 are satisfied for $0 < \mu < 1 - \mu_h \mu_v$ then A2 is satisfied and so Theorem 2 holds.*

Proof. The proof can be found in [Balibrea-Iniesta *et al.*, 2015]. ■

3. The Autonomous Lozi Map

In this section, we show that Assumptions 1 and 2 of the Conley–Moser conditions hold for the autonomous Lozi map. Typically, it has been difficult to show that Assumption 2 holds for specific maps. However, the relatively simple form of the Lozi map allows us to demonstrate Assumption 2 explicitly.

The (autonomous) Lozi map is defined as $L(x, y) = (1 + y - a|x|, bx)$, where $a, b \in \mathbb{R}$:

$$L(x, y) = (1 + y - a|x|, -x). \tag{21}$$

This map is invertible with inverse

$$L^{-1}(x, y) = (-y, x + a|y| - 1). \tag{22}$$

For our purposes we will consider the situation where the Lozi map is orientation and area preserving, which occurs when $b = -1$. Henceforth, b will be fixed at this value and we will view a as a parameter.

The setup for the autonomous problem is as follows. We consider the map

$$L : S \mapsto \mathbb{R}^2,$$

where the square $S = \{(x, y) \in \mathbb{R}^2 : |x| \leq R, |y| \leq R\}$ and the boundaries of the square are

$$L_1 = \{(x, y) \in \mathbb{R}^2 \,|\, y = R\},$$
$$L_2 = \{(x, y) \in \mathbb{R}^2 \,|\, y = -R\},$$
$$L_3 = \{(x, y) \in \mathbb{R}^2 \,|\, x = R\},$$
$$L_4 = \{(x, y) \in \mathbb{R}^2 \,|\, x = -R\}.$$

Furthermore, we need to define the subsets of the boundaries of the square S as follows:

$$L_1^+ = \{(x, y) \in \mathbb{R}^2 \,|\, x \geq 0, y = R\},$$
$$L_1^- = \{(x, y) \in \mathbb{R}^2 \,|\, x < 0, y = R\},$$
$$L_2^+ = \{(x, y) \in \mathbb{R}^2 \,|\, x \geq 0, y = -R\},$$
$$L_2^- = \{(x, y) \in \mathbb{R}^2 \,|\, x < 0, y = -R\},$$
$$L_3^+ = \{(x, y) \in \mathbb{R}^2 \,|\, x = R, y \geq 0\},$$
$$L_3^- = \{(x, y) \in \mathbb{R}^2 \,|\, x = R, y < 0\},$$

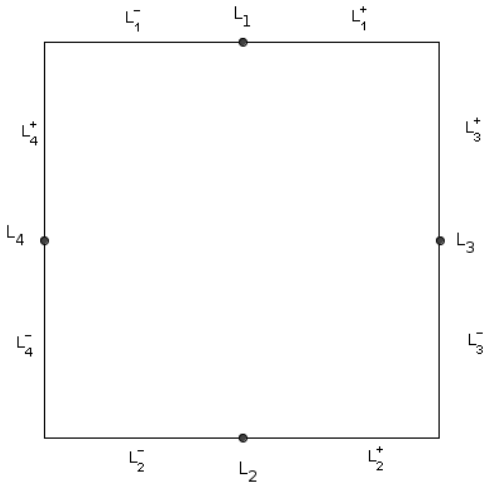

Fig. 1. Geometrical setting: Boundaries and subsets of the boundaries of the square S.

$$L_4^+ = \{(x, y) \in \mathbb{R}^2 \,|\, x = -R, y \geq 0\},$$
$$L_4^- = \{(x, y) \in \mathbb{R}^2 \,|\, x = -R, y < 0\},$$

as shown in Fig. 1.

At this moment, we can state the main result of this section; the existence of the chaotic saddle for the Lozi autonomous map.

Theorem 4. *For $a > 4$, Assumptions 1 and 2 hold for the autonomous Lozi map, and therefore, it possesses a chaotic saddle inside the square S.*

The proof of this theorem is carried out in the following subsections.

3.1. *Verification of Assumption 1 of the autonomous Conley–Moser conditions*

In this section, we will show how the map L acts on the square S. In order to do that, we want to see how the boundaries of the square S are transformed. This action can be seen in Fig. 2.

First, we begin with the map L acting on the upper boundary, L_1,[2]

$$L(L_1) = L(x, R) = (1 + R - a|x|, -x)$$

[2]For notational convenience henceforth we will denote the image of a point (x, y) under L by (X, Y).

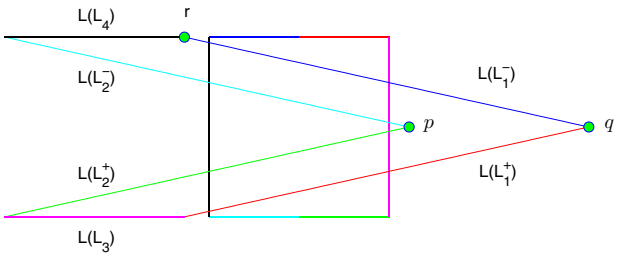

Fig. 2. L mapping S.

$$\begin{cases} X = 1 + R - a|x| \\ Y = -x \end{cases}$$

$$|y| = \frac{1 + R - x}{a}$$

$$\Rightarrow \begin{cases} y = \dfrac{1+R}{a} - \dfrac{x}{a}, & x < 0 \ \ (L_1^-) \\ y = \dfrac{x}{a} - \dfrac{1+R}{a}, & x \geq 0 \ \ (L_1^+). \end{cases} \tag{23}$$

We do the same but for the lower boundary, L_2,

$$L(L_2) = L(x, -R) = (1 - R - a|x|, -x)$$

$$\begin{cases} X = 1 - R - a|x| \\ Y = -x \end{cases}$$

$$|y| = \frac{1 - R - x}{a}$$

$$\Rightarrow \begin{cases} y = \dfrac{1-R}{a} - \dfrac{x}{a}, & x < 0 \ \ (L_2^-) \\ y = \dfrac{x}{a} - \dfrac{1-R}{a}, & x \geq 0 \ \ (L_2^+). \end{cases} \tag{24}$$

Now we see the map L acting on the right side, L_3,

$$L(L_3) = L(R, y) = (1 + y - aR, -R)$$

$$\begin{cases} X = 1 + y - aR \\ Y = -R \end{cases} \tag{25}$$

and the left side, L_4,

$$L(L_4) = L(-R, y) = (1 + y - aR, R)$$

$$\begin{cases} X = 1 + y - aR \\ Y = R. \end{cases} \tag{26}$$

From these computations we can set that the horizontal boundaries L_1 and L_2 are mapped by L to affine lines with slopes $|m| = 1/a$ passing through the points $q = (1 + R, 0)$ and $p = (1 - R, 0)$ respectively that must be outside the domain S as we will see later. Moreover, vertical lines are mapped to horizontal lines. From Fig. 2, we can observe how the strips are formed. In this case, the set $L(S) \cap S$ is the union of the two horizontal strips H_1 and H_2.

On the other hand, we want to show L^{-1} acting on S, as is shown in Fig. 3. As we did before, we start with L^{-1} acting on the upper side L_1.

$$L^{-1}(L_1) = L^{-1}(x, R) = (-R, x + aR - 1)$$

$$\begin{cases} X = -R \\ Y = x + aR - 1 \end{cases} \tag{27}$$

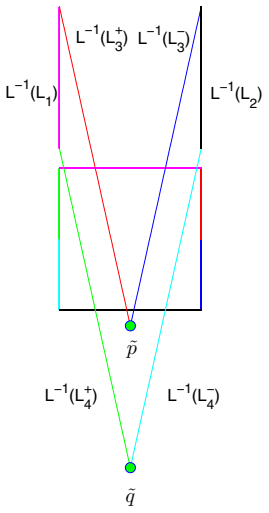

Fig. 3. L^{-1} mapping S.

and L^{-1} acting on the lower side, L_2,

$$L^{-1}(L_2) = L^{-1}(x, -R) = (R, x + aR - 1)$$
$$\begin{cases} X = R \\ Y = x + aR - 1. \end{cases} \tag{28}$$

Now we focus on L^{-1} acting on the right side, L_3,

$$L^{-1}(L_3) = L^{-1}(R, y) = (-y, R + a|y| - 1)$$
$$\begin{cases} X = -y \\ Y = R + a|y| - 1 \end{cases}$$
$$y = R + a|x| - 1$$
$$\Rightarrow \begin{cases} y = R + ax - 1, & y < 0 \ \ (L_3^-) \\ y = R - ax - 1, & y \geq 0 \ \ (L_3^+) \end{cases} \tag{29}$$

and L^{-1} acting on the left side, L_4,

$$L^{-1}(L_4) = L^{-1}(-R, y) = (-y, -R + a|y| - 1)$$
$$\begin{cases} X = -y \\ Y = -R + a|y| - 1 \end{cases}$$
$$y = a|x| - (1 + R)$$
$$\Rightarrow \begin{cases} y = ax - (1 + R), & y < 0 \ \ (L_4^-) \\ y = -ax - (1 + R), & y \geq 0 \ \ (L_4^+). \end{cases} \tag{30}$$

From this we can observe that the vertical boundaries L_3 and L_4 are mapped by L^{-1} to affine lines with slopes $|m| = a$ passing through the points $\tilde{p} = (0, R - 1)$ and $\tilde{q} = (0, -(1 + R))$ respectively, which are outside the square, and horizontal lines are mapped to vertical lines. As we show in Fig. 3, the union of the vertical strips V_1 and V_2 is the set $L^{-1}(S) \cap S$.

Now that we know how the square S is mapped under L and L^{-1} we have to set some conditions on the size of S, that is the value R. We have to keep in mind two conditions.

The first one is that we need the two horizontal strips and the two vertical strips to cross each other. (We illustrate this idea in Fig. 2.) For that reason, we need the point p to have first coordinate greater than R and the point $\tilde{p}$ to have second coordinate lower than $-R$. Because of the symmetry of the problem, we reflect only on the condition for p

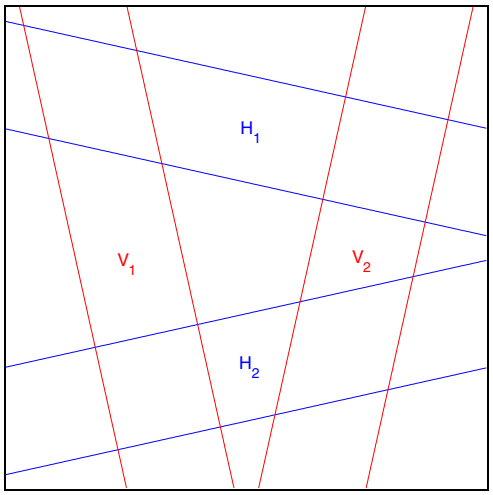

Fig. 4. Vertical and horizontal strips. $H_1 \cup H_2 := L(S) \cap S$ and $V_1 \cup V_2 := L^{-1}(S) \cap S$.

in the next inequality

$$1 - R \geq R \Leftrightarrow \frac{1}{2} \geq R. \tag{31}$$

On the other hand, the second issue is that we need the area of intersection between the strips, represented for instance in Fig. 4, to be inside the domain S. This is achieved when the point $r = L(L_1^-) \cap \{y = R\}$ has first coordinate lower than $-R$, as we can see in Fig. 2.

$$\begin{aligned} r &= L(L_1^-) \cap \{y = R\} \\ &= (1 + R - a|x|, -x)|_{-x=R} \\ &= (1 + R - aR, R). \end{aligned} \tag{32}$$

So this last assumption is translated into

$$1 + R - aR < -R \tag{33}$$

and this holds when

$$R \geq \frac{1}{a - 2}. \tag{34}$$

Combining these two conditions we have,

$$\frac{1}{a - 2} \leq R \leq \frac{1}{2}. \tag{35}$$

This last inequality only makes sense when $a \geq 4$.

Once we have set these conditions, we can take

$$R(a) = \frac{1}{2}\left(\frac{1}{a-2} + \frac{1}{2}\right) = \frac{a}{4(a-2)}, \quad \text{for every } a \geq 4, \tag{36}$$

which is the midpoint of the interval

$$\left[\frac{1}{a-2}, \quad \frac{1}{2}\right].$$

Now we start proving the first assumption, A1, for the autonomous Conley–Moser conditions. For this purpose, we need to define the vertical (V_1 and V_2) and the horizontal (H_1 and H_2) strips. To obtain the horizontal strips we will map forward by L the square S and make the intersection with the same square. To get the vertical strips we will map backward by L^{-1} the square S and intersect it with S, that is

$$\begin{aligned} H_1 \cup H_2 &:= L(S) \cap S \\ V_1 \cup V_2 &:= L^{-1}(S) \cap S \end{aligned} \tag{37}$$

where H_1 is the upper half part of $L(S) \cap S$ and H_2 is the lower half part of $L(S) \cap S$, V_1 is the left half part of $L^{-1}(S) \cap S$ and V_2 is the right half part of $L^{-1}(S) \cap S$. We will use the following notation

$$\begin{aligned} H_1 &:= (L(S) \cap S)^+, && \text{where } y > 0, \\ H_2 &:= (L(S) \cap S)^-, && \text{where } y < 0, \\ V_1 &:= (L^{-1}(S) \cap S)^-, && \text{where } x < 0, \\ V_2 &:= (L^{-1}(S) \cap S)^+, && \text{where } x > 0. \end{aligned} \tag{38}$$

These strips can be seen in Fig. 4.

It is easy to see from expressions in (38) that L maps V_i homeomorphically onto H_i, $(L(V_i) = H_i)$ for $i = 1, 2$. Furthermore, the horizontal boundaries of V_i map to the horizontal boundaries of H_i and the vertical boundaries of V_i map to the vertical boundaries of H_i. Moreover, V_i are μ_v-vertical strips because its vertical boundaries are μ_v-vertical curves where $|\mu_v| = 1/a$. And H_i are μ_h-horizontal strips because its horizontal boundaries are μ_h-horizontal curves where $|\mu_h| = 1/a$.

Remark 3.1. We have to take care around $|\mu_v| = 1/a$. The slope of the vertical lines is a but seen as horizontal curves. We must see this slope rate as if the vertical lines were μ_v-vertical curves and so $|\mu_v| = 1/a$.

We have to keep in mind that the product of the slopes of the strips has to be less than 1 as it is required in the Conley–Moser conditions. In our case $|\mu_h| = |\mu_v| = 1/a$. Therefore

$$|\mu_h \cdot \mu_v| = \left|\frac{1}{a} \cdot \frac{1}{a}\right| = \frac{1}{a^2} \tag{39}$$

and the condition of the slopes of A_1 is satisfied.

3.2. *Verification of Assumption 2 of the autonomous Conley–Moser conditions*

The second assumption describes how the map L bends and makes thinner strips on each iteration. Moreover, we obtain this rate which in our assumption is called ν_v. Lets take V — a μ_v-vertical strip contained, for instance, in V_2 ($V \subset V_2$). As we can see in Fig. 5, we name the vertices of V_2 as $v_1 = (v_{1_x}, R)$, $v_2 = (v_{2_x}, R)$, $v_3 = (v_{3_x}, -R)$ and $v_4 = (v_{4_x}, -R)$ and the vertices which delimit V are $q_1 = (q_{1_x}, R)$, $q_2 = (q_{2_x}, R)$, $q_3 = (q_{3_x}, -R)$ and $q_4 = (q_{4_x}, -R)$. We assume that

$$\begin{aligned} v_{1_x} < q_{1_x} < q_{2_x} < v_{2_x} \\ v_{3_x} < q_{3_x} < q_{4_x} < v_{4_x} \end{aligned} \tag{40}$$

and

$$d(V) = |q_{2_x} - q_{1_x}| = |q_{4_x} - q_{3_x}|.$$

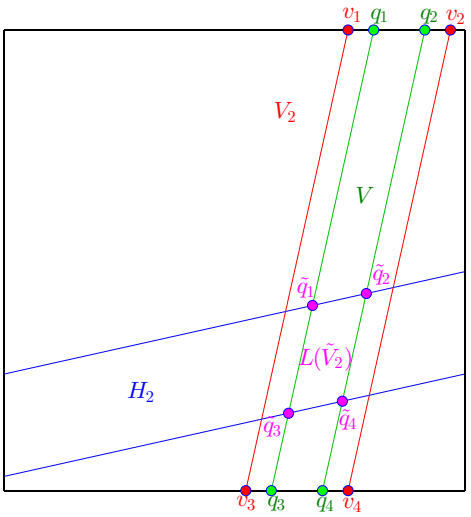

Fig. 5. $V \subset V_2$ strip and $L(\tilde{V}_2) \equiv V \cap H_2$.

The vertical boundaries of V are the straight lines with slope rate a (because V is μ_v-vertical strip) and which pass through the points q_1 and q_2 respectively:

$$\begin{aligned} y_{q_1} &= ax + R - aq_{1_x} \\ y_{q_2} &= ax + R - aq_{2_x} \end{aligned} \tag{41}$$

We need to determine $\tilde{V}_2 \equiv L^{-1}(V) \cap V_2$. Since we do not know how L^{-1} acts on V, first we obtain $L(\tilde{V}_2) \equiv V \cap L(V_2) = V \cap H_2$ and after that, we will recover $\tilde{V}_2$ by iterating $L(\tilde{V}_2)$ backward. V cuts H_2 at four points: $\tilde{q}_1$, $\tilde{q}_2$, $\tilde{q}_3$ and $\tilde{q}_4$ and we can describe them as follows:

$$\tilde{q}_1 : y_{q_1} \cap \left\{ y = \frac{x - (1-R)}{a} \right\}$$

$$\Rightarrow \begin{cases} y = \dfrac{x - (1-R)}{a} \\ y = ax + R - aq_{1_x}. \end{cases} \tag{42}$$

Solving these two equations gives the coordinates of $\tilde{q}_1$:

$$\begin{aligned} \tilde{q}_{1_x} &= \frac{a^2 q_{1_x} - aR - 1 + R}{a^2 - 1} \\ \tilde{q}_{1_y} &= \frac{aq_{1_x} + aR - a - R}{a^2 - 1}. \end{aligned} \tag{43}$$

We continue the same procedure for the rest of the points

$$\tilde{q}_2 : y_{q_2} \cap \left\{ y = \frac{x - (1-R)}{a} \right\}$$

$$\Rightarrow \begin{cases} y = \dfrac{x - (1-R)}{a} \\ y = ax + R - aq_{2_x} \end{cases} \tag{44}$$

and the coordinates for $\tilde{q}_2$ are

$$\begin{aligned} \tilde{q}_{2_x} &= \frac{a^2 q_{2_x} - aR - 1 + R}{a^2 - 1} \\ \tilde{q}_{2_y} &= \frac{aq_{2_x} + aR - a - R}{a^2 - 1}. \end{aligned} \tag{45}$$

In the case of $\tilde{q}_3$ we solve

$$\tilde{q}_3 : y_{q_1} \cap \left\{ y = \frac{x - (1+R)}{a} \right\}$$

$$\Rightarrow \begin{cases} y = \dfrac{x - (1+R)}{a} \\ y = ax + R - aq_{1_x} \end{cases} \tag{46}$$

with coordinates

$$\begin{aligned} \tilde{q}_{3_x} &= \frac{a^2 q_{1_x} - aR - 1 - R}{a^2 - 1} \\ \tilde{q}_{3_y} &= \frac{aq_{1_x} - aR - a - R}{a^2 - 1}. \end{aligned} \tag{47}$$

Finally, to obtain $\tilde{q}_4$ we solve the system

$$\tilde{q}_4 : y_{q_2} \cap \left\{ y = \frac{x - (1+R)}{a} \right\}$$

$$\Rightarrow \begin{cases} y = \dfrac{x - (1+R)}{a} \\ y = ax + R - aq_{2_x} \end{cases} \tag{48}$$

therefore its coordinates are

$$\begin{aligned} \tilde{q}_{4_x} &= \frac{a^2 q_{2_x} - aR - 1 - R}{a^2 - 1} \\ \tilde{q}_{4_y} &= \frac{aq_{2_x} - aR - a - R}{a^2 - 1}. \end{aligned} \tag{49}$$

At this moment, we have given a precise description of $L(\tilde{V}_2)$; it is a strip delimited by the four vertices from above and the straight lines y_{q_1}, y_{q_2}, $y = \frac{x-(1-R)}{a}$ and $y = \frac{x-(1+R)}{a}$. In order to recover $\tilde{V}_2$ we should map it backward by L^{-1}. By continuity, and since L is orientation preserving, the points which are leading to $y = R$ are $L^{-1}(\tilde{q}_4)$ and $L^{-1}(\tilde{q}_3)$ and the points that are mapped to $y = -R$ are $L^{-1}(\tilde{q}_2)$ and $L^{-1}(\tilde{q}_1)$, and therefore

$$\begin{aligned} d(\tilde{V}_2) &= |L^{-1}(\tilde{q}_{4_x}) - L^{-1}(\tilde{q}_{3_x})| \\ &= |L^{-1}(\tilde{q}_{2_x}) - L^{-1}(\tilde{q}_{1_x})|. \end{aligned} \tag{50}$$

For instance, we compute $L^{-1}(\tilde{q}_{4_x})$ and $L^{-1}(\tilde{q}_{3_x})$

$$\begin{aligned} L^{-1}(\tilde{q}_{4_x}) &= L^{-1}\left(\frac{a^2 \tilde{q}_{2_x} - aR - 1 - R}{a^2 - 1}, \frac{a\tilde{q}_{2_x} - aR - a - R}{a^2 - 1} \right) \\ &= \left(\frac{aR + a + R - a\tilde{q}_{2_x}}{a^2 - 1}, \frac{a^2 \tilde{q}_{2_x} - aR - 1 - R}{a^2 - 1} + \frac{a|a\tilde{q}_{2_x} - aR - a - R|}{a^2 - 1} - 1 \right) \end{aligned}$$

$$\overset{(*)}{=} \left(\frac{aR+a+R-a\tilde{q}_{2_x}}{a^2-1}, \frac{a^2q_{2_x}-aR-1-R-a^2q_{2_x}+a^2R+a^2+aR-a^2+1}{a^2-1}\right)$$

$$= \left(\frac{aR+a+R-a\tilde{q}_{2_x}}{a^2-1}, R\right). \tag{51}$$

In $(*)$ we have used the fact that $a\tilde{q}_{2_x}-aR-a-R<0$ as $\tilde{q}_{2_x} < R$ and $a > 0$. The computations for $L^{-1}(\tilde{q}_2)$ are analogous, so

$$L^{-1}(\tilde{q}_{3_x}) = \left(\frac{a+aR+R-aq_{1_x}}{a^2-1}, R\right). \tag{52}$$

Using (50), we can compute $d(\tilde{V}_2)$

$$d(\tilde{V}_2) = \frac{|a+aR+R-aq_{1_x}-a-aR-R+aq_{2_x}|}{a^2-1}$$

$$= \frac{a}{a^2-1}\cdot|q_{2_x}-q_{1_x}| = \nu_v \cdot d(V). \tag{53}$$

Therefore, we only need the rate ν_v to be less than 1 and that holds when $a > \frac{1+\sqrt{5}}{2}$:

$$\frac{a}{a^2-1} < 1 \Leftrightarrow a^2-a-1>0 \Leftrightarrow a > \frac{1+\sqrt{5}}{2} = \Phi. \tag{54}$$

The last issue of Assumption 2 that remains to be proved is that $\tilde{V}_i$ is a μ_v-vertical strip. In order to prove this we realize that $L(\tilde{V}_i) = V \cap L(V_i) = V \cap H_i$ is a μ_h-horizontal strip since its boundaries are μ_h-horizontal curves. As we know by Assumption 1, by F^{-1} horizontal boundaries of horizontal strips map to horizontal boundaries of vertical strips and vertical boundaries of vertical strips map to vertical boundaries of horizontal strips and it is clear that this vertical boundaries of $\tilde{V}_i$ are μ_v-horizontal curves. Therefore, the second assumption is already proven and hence, using Theorem 4, the existence of the chaotic saddle inside S is proven.

4. Nonautonomous Lozi Map

In this section, we prove that Assumptions 1 and 3 of the nonautonomous Conley–Moser conditions hold for the nonautonomous Lozi map. We begin by developing the set-up for the problem. We define the maps L_n and the domains S_n as follows:

$$L_n(x,y) = (1+y-a(n)|x|, -x) \tag{55}$$

and

$$L_n^{-1}(x,y) = (-y, x+a(n)|y|-1) \tag{56}$$

where $a(n) = a+\epsilon(1+\cos(n))$, $a > 4$. The domains can be set as $S_n = [-R(n), R(n)] \times [-R(n), R(n)]$ where

$$R(n) = \frac{a(n)}{4(a(n)-2)}. \tag{57}$$

Although the domain may change with each iteration, in this example we can consider a fixed domain in order to simplify the proof of Theorem 5. Therefore we define the domain as:

$$S = \sup_{n\in\mathbb{Z}}([-R(n), R(n)] \times [-R(n), R(n)])$$

$$= [-R, R] \times [-R, R] \tag{58}$$

where

$$R = \sup_{n\in\mathbb{Z}} \frac{a(n)}{4(a(n)-2)}. \tag{59}$$

To find this value we examine the monotonicity of the function

$$f(a(n)) = \frac{a(n)}{4(a(n)-2)} \tag{60}$$

for $a(n) \neq 2$. This function always decreases since its derivate is negative when $a(n) \neq 2$. Therefore, the supreme of this value is determined from the following relations:

$$\inf_{n\in\mathbb{Z}} a(n) = a+\epsilon(1-1) = a \tag{61}$$

and

$$R = \sup_{n\in\mathbb{Z}} R(n) = \frac{\inf_{n\in\mathbb{Z}} a(n)}{4\left(\inf_{n\in\mathbb{Z}} a(n)-2\right)} = \frac{a}{4(a-2)}. \tag{62}$$

As we did in the autonomous case, we must check conditions similar to inequalities (31) and (33) in order to obtain strips of four vertices totally included in the maximal domain S.

By the symmetry of the problem, as it is shown in Fig. 4, the first condition, (31), is satisfied since the point p does not depend on the iteration n. So this condition holds when

$$R < \frac{1}{2}. \tag{63}$$

The second condition is analogous to (33), and it also holds. We want the point r to cut the horizontal

line $y = R$ out from the domain S and it must have first coordinate lower than $-R$.

$$\begin{aligned} r &= L_n(L_1^-) \cap \{y = R\} \\ &= (1 + R - a(n)|x|, -x)|_{-x=R} \\ &= (1 + R - a(n)R, R) \end{aligned} \tag{64}$$

therefore, we must determine if the following inequality holds

$$1 + R - a(n)R < -R \Leftrightarrow 1 < (a(n) - 2)R \quad \text{for all } n \in \mathbb{Z} \tag{65}$$

and it does hold since

$$(a(n) - 2)R > (a - 2)\frac{a}{4(a - 2)} = \frac{a}{4} > 1 \tag{66}$$

when $a > 4$ for all $n \in \mathbb{Z}$.

Henceforth, we set $S = S_n$ for all $n \in \mathbb{Z}$ and we can state the main nonautonomous theorem.

Theorem 5. *For $a(n) = a + \epsilon(1 + \cos(n))$ where $a > 4$ and ϵ small, Assumptions 1 and 3 of the nonautonomous Conley–Moser conditions hold for the nonautonomous Lozi map L_n, and therefore it possesses a chaotic saddle, Λ_n, inside the square S. In other words, $\{\Lambda_n, L_n\}_{n=-\infty}^{+\infty}$ is an infinite sequence of chaotic invariant sets where*

$$\Lambda \equiv \bigcup_{n \in \mathbb{Z}} \Lambda_n,$$

contains an uncountable infinity of orbits, each of them unstable (of saddle type), and the dynamics on the invariant set exhibits sensitive dependence on initial conditions.

From now on, we see how these two assumptions are held. First of all, we construct the horizontal and vertical strips as in the autonomous case. Then, we check the third assumption, the *cone condition*, to quantify the folding and stretching of the strips.

4.1. *Verification of Assumption 1 for the nonautonomous Conley–Moser conditions*

We have defined the bi-infinite sequence of maps and domains

$$\{L_n, S\}_{n=-\infty}^{+\infty}, \quad L_n : S \to \mathbb{R}^2 \tag{67}$$

satisfying

$$L_n(S) \cap S \neq \emptyset, \quad \forall\, n \in \mathbb{Z}.$$

Now we define the main geometrical structures of this problem, the horizontal and the vertical strips. In this context we will proceed as in the autonomous case adding the iteration variable

$$\begin{aligned} H_1^{n+1} \cup H_2^{n+1} &:= L_n(S) \cap S \\ V_1^n \cup V_2^n &:= L_n^{-1}(S) \cap S \end{aligned} \tag{68}$$

where H_1^{n+1} is the upper half part of $L_n(S) \cap S$ and H_2^{n+1} is the lower half part of $L_n(S) \cap S$, V_1^n is the left half part of $L_n^{-1}(S) \cap S$ and V_2^n is the right half part of $L_n^{-1}(S) \cap S$. We will use the following notation

$$\begin{aligned} H_1^{n+1} &:= (L_n(S) \cap S)^+, \quad \text{where } y > 0, \\ H_2^{n+1} &:= (L_n(S) \cap S)^-, \quad \text{where } y < 0, \\ V_1^n &:= (L_n^{-1}(S) \cap S)^-, \quad \text{where } x < 0, \\ V_2^n &:= (L_n^{-1}(S) \cap S)^+, \quad \text{where } x > 0. \end{aligned} \tag{69}$$

We are giving only the vertices of H_1^{n+1} and V_1^n. The vertices of H_2^{n+1} and V_2^n are symmetric with respect to $y = 0$ and $x = 0$ respectively. We show H_i^{n+1} and V_i^n in Fig. 6.

$$h_{11} : \{x = -R\} \cap \left\{y = \frac{1 + R - x}{a(n)}\right\} \Rightarrow \begin{cases} h_{11_x} = -R \\ h_{11_y} = \dfrac{1 + 2R}{a(n)} \end{cases} \tag{70}$$

$$h_{12} : \{x = R\} \cap \left\{y = \frac{1 + R - x}{a(n)}\right\} \Rightarrow \begin{cases} h_{12_x} = R \\ h_{12_y} = \dfrac{1}{a(n)} \end{cases} \tag{71}$$

$$h_{13} : \{x = R\} \cap \left\{y = \frac{1 - R - x}{a(n)}\right\} \Rightarrow \begin{cases} h_{13_x} = R \\ h_{13_y} = \dfrac{1 - 2R}{a(n)} \end{cases} \tag{72}$$

$$h_{14} : \{x = -R\} \cap \left\{y = \frac{1 - R - x}{a(n)}\right\} \Rightarrow \begin{cases} h_{14_x} = -R \\ h_{14_y} = \dfrac{1}{a(n)} \end{cases} \tag{73}$$

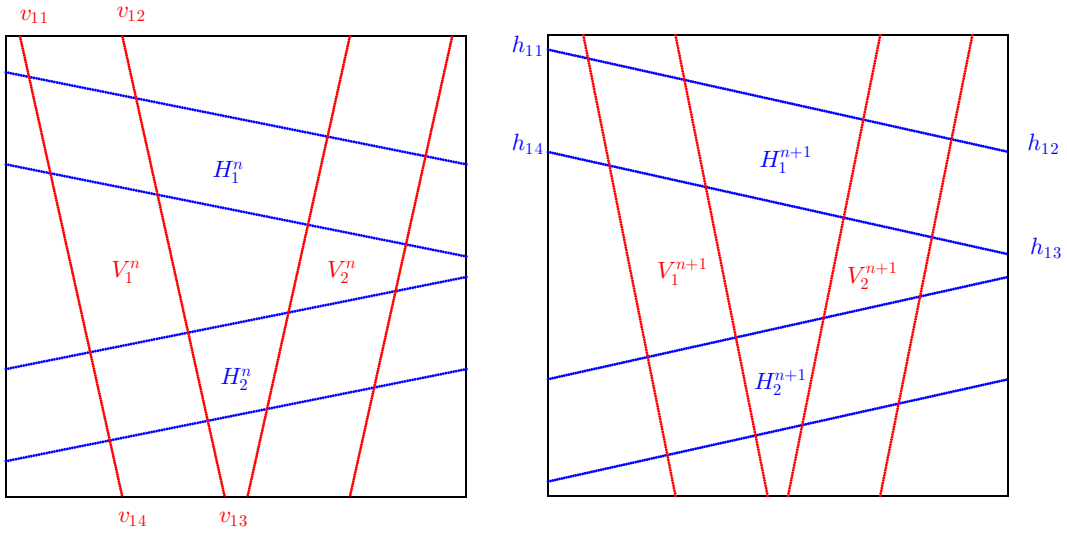

(a) $n_0 = n$ (b) $n_0 = n+1$

Fig. 6. Vertical and horizontal strips. $L_n(V_i^n) = H_i^{n+1}$, $i = 1, 2$.

and the computations for the vertices of V_1^n are similar

$$v_{11} : \{y = R\} \cap \{y = -R - a(n)x - 1\}$$

$$\Rightarrow \begin{cases} v_{11_x} = \dfrac{-2R-1}{a(n)} \\ v_{11_y} = R \end{cases} \tag{74}$$

$$v_{12} : \{y = R\} \cap \{y = R - a(n)x - 1\}$$

$$\Rightarrow \begin{cases} v_{12_x} = \dfrac{-1}{a(n)} \\ v_{12_y} = R \end{cases} \tag{75}$$

$$v_{13} : \{y = -R\} \cap \{y = R - a(n)x - 1\}$$

$$\Rightarrow \begin{cases} v_{13_x} = \dfrac{2R-1}{a(n)} \\ v_{13_y} = -R \end{cases} \tag{76}$$

$$v_{14} : \{y = -R\} \cap \{y = -R - a(n)x - 1\}$$

$$\Rightarrow \begin{cases} v_{14_x} = \dfrac{-1}{a(n)} \\ v_{14_y} = -R. \end{cases} \tag{77}$$

As it is defined above, V_i^n and H_i^{n+1} are μ_v^n-vertical strips and μ_h^{n+1}-horizontal strips respectively with $\mu_v^n = 1/a(n)$ and $\mu_h^{n+1} = 1/a(n+1)$. Taking into account Remark 4.1 and due to reasons explained afterwards, by convenience, we can choose

$$\mu_v = \mu_h = \frac{a - \sqrt{a^2 - 4}}{2} > \frac{1}{a(n)}, \tag{78}$$

for all $n \in \mathbb{Z}$ and $a > 4$.

Remark 4.1. Note that if V is a μ_v-vertical strip and $\mu_v \leq \mu_v^*$, therefore V is a μ_v^*-vertical strip:

$$|x_1 - x_2| \leq \mu_v |y_1 - y_2| \leq \mu_v^* |y_1 - y_2|.$$

The same argument could be used for horizontal strips.

L_n is a homeomorphism on the whole plane and so also on S. Therefore

$$L_n(V_i^n) = H_i^{n+1}, \quad i = 1, 2. \tag{79}$$

We should also define

$$\begin{aligned} L_n(V_i^n) \cap V_j^{n+1} &\equiv H_{ij}^{n+1} \\ V_i^n \cap L_n^{-1}(V_j^{n+1}) &\equiv L_n^{-1}(H_{ij}^{n+1}) \equiv V_{ji}^n. \end{aligned} \tag{80}$$

Let $\{A^n\}_{n=-\infty}^{+\infty}$ denote a sequence of 2×2 matrices such that

$$A_{ij}^n = \begin{cases} 0 & \text{if } L_n(V_i^n) \cap V_j^{n+1} \\ & \quad = H_i^{n+1} \cap V_j^{n+1} = \emptyset \\ 1 & \text{if } L_n(V_i^n) \cap V_j^{n+1} \\ & \quad = H_i^{n+1} \cap V_j^{n+1} \neq \emptyset. \end{cases} \tag{81}$$

In our case, we can ensure that

$$A^n = \begin{pmatrix} 1 & 1 \\ 1 & 1 \end{pmatrix}. \tag{82}$$

We know that H_i^{n+1} are horizontal strips formed by two μ_h-horizontal curves that rest on the lines $x = R$ and $x = -R$ and V_j^{n+1} are vertical strips formed by two μ_v-vertical curves that lead from $y = R$ to $y = -R$. So applying the *Fixed Point Theorem*, these straight lines get cut in four vertices that together with the two horizontal and the two vertical lines form H_{ij}^{n+1}. These sets are μ_h-horizontal strips because their boundaries are contained in V_j^{n+1} due to their construction $(H_i^{n+1} \cap V_j^{n+1})$.

Furthermore, due to the fact that L_n is homeomorphism and the construction of the strips, L_n maps V_{ji}^n onto H_{ij}^{n+1}. It is clear from (80) that

$$\begin{aligned} L_n^{-1}(H_{ij}^{n+1}) = V_{ji}^n = L_n^{-1}(V_j^{n+1}) \cap V_i^n \\ \Rightarrow L_n^{-1}(H_{ij}^{n+1}) \subset V_i^n \end{aligned} \tag{83}$$

so

$$L_n^{-1}(\partial_h H_{ij}^{n+1}) \subset \partial_h V_i^n. \tag{84}$$

Finally we need to prove $\mu_v \mu_h < 1$. We know that $\mu_v = \mu_h = \frac{a-\sqrt{a^2-4}}{2}$ and

$$\mu_v \cdot \mu_h = \left(\frac{a - \sqrt{a^2-4}}{2} \right)^2 < 1 \tag{85}$$

so Assumption 1 is proven.

4.2. *The Cone condition. Assumption A3 of the nonautonomous Conley–Moser conditions*

As we stated earlier, the second assumption of the Conley–Moser conditions can be replaced by another condition named the *Cone condition*. Given any point $z_0 = (x_0, y_0) \in \mathcal{H}^{n+1}$ and any $(\xi_{z_0}, \eta_{z_0}) \in S^s_{\mathcal{H}^{n+1}}$ (which by definition, $|\xi_{z_0}| \leq \mu_v |\eta_{z_0}|$), we have that

$$\begin{aligned} DL_n^{-1}(z_0) \cdot (\xi_{z_0}, \eta_{z_0}) &= \begin{pmatrix} 0 & -1 \\ 1 & a(n)\text{sign}(y) \end{pmatrix} \begin{pmatrix} \xi_{z_0} \\ \eta_{z_0} \end{pmatrix} \\ &= \begin{pmatrix} -\eta_{z_0} \\ \xi_{z_0} + a(n)\text{sign}(y)\eta_{z_0} \end{pmatrix} \end{aligned} \tag{86}$$

and (86) belongs to $S^s_{\mathcal{V}^n}$ if and only if the inequality

$$|-\eta_{z_0}| = |\eta_{z_0}| \leq \mu_v |\xi_{z_0} + a(n)\text{sign}(y)\eta_{z_0}| \tag{87}$$

holds and this is true since

$$\begin{aligned} &\mu_v |\xi_{z_0} + a(n)\text{sign}(y)\eta_{z_0}| \\ &\quad \geq \mu_v (a(n)|\eta_{z_0}| - |\xi_{z_0}|) \\ &\quad \geq \mu_v (a(n)|\eta_{z_0}| - \mu_v |\eta_{z_0}|) \\ &\quad = \mu_v (a(n) - \mu_v)|\eta_{z_0}| \overset{(*)}{\geq} |\eta_{z_0}|. \end{aligned} \tag{88}$$

Last part of the inequality, $(*)$, hold when $\mu_v(a(n) - \mu_v) \geq 1$ and that is satisfied when

$$\begin{aligned} \mu_v &\in \left[\frac{a(n) - \sqrt{a(n)^2 - 4}}{2}, \frac{a(n) + \sqrt{a(n)^2 - 4}}{2} \right] \\ &= I_n. \end{aligned} \tag{89}$$

We need to prove that $\mu_v \in I_n$ for every $n \in \mathbb{Z}$, or, equivalently

$$\begin{aligned} \mu_v \in \bigcap_{n \in \mathbb{Z}} I_n = \Bigg[&\sup_{n \in \mathbb{Z}} \frac{a(n) - \sqrt{a(n)^2 - 4}}{2}, \\ &\inf_{n \in \mathbb{Z}} \frac{a(n) + \sqrt{a(n)^2 - 4}}{2} \Bigg] \\ = &\left[\frac{a - \sqrt{a^2-4}}{2}, \frac{a + \sqrt{a^2-4}}{2} \right]. \end{aligned} \tag{90}$$

Finally, we can set a general value for μ_h and μ_v that hold for the last inequalities

$$\mu_h = \mu_v = \frac{a - \sqrt{a^2-4}}{2} \tag{91}$$

and we can observe that

$$\mu_h \cdot \mu_v = \left(\frac{a - \sqrt{a^2-4}}{2} \right)^2 < 1. \tag{92}$$

Since $z_0 \in \mathcal{H}^{n+1}$ is an arbitrary point, the inclusion $DL_n^{-1}(S^s_{\mathcal{H}^{n+1}}) \subset S^s_{\mathcal{V}^n}$ is proven.

To finish the proof of Assumption 3, we only need to prove the inequality

$$|\eta_{f_n^{-1}(z_0)}| \geq \frac{1}{\mu}|\eta_{z_0}| \tag{93}$$

for $0 < \mu < 1 - \mu_h\mu_v$ and $z_0 \in \mathcal{H}^{n+1}$, $(\xi_{z_0}, \eta_{z_0}) \in S^s_{\mathcal{H}^{n+1}}$ because

$$|\xi_{f_n(z_0)}| \geq \frac{1}{\mu}|\xi_{z_0}|, \quad z_0 \in \mathcal{V}^n, \quad (\xi_{z_0}, \eta_{z_0}) \in S^u_{\mathcal{V}^n} \tag{94}$$

is proved by using a similar argument.

$$\begin{aligned} |\eta_{f_n^{-1}(z_0)}| &\geq |\xi_{z_0} + a(n)\text{sign}(y)\eta_{z_0}| \\ &\geq a(n)|\eta_{z_0}| - |\xi_{z_0}| \geq a(n)|\eta_{z_0}| - \mu_v|\eta_{z_0}| \\ &= (a(n) - \mu_v)|\eta_{z_0}| \geq \frac{1}{\mu}|\eta_{z_0}| \end{aligned} \tag{95}$$

so it follows that

$$\mu \geq \frac{1}{a(n) - \mu_v}. \tag{96}$$

Taking into account this last inequality and the condition $0 < \mu < 1 - \mu_h\mu_v$, we have the following chain of inequalities

$$\frac{1}{a(n) - \mu_v} \leq \mu \leq 1 - \mu_h\mu_v \tag{97}$$

and this last inequality is satisfied provided that $a > 4$ so the proof of Assumption 3 is complete.

The proof of the second inclusion $DL_n(S^u_{\mathcal{V}^n}) \subset S^u_{\mathcal{H}^{n+1}}$ is similar.

5. The Visualization of the Chaotic Saddle

In this section the chaotic saddle for the autonomous and for the nonautonomous cases are displayed by using the discrete Lagrange descriptors (DLD). This tool explained in [Lopesino *et al.*, 2015] consists of evaluating the p-norm of an orbit generated by a two-dimensional map, in our case the Lozi map. For instance, let

$$\{x_n, y_n\}_{n=-N}^{n=N}, \quad N \in \mathbb{N}, \tag{98}$$

denote an orbit of a point. The DLD is defined as follows:

$$MD_p = \sum_{i=-N}^{N-1} |x_{i+1} - x_i|^p + |y_{i+1} - y_i|^p, \quad p \leq 1. \tag{99}$$

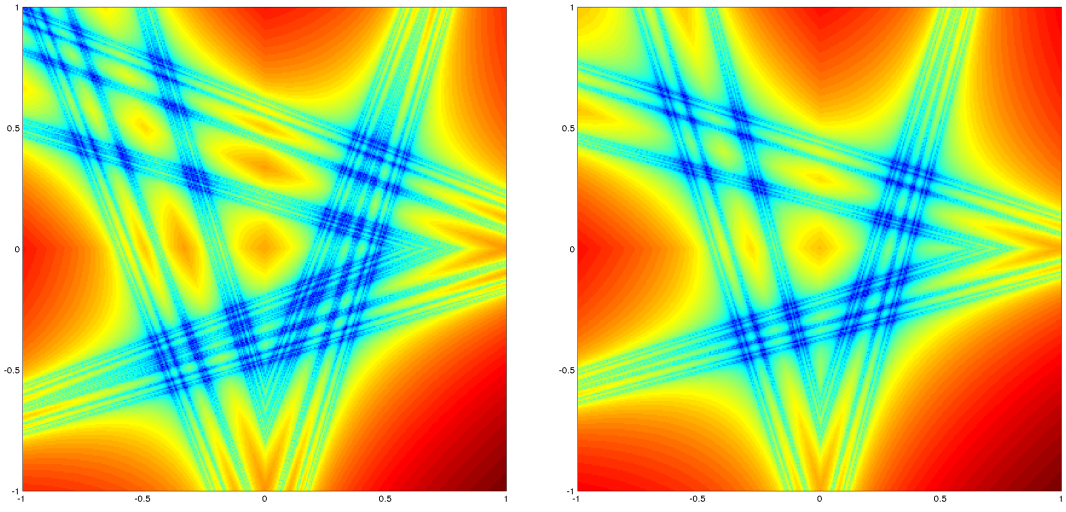

(a) (b)

Fig. 7. Chaotic saddle for different values of a. These panels show contours of MD_p for $p = 0.25$ and $N = 20$, with a grid point spacing of 0.005. Chaotic S with (a) $a = 3$, (b) $a = 3.5$, (c) $a = 4$ and (d) $a = 4.5$.

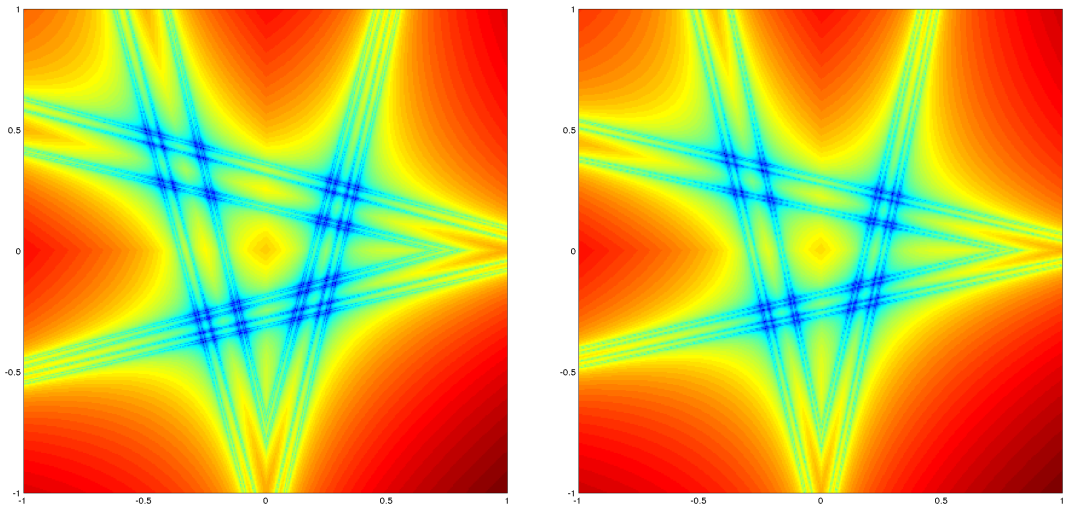

(c) (d)

Fig. 7. (*Continued*)

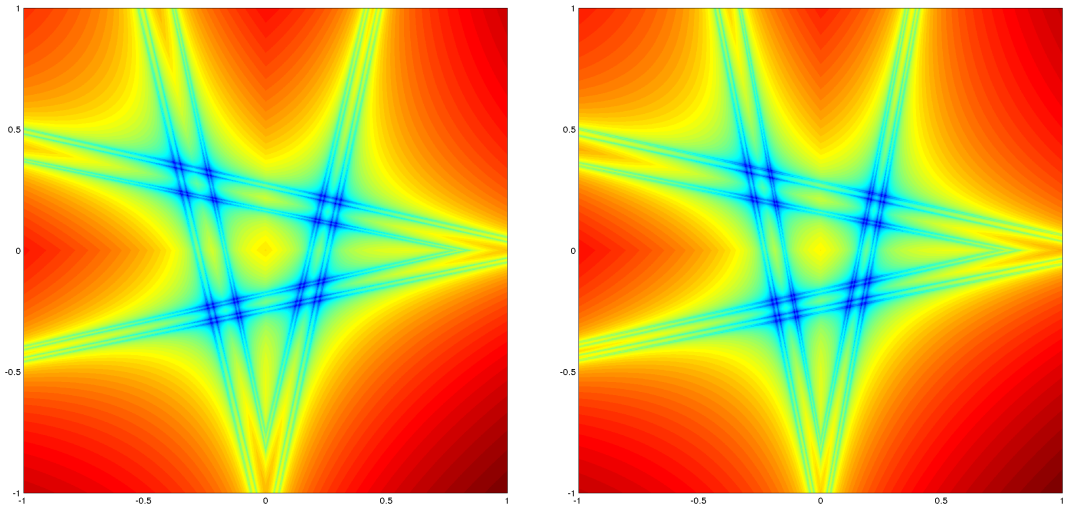

(a) (b)

Fig. 8. Chaotic saddle for different starting time iteration. These panels show contours of MD_p for $p = 0.25$, $A = 4.5 + \epsilon(1 + \cos(n))$ and $N = 100$, with a grid point spacing of 0.001. Chaotic S with (a) $n_0 = -3$, (b) $n_0 = -1$, (c) $n_0 = 1$ and (d) $n_0 = 3$.

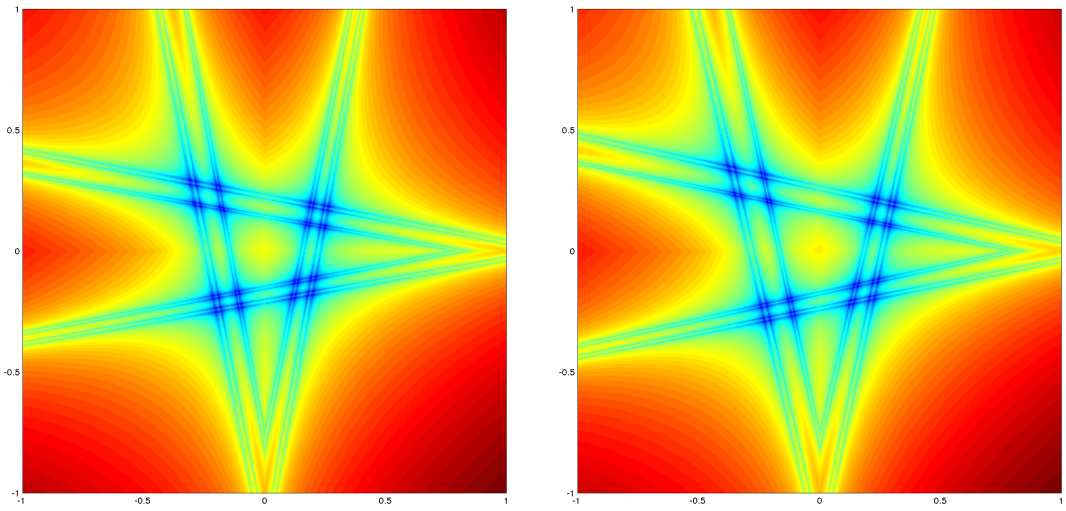

(c) (d)

Fig. 8. (*Continued*)

We are interested in showing the phase space where the chaotic saddle exists, therefore our study region is the square S. We prepare a set of initial conditions by fixing a spatial grid and then expression (99) is applied to the initial conditions belonging to this grid.

The Chaotic Saddle for the Autonomous Case. Figure 7 shows the chaotic saddle of the Lozi map for different values of a. It is confirmed that only when $a \geq 4$, the set is wholly contained in the square S.

The Chaotic Saddle for the Nonautonomous Case. Figure 8 shows by means of the DLD tool, how the chaotic saddle evolves with the iterations when the autonomous system is perturbed.

6. Summary and Conclusions

In this paper we have considered the Lozi map, both in its autonomous and nonautonomous versions, and provided necessary conditions for the map to possess a chaotic invariant set. This is accomplished by using autonomous and nonautonomous versions of the Conley–Moser conditions, in particular, we used the sharpened conditions for nonautonomous maps given in [Balibrea-Iniesta *et al.*, 2015] to show that the nonautonomous chaotic invariant set is hyperbolic. In the course of the proof, we provide a precise characterization of what is meant by the phrase "hyperbolic chaotic invariant set" for nonautonomous dynamical systems. At the end of this paper we have used the DLD to visualize the chaotic saddle for different parameters.

Acknowledgments

The research of C. Lopesino, F. Balibrea-Iniesta and A. M. Mancho is supported by the MINECO under grant MTM2014-56392-R. The research of S. Wiggins is supported by ONR Grant No. N00014-01-1-0769. We acknowledge support from MINECO: ICMAT Severo Ochoa project SEV-2011-0087.

References

Alekseev, V. M. [1968a] "Quasirandom dynamical systems, I," *Math. USSR-Sb.* **5**, 73–128.

Alekseev, V. M. [1968b] "Quasirandom dynamical systems, II," *Math. USSR-Sb.* **6**, 505–560.

Alekseev, V. M. [1969] "Quasirandom dynamical systems, III," *Math. USSR-Sb.* **6**, 1–43.

Balibrea-Iniesta, F., Lopesino, C., Wiggins, S. & Mancho, A. M. [2015] "Chaotic dynamics in nonautonomous maps: Application to the nonautonomous Hénon map," *Int. J. Bifurcation and Chaos* **25**, 1550172-1–14.

Chastaing, J.-Y., Bertin, E. & Géminard, J.-C. [2015] "Dynamics of the bouncing ball," *Am. J. Phys.* **83**, 518.

Devaney, R. & Nitecki, Z. [1979] "Shift automorphisms in the Hénon mapping," *Comm. Math. Phys.* **67**, 137–179.

Holmes, P. J. [1982] "The dynamics of repeated impacts with a sinusoidally vibrating table," *J. Sound Vibr.* **84**, 173–189.

Lerman, L. & Silnikov, L. [1992] "Homoclinical structures in nonautonomous systems: Nonautonomous chaos," *Chaos* **2**, 447–454.

Lopesino, C., Balibrea, F., Wiggins, S. & Mancho, A. [2015] "Lagrangian descriptors for two dimensional, area preserving, autonomous and nonautonomous maps," *Commun. Nonlin. Sci. Numer. Simul.* **27**, 40–51.

Lozi, R. [1978] "Un attracteur etrange (?) du type attracteur de Henon," *J. de Phys. Coll.* **39**, C5-9–C5-10.

Moser, J. [1973] *Stable and Random Motions in Dynamical Systems*, Annals of Mathematical Studies, Vol. 77 (Princeton University Press).

Stoffer, D. [1988a] "Transversal homoclinic points and hyperbolic sets for non-autonomous maps I," *J. Appl. Math. Phys.* (*ZAMP*) **39**, 518–549.

Stoffer, D. [1988b] "Transversal homoclinic points and hyperbolic sets for non-autonomous maps II," *J. Appl. Math. Phys.* (*ZAMP*) **39**, 783–812.

Wiggins, S. [1999] "Chaos in the dynamics generated by sequences of maps, with applications to chaotic advection in flows with aperiodic time dependence," *Z. Angew. Math. Phys.* (*ZAMP*) **50**, 585–616.

Wiggins, S. [2003] *Introduction to Applied Nonlinear Dynamical Systems and Chaos*, 2nd edition (Springer).

Wiggins, S. & Mancho, A. M. [2014] "Barriers to transport in aperiodically time-dependent two-dimensional velocity fields: Nekhoroshev's theorem and nearly invariant tori," *Nonlin. Process. Geophys.* **21**, 165–185.

CHAPTER 4

Discussion

This work provides a theoretical framework for LDs from a clear and precise definition of the singularity notion from which theorems are obtained. In this Chapter we provide further remarks on the definition of singular features and their applicability. We focus our analysis on discrete Lagrangian descriptors for maps. In particular we extend the discussion on some technical details by presenting several examples. We also mention several contexts in which our specific contribution on discrete Lagrangian descriptors has been used and discuss about its advantages.

The characterization of manifolds in maps as singular features of the discrete Lagrangian descriptor is performed by stating that the discrete Lagrangian descriptor, MD_p has not a defined derivative at points that lie on the manifold. This is because the directional derivative of the Lagrangian descriptor in a direction transversal to the manifold is either unbounded when $p < 1$ or simply discontinuous for the case $p = 1$. We further discuss the presence of singularities in MD_p. We consider the rotated linear saddle discussed in Chapter 3:

$$F(x, y) = A \begin{pmatrix} x \\ \\ y \end{pmatrix} \tag{4.1}$$

where

$$A = \begin{pmatrix} \frac{1}{\lambda} + \lambda & \frac{1}{\lambda} - \lambda \\ \\ \frac{1}{\lambda} - \lambda & \frac{1}{\lambda} + \lambda \end{pmatrix} = \frac{1}{2\lambda} \begin{pmatrix} 1 + \lambda^2 & 1 - \lambda^2 \\ \\ 1 - \lambda^2 & 1 + \lambda^2 \end{pmatrix} \tag{4.2}$$

Here $\lambda > 1$. It is easy to see that the stable and the unstable manifolds are given by the vectors $(1, 1)$ and $(1, -1)$ respectively. Let us consider that $MD_p = MD_p^+ + MD_p^-$. The exact expression for MD_p^+ (expression MD_p^- is analogous) applied to trajectories in map (4.1) is:

$$\begin{aligned} MD_p^+ = \quad & \sum_{i=0}^{N-1} \frac{1}{\lambda^{(i+1)p}} |(\lambda^{2(i+1)} - \lambda^{2(i+1)-1} - \lambda + 1)x_0 + (-\lambda^{2(i+1)} + \lambda^{2(i+1)-1} - \lambda + 1)y_0|^p \\ & + \tfrac{1}{\lambda^{(i+1)p}} |(-\lambda^{2(i+1)} + \lambda^{2(i+1)-1} - \lambda + 1)x_0 + \lambda^{2(i+1)} - \lambda^{2(i+1)-1} - \lambda + 1)y_0|^p \end{aligned} \tag{4.3}$$

This is an example in which *each term on this sum has singularities along two different lines.* In particular, for each i and λ, we have

$$y_0 = \frac{\lambda^{2(i+1)} - \lambda^{2(i+1)-1} - \lambda + 1}{\lambda^{2(i+1)} - \lambda^{2(i+1)-1} + \lambda - 1} x_0 = m(\lambda, i) x_0 \tag{4.4}$$

and

$$y_0 = -\frac{1}{m(\lambda, i)} x_0 \tag{4.5}$$

where $m(\lambda, i)$ and $-\frac{1}{m(\lambda, i)}$[1] are, respectively, the slopes of the singular lines. The presence of these terms having singularities along lines which do not correspond to manifolds, is not an obstacle for visualizing manifolds using MD_p as it is possible to show that at large N, $m \simeq 1$ and thus the largest contributions in the summation correspond to terms aligned with the manifolds.

Additionally, we consider the following two dimensional area-preserving map denoted by f,

$$(f): \quad \begin{cases} x_{n+1} &= 2x_n \\ y_{n+1} &= \frac{1}{2} y_n + g(x_n) \end{cases} \tag{4.6}$$

with $g : \mathbb{R} \to [0, \infty)$ a smooth function satisfying $g(x) = 0$ for all $x \notin [0, 1]$ and $g(x) > 0$ if $x \in (0, 1)$.

The inverse map of f is as follows,

$$(f^{-1}): \quad \begin{cases} x_n &= \frac{1}{2} x_{n+1} \\ y_n &= 2y_n - 2g(\frac{1}{2} x_{n+1}) \end{cases} \tag{4.7}$$

The simple form of the map allows the orbits to be analytically computed through an arbitrary point (x_0, y_0):

$$x_n = 2^n x_0 \quad \text{for any } n \in \mathbb{Z}, \tag{4.8}$$

$$y_n = \frac{1}{2^n} y_0 + \sum_{i=0}^{n-1} \frac{1}{2^{n-1-i}} g(2^i x_0) \qquad \text{for any } n \geq 1, \tag{4.9}$$

$$y_{-n} = 2^n y_0 - \sum_{i=1}^{n} 2^{n+1-i} g\left(\frac{1}{2^i} x_0\right) \qquad \text{for any } n \geq 1. \tag{4.10}$$

It is easy to show that the origin $(0, 0)$ is a global saddle point, since the function g is zero over the interval $(-\infty, 0] \cup [1, \infty)$. Moreover, its corresponding stable and unstable manifolds can be computed explicitly and have the following form:

$$W^s(0, 0) = \{(x, y) \in \mathbb{R}^2 : x = 0\}, \tag{4.11}$$

[1]There is a missprint in the article *Lagrangian descriptors for two dimensional, area-preserving, autonomous and nonautonomous maps* in Section 3.1 where the slope of the invariant manifold is computed.

$$W^u(0,0) = \{(x,y) \in \mathbb{R}^2 : y = \bar{y}(x) = \sum_{i=1}^{\infty} \frac{1}{2^{i-1}} g\left(\frac{1}{2^i}x\right)\}. \tag{4.12}$$

The curve $\{y = \bar{y}(x)\}$ coincides with the line $\{y = 0\}$ for $x \leq 0$. Its shape changes for $x > 0$ since $g > 0$ over the interval $(0, 1)$. The left hand panel in Figure 4.1 a) shows the unstable manifold for positive x for the particular choice $g(x) = \sin^2(\pi x)$. Since we have analytical expressions for the stable and unstable manifolds of the saddle point at the origin, it is straightforward to verify the manner in which MD_p reveals the stable and unstable manifolds. Figure 4.1 b) shows the contours of the Lagrangian descriptor for $N = 50$ and $p = 0.25$, confirming that MD_p accurately reveals the stable and unstable manifolds of the saddle point at the origin.

Figure 4.2 plots contours of the two components of the gradient of MD_p for the map 4.6. Clearly, the stable and unstable manifolds correspond to singular features of MD_p as defined in our work. We next provide an analytical discussion on the performance of MD_p for this example. We consider its expression:

$$MD_p = \sum_{i=-N-1}^{N} |x_{i+1} - x_i|^p + |y_{i+1} - y_i|^p, \quad \text{(with } p \leq 1) \tag{4.13}$$

applied to the sequences $\{(x_n, y_n)\}_{n=-\infty}^{+\infty}$ generated by f (and until $N = 50$ iterations). The terms composing the sum (4.13) with respect to the initial condition points (x_0, y_0),

$$|x_{n+1} - x_n| = |2x_n - x_n| = |x_n| = 2^n|x_0| \qquad \text{for every } n = (-N-1), \cdots, N, \tag{4.14}$$

$$|y_{n+1} - y_n| = \left|\frac{1}{2}y_n + g(x_n) - y_n\right| = \left|g(x_n) - \frac{1}{2}y_n\right| =$$

$$\left|g(2^n x_0) - \frac{1}{2^{n+1}}y_0 - \sum_{i=0}^{n-1} \frac{1}{2^{n-i}} g(2^i x_0)\right| \qquad \text{for every } n = 0, \cdots, N, \tag{4.15}$$

$$|y_{-n+1} - y_{-n}| = \left|y_{-n+1} - 2y_{-n+1} + 2g\left(\frac{1}{2}x_{-n+1}\right)\right| = \left|2g\left(\frac{1}{2}x_{-n+1}\right) - y_{-n+1}\right| =$$

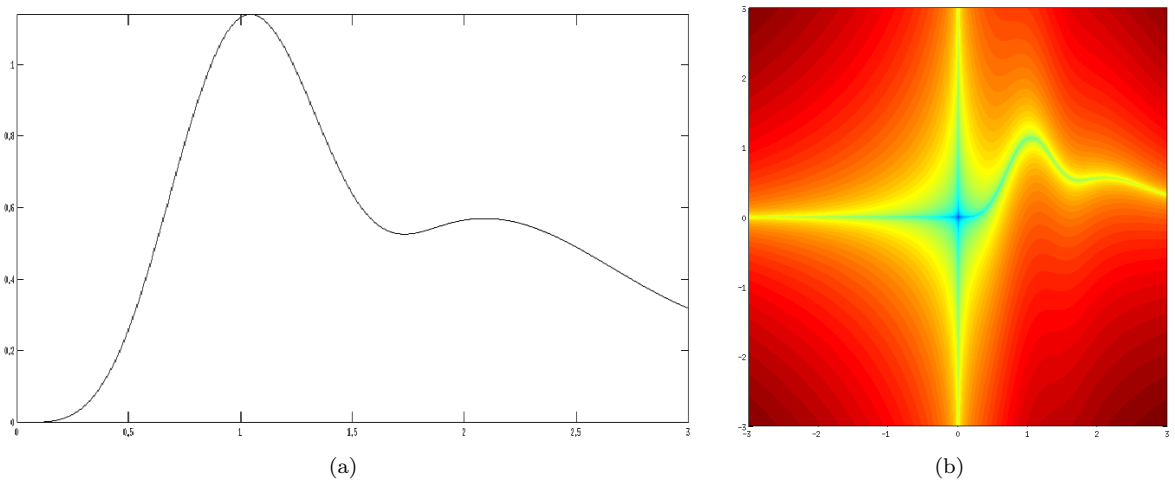

(a) (b)

Figure 4.1: a) The graph of the unstable manifold, $y = \bar{y}(x) = \sum_{i=1}^{\infty} \frac{1}{2^{i-1}} g\left(\frac{1}{2^i}x\right)$ over the interval $[0, 3]$, where we have taken $g(x) = \sin^2(\pi x)$; b) contours of the Lagrangian descriptor MD_p evaluated for the map f with $g(x) = \sin^2(\pi x)$ for $N = 50$ iterations and $p = 0.25$.

$$\left| 2g\left(\frac{1}{2^n}x_0\right) - 2^{n-1}y_0 + \sum_{i=1}^{n-1} 2^{n-i} g\left(\frac{1}{2^i}x_0\right) \right| \qquad \text{for every } n = 1, \cdots, (N+1). \tag{4.16}$$

From these last three equations, one sees that the highest order singularities (of order 2^N) correspond to the increments $|x_{N+1} - x_N|$ and $|y_{-N-1} - y_{-N}|$, that is, to equations 4.14 and 4.16 with $n = N$ and $n = N+1$ respectively, which give rise to the singular features located at the curves,

$$C_1(N) \equiv \{x_0 = 0\} \quad , \quad C_2(N) \equiv \{y_0 = \frac{1}{2^{N-2}} g\left(\frac{1}{2^N}x_0\right) + \sum_{i=1}^{N-1} \frac{1}{2^{i-1}} g\left(\frac{1}{2^i}x_0\right)\}. \tag{4.17}$$

The first curve $C_1(N)$ coincides with the stable manifold $W^s(f,(0,0))$ for every $N > 0$ and the second one $C_2(N)$ converges to $W^u(f,(0,0)) \equiv \{y_0 = \bar{y}(x_0)\}$ for an increasing number of iterations N.

The discussion of these two examples clarifies that our statement on Lagrangian descriptors is not that *singular features* of the Lagrangian descriptors are manifolds. Rather, the assertion is that manifolds coincide with *singular features*.

Finally, we remark that both examples show that singularities are aligned with manifolds for a sufficiently large number of iterations N, and thus the unbounded character of MD_p in the limit $N \to$ infinity, which would make it impossible to consider a derivative in this limit, does not affect the described construction, since singularities are defined for any finite N and it is not necessary to take the limit $N \to$ infinity.

Discrete Lagrangian descriptors are proving to be one of the simplest methods for implementing and displaying with great detail the geometrical features associated to trajectory solutions of maps. Another method used with this purpose is the PIM procedure, which has been employed to obtain the chaotic saddle of a map, although it is designed to detect only points belonging to a chaotic saddle and does not detect its invariant manifolds (Nusse and Yorke, 1989). The method is computationally expensive in terms of time and memory. Other well-known numerical methods to compute periodic points are those that use fixed point theorems,

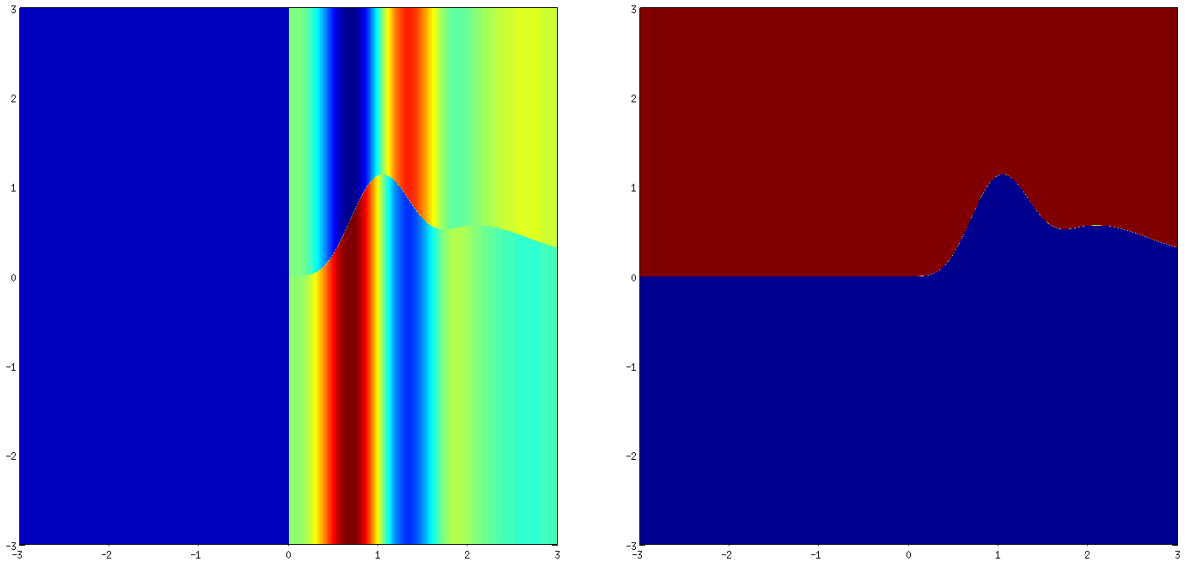

Figure 4.2: The two panels show the the modulus of the gradient components $\partial/\partial x$ and $\partial/\partial y$ (left and right, respectively) of the Lagrangian descriptor $MD_{p=1}$ applied to the map f (with $g(x) = \sin^2(\pi x)$ over the interval $(0,1)$) and evaluated for $N = 50$ iterations.

such as Newton's method. All these methods follow an iterative procedure and require the calculation of the derivative. The iteration stops when a desired accuracy of the solution is reached by tuning a threshold parameter.

In order to compare the output of MD_p and those obtained by fixed point theorems we recall results reported in Maličký (2012) by considering the following example:

$$\begin{cases} x_{n+1} &= x_n(4 - x_n - y_n) \\ y_{n+1} &= x_n y_n \end{cases} \tag{4.18}$$

The dynamics of this example has been studied in great detail in Maličký (2012) and Balibrea (2016) inside the triangle Δ of vertices $(0,0)$, $(4,0)$ and $(0,4)$. The map associated with Eq. (4.18) is $F(x,y) = (x(4-x-y), xy)$ and Δ is invariant under the action of F, i.e., $F(\Delta) = \Delta$. Figure 4.3 shows different outputs of the dynamics of system 4.18 inside Δ obtained with the different methods. Outputs are similar for both techniques, although simplicity and computing time are much lower for the MD_p. Figure 4.3 a) was computed in $C++$ language and Mathematica, obtaining similar results in both cases. According to Maličký (2017), the computational time was 2-3 days, while Figure 4.3 b), which shows the result of MD_p, it is just a few seconds.

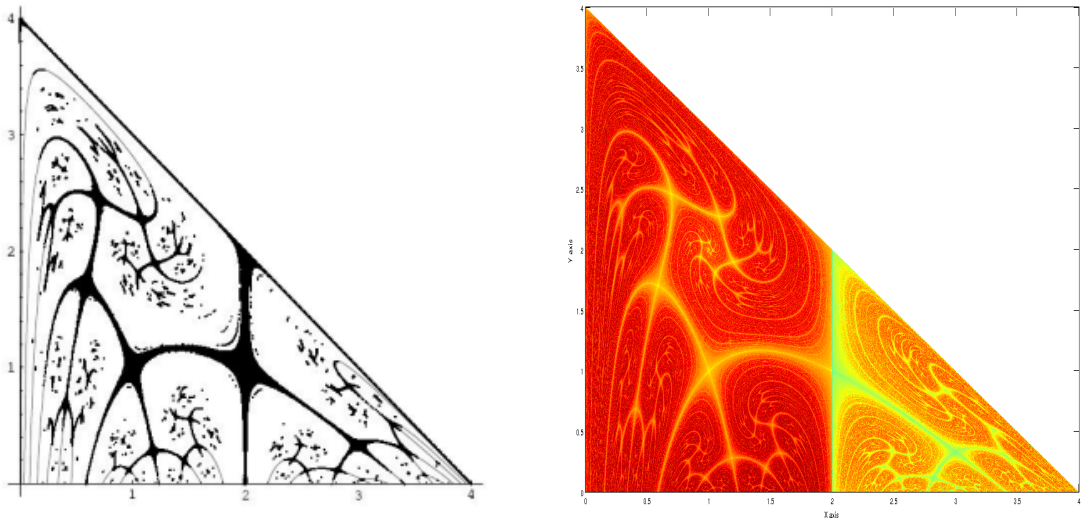

(a) (b)

Figure 4.3: Outputs of the dynamics of system 4.18 using (a) fixed point methods (periodic saddle points of period less than 36) and (b) DLD inside the triangule Δ for $p = 0.1$ and $N = 30$ iterations in a grid size of 4000×4000.

CHAPTER 5

Conclusions and perspectives

Finally, we briefly summarize the contributions of this work and highlight open questions related to our results that could guide future research.

One of the main goals of this work is to provide a theoretical framework for Lagrangian descriptors in aperiodically time-dependent dynamical systems. To this end, we first extend the definition of LDs to the discrete context in a manner that simplifies calculations. A definition for *singular features* from which theorems are obtained for four particular examples is stated more precisely. Normal Form theory and Hartman-Grobman theorem are applied to the C^1 version for two dimensional Hamiltonian systems. Using similar ideas, the new definition of discrete Lagrangian descriptors is adapted to continuous time dynamical systems. As in the discrete setting, we provide rigorous proofs for four particular examples built from a hyperbolic point. Our proofs are based on settings for which we have a priori knowledge of the manifold of a hyperbolic point, and we prove the presence of defined singularities aligned with these curves in the framework of our particular LD. A more general result that we have not obtained, but which could guide future efforts, would be to prove that geometrical structures related to hyperbolic trajectories with no material flux are aligned with singular features of the LD. Additionally, other results could lead to further definitions for the kind of singular features observed in contexts different to those studied, or which would yield proofs of their presence on the particular LD, function M, used in many applications (de la Cámara *et al.*, 2012, 2013; Curbelo *et al.*, 2017a; Smith and Mc Donald, 2014; Rempel *et al.*, 2013; Garcia-Garrido *et al.*, 2015, 2016; Craven and Hernandez, 2015, 2016). The visualizations provided by the discrete LDs, versus others that have been used in Maličký (2012), support the idea that the representational power of this tool could support further theoretical findings for maps, as well as suggesting the presence of objects on which formal proofs could be performed.

Furthermore, in the continuous time setting, we discuss results that show the ability of LDs to reveal invariant sets such as n-tori which are just an extension of the ergodic partition theory. We illustrate this in two examples: the planar harmonic oscillator and the three dimensional ABC flow. These results on the ability of LDs to reveal tori-like invariant sets have already started to be applied in the atmospheric context as tools that allow the identification of the vortex core and vortex boundaries in the stratospheric polar vortex (Curbelo *et al.*, 2017b). The power of this tool in the exploration of high dimensional systems is yet to be exploited. For instance, open questions in the context of astrodynamics like the 3 body problem (or its restricted version), for which these type of visualization tools could provide novel insights. A first step in this direction would be to address well-known problems in this topic and explore them from this perspective. In geophysical contexts, 3D studies with LDs are being carried out in the stratosphere (Curbelo *et al.*, 2017a,b) that reveal the presence of Normally Hyperbolic Invariant Manifolds.

Our final result addresses the challenge of rigorously proving the presence of chaotic invariant sets in aperiodically time-dependent systems. To this end, we have studied the autonomous and nonautonomous Lozi map in its orientation and area-preserving version. We have applied first and second Conley-Moser conditions to prove the existence of a chaotic saddle in the autonomous version of the Map. Proof that the first and third Conley-Moser conditions are satisfied for the nonautonomous aperiodic version under certain parameters would enable us to address the aforementioned challenge. Discrete LDs allow a visualization of

the chaotic behavior of the Lozi map as parameters are varied.

Conclusiones y trabajo futuro

Para concluir, resumimos brevemente las contribuciones de este trabajo y destacamos las preguntas abiertas relacionadas con nuestros resultados que podrían orientar futuras investigaciones.

Uno de los principales objetivos de este trabajo ha sido el de proporcionar un marco teórico para los descriptores Lagrangianos en sistemas dinámicos dependientes del tiempo. Para ello, primero hemos ampliado la definición de los LDs al contexto discreto de manera que se simplifiquen los cálculos. Se hace precisa una definición para caracterizar los *rasgos singulares* a partir de la cual se obtienen teoremas en cuatro ejemplos particulares. La teoría de la forma normal y el teorema de Hartman-Grobman se aplican en su versión C^1 para sistemas hamiltonianos bidimensionales. Usando ideas similares, la nueva definición de descriptores Lagrangianos discretos se adapta a sistemas dinámicos continuos. Al igual que en el caso discreto, proporcionamos demostraciones rigurosas para cuatro ejemplos particulares construidos a partir de un punto hiperbólico. Nuestras demostraciones se basan en situaciones para las que tenemos un conocimiento a priori de la variedad de un punto hiperbólico, y además demostramos la presencia de singularidades, en el sentido definido, alineadas con estas curvas en el marco de nuestro descriptor lagrangiano. Un resultado más general que no hemos obtenido pero que podría guiar los esfuerzos futuros sería demostrar que estructuras geométricas a través de las cuales no hay flujo material están alineadas con propiedades singulares del LD. Además, otros resultados podrían abordar definiciones adicionales para las propiedades singulares observadas en diferentes contextos a los estudiados o que permitirían demostrar su presencia en la función M, en su verión original distinta a la propuesta en este trabajo, y que ha sido utilizada en muchas aplicaciones (de la Cámara *et al.*, 2012, 2013; Curbelo *et al.*, 2017a; Smith and Mc Donald, 2014; Rempel *et al.*, 2013; Garcia-Garrido *et al.*, 2015, 2016; Craven and Hernandez, 2015, 2016). Las visualizaciones proporcionadas por los LD discretos, en comparación con otros métodos que se han utilizado en Maličký (2012), respaldan la idea de que la habilidad de representación de esta herramienta podría derivar en hallazgos teóricos adicionales para mapas y sugerir la presencia de objetos sobre los que se podrían realizar demostraciones formales.

Además, en el caso continuo, hemos discutido los resultados que muestran la capacidad de los LD para revelar conjuntos invariantes como los n-toros. Estos resultados son solo una extensión directa de la teoría de partición ergódica. Hemos ilustrado esto con dos ejemplos: el oscilador armónico plano y el flujo ABC tridimensional. Estos resultados acerca de la capacidad de los LD para revelar conjuntos invariantes tipo toro ya han comenzado a aplicarse en el contexto atmosférico como herramientas que permiten la identificación del núcleo y los bordes del vórtice polar estratosférico (Curbelo *et al.*, 2017b). La habilidad de esta herramienta en la exploración de sistemas n-dimensionales aún no se ha explorado exhaustivamente. Por ejemplo, todavía quedan preguntas abiertas en el contexto de la astrodinámica, como el problema de 3 cuerpos (o en su versión restringida), para los cuales este tipo de herramientas de visualización podrían proporcionar nuevos conocimientos. Un primer paso en esta dirección sería abordar problemas ampliamente conocidos y explorarlos desde esta perspectiva. Actualmente, en contextos geofísicos, se han realizado estudios 3D con LD en la estratosfera (Curbelo *et al.*, 2017a,b) y han revelado la presencia de variedades invariantes normalmente hiperbólicas.

Nuestro último resultado ha abordado el reto de probar rigurosamente la presencia de conjuntos invariantes caóticos en sistemas dependientes del tiempo de forma no periódica. Para ello, hemos estudiado el mapa Lozi autónomo y no autónomo en la versión en la que se preserva su orientación y su área. Hemos aplicado la primera y segunda condición de Conley-Moser para demostrar la existencia de un conjunto caótico en la versión autónoma de dicho mapa. El hecho de haber demostrado que la primera y la tercera condición de Conley-Moser se cumplen para la versión aperiódica no autónoma bajo ciertos parámetros nos permite abordar

el desafío antes mencionado. Los LD discretos permiten una visualización del comportamiento caótico del mapa Lozi a medida que los parámetros son variados.

Bibliography

Alekseev, V. M. (1968a). Quasirandom dynamical systems. I. *Math. USSR-Sb*, **5**, 73–128.

Alekseev, V. M. (1968b). Quasirandom dynamical systems. II. *Math. USSR-Sb*, **6**, 505–560.

Alekseev, V. M. (1969). Quasirandom dynamical systems. III. *Math. USSR-Sb*, **7**, 1–43.

Aref, H. (1984). Stirring by chaotic advection. *J. Fluid Mech.*, **143**, 1–21.

Aref, H. (2002). The development of chaotic advection. *Phys. Fluids.*, **14**, 1315–1325.

Arnold, V. I. (1973). *Ordinary Differential Equations.* MIT Press.

Aurell, E., Boffeta, G., Crisanti, A., Paladin, G., and Vulpiani, A. (1997). Predictability in the large: An extension of the concept of Lyapunov exponent. *J. Phys. A :Math. Gen.*, **30**, 1–26.

Balibrea, F. (2016). Los secretos de algunas sucesiones de números enteros. *Materials Matemàtics*, (2), 1–32.

Balibrea-Iniesta, F., Lopesino, C., Wiggins, S., and Mancho, A. M. (2015). Chaotic Dynamics in Nonautonomous Maps: Application to the Nonautonomous Hénon Map. *Int. J. Bifurcation and Chaos*, **25**, 1550172.

Batchelor, G. K. (1967). *An Introduction to Fluid Dynamics*. Cambridge University Press, Cambridge,.

Beron-Vera, F. J., Olascoaga, M. J., and Goni, G. J. (2010). Surface Ocean Mixing Inferred from Different Multisatellite Altimetry Measurements. *J. Phys. Oceanogr.*, **40**, 2466–2480.

Branicki, M. and Wiggins, S. (2010). Finite-time Lagrangian transport analysis: stable and unstable manifolds of hyperbolic trajectories and Finite-time Lyapunov exponents. *Nonlin. Proc. Geophys.*, **17**, 1–36.

Chastaing, J. Y., Bertin, E., and Géminard, J. C. (2015). Dynamics of the bouncing ball. *Am. J. Phys.*, **83**, 518.

Coddington, E. A. and Levinson, N. (1955). *Theory of Ordinary Differential Equations*. McGraw-Hill, New York.

Coulliette, C. and Wiggins, S. (2001). Intergyre transport in a wind-driven, quasigeostrophic double gyre: an application of lobe dynamics. *Nonlin. Proc. Geophys.*, **8**, 69–94.

Craven, G. T. Junginger, A. and Hernandez, R. (2017). Deconstructing field-induced ketene isomerization through Lagrangian descriptors. *Phys. Review E*, **96**(2), 022222.

Craven, G. T. and Hernandez, R. (2015). Lagrangian descriptors of thermalized transition states on time-varying energy surfaces. *Phys. Rev. Lett.*, **115**, 148301.

Craven, G. T. and Hernandez, R. (2016). Deconstructing field-induced ketene isomerization through Lagrangian descriptors. *Phys. Chem. Chem. Phys*, **18**(5), 4008–4018.

Curbelo, J., Garcia-Garrido, V. J., Mechoso, C. R., Mancho, A. M., Wiggins, S., and Niang, C. (2017a). Insights into the three-dimensional Lagrangian geometry of the Antarctic polar vortex. *Nonlin. Processes Geophys*, **24**(3), 379–392.

Curbelo, J., Mechoso, C. R., Mancho, A. M., and Wiggins, S. (2017b). Lagrangian study of the final warming in the southern stratosphere during 2002. *submitted to Climate dynamics*.

de la Cámara, A., Mechoso, C. R., Ide, K., R. Walterscheid, and Schubert, G. (2010). Polar night vortex breakdown and large-scale stirring in the southern stratosphere. *Climate Dynamics*, **35**(6), 965–975.

de la Cámara, A., Mancho, A. M., Ide, K., Serrano, E., and Mechoso, C. (2012). Routes of transport across the Antarctic polar vortex in the southern spring. *J. Atmos. Sci.*, **69**(2), 753–767.

de la Cámara, A., Mechoso, C. R., Serrano, E., and Ide, K. (2013). Quasi-horizontal transport within the Antarctic polar night vortex: Rossby wave breaking evidence and Lagrangian structures. *J. Atmos. Sci.*, **70**, 2982–3001.

Devaney, R. L. and Nitecki, Z. (1979). Shift automorphisms in the Hénon mapping. *Comm. Math. Phys.*, **67**, 137–148.

d'Ovidio, F., Fernández, V., Hernández-García, E., and López, C. (2004). Mixing structures in the Mediterranean Sea from finite-size Lyapunov exponents. *Geopys. Res. Lett.*, **31**(L17203).

Farazmand, M. and Haller, G. (2012). Computing Lagrangian Coherent Structures from variational LCS theory. *Chaos*, **22**(013128).

Froyland, G. and Padberg-Gehle, K. (2014). Almost-invariant and finitetime coherent sets: directionality, duration, and diffusion, Ergodic Theory, Open Dynamics, and Coherent Structures. *Proc. Math. Stat.*, **70**, 171–216.

Froyland, G., Horenkamp, C., Rossi, V., Santitissadeekom, N., and Gupta, A. S. (2012). Three-dimensional characterization and tracking of an agulhas ring. *Ocean Model.*, **52-53**, 69–75.

Garcia-Garrido, V. J., Mancho, A. M., and Wiggins, S. (2015). A dynamical systems approach to the surface search for debris associated with the disappearance of flight MH370. *Nonlin. Proc. Geophys.*, **22**, 701–712.

Garcia-Garrido, V. J., Ramos, A., Mancho, A. M., Coca, J., and Wiggins, S. (2016). A dynamical systems perspective for a real-time response to a marine oil spill. *Marine Pollution Bulletin.*, pages 1–10.

Hadjighasem, A., Farazmand, M., Blazevski, D., Froyland, G., and Haller, G. (2017). A critical comparison of Lagrangian methods for coherent structure detection. *Chaos*, **27**(5), 053104.

Haller, G. and Beron-Vera, F. J. (2012). Geodesic theory of transport barriers in two-dimensional flows. *Physica D*, **241**, 1680–1702.

Holmes, P. J. (1982). The dynamics of repeated impacts with a sinusoidally vibrating table. *J. Sound Vibr.*, **84**, 173–189.

Junginger, A. and Hernandez, R. (2016). Uncovering the geometry of barrierless reactions using Lagrangian descriptors. *J. Phys. Chem. B*, **120**(8), 1720–1725.

Junginger, A., Craven, G. T., Bartsch, T., Revuelta, F., Borondo, F., Benito, R. M., and Hernandez, R. (2016). Transition state geometry of driven chemical reactions on time-dependent double-well potentials. *Phys. Chem. Chem. Phys.*, **18**, 30270.

Koon, W. S., Lo, M. W., Marsden, J. E., and Ross, S. D. (2000). Heteroclinic connctions between orbits and resonance transitios in celestial mechanics. *Chaos*, **10**, 427–469.

Lekien, F., Shadden, S. C., and Marsden, J. E. (2007). Lagrangian coherent structures in n-dimensional systems. *J. of Mathematical Physics*, **48**(6), 065404.

Lerman, L. and Silnikov, L. (1992). Homoclinical structures in nonautonomous systems: Nonautonomous chaos. *Chaos*, **2**, 447–454.

Levnajić, Z. and Mezić, I. (2010). Ergodic theory and visualization. i. mesochronic plots for visualization of ergodic partition and invariant sets. *Chaos*, **20**(3).

Madrid, J. A. J. and Mancho, A. M. (2009). Distinguished trajectories in time dependent vector fields. *Chaos*, **19**, 013111.

Malhotra, N. and Wiggins, S. (1998). Geometric structures, lobe dynamics, and Lagrangian transport in flows with aperiodic timedependence, with applications to Rossby wave flow. *J. Nonlinear Science*, **8**, 401–456.

Maličký, P. (2012). Interior periodic points of a Lotka-Volterra map. *Journal of Difference Equations and Applications*, **18**(4), 553–567.

Maličký, P. (2017). Personal communication.

Mancho, A. M., Small, D., and Wiggins, S. (2004). Computation of hyperbolic and their stable and unstable manifolds for oceanographic flows represented as data sets. *Nonlin. Proc. Geophys.*, **11**, 17–33.

Mancho, A. M., Small, D., and Wiggins, S. (2006). A tutorial on dynamical systems concepts applied to Lagrangian transport in oceanic flows defined as finite time data sets: Theoretical and computational issues. *Phys. Rep.*, **237**(3-4).

Mancho, A. M., Hernández-García, E., Small, D., Wiggins, S., and Fernández, V. (2008). Lagrangian transport through an ocean front in the North-Western Mediterranean Sea. *J. Phys. Oceanogr*, **38**(6), 1222–1237.

Mancho, A. M., Wiggins, S., Curbelo, J., and Mendoza, C. (2013). Lagrangian Descriptors: A Method for Revealing Phase Space Structures of General Time Dependent Dynamical Systems. *Communications in Nonlinear Science and Numerical Simulation*, **18**, 3530–3557.

Manney, G. L. and Lawrence, Z. D. (2016). The major stratospheric final warming in 2016: dispersal of vortex air and termination of Arctic chemical ozone loss. *Atmos. Chem. Phys.*, **16**, 15371–15396.

Mendoza, C. and Mancho, A. M. (2010). The hidden geometry of ocean flows. *Phys. Rev. Lett.*, **105**(3), 038501.

Mendoza, C. and Mancho, A. M. (2012). Review Article: "The Lagrangian description of aperiodic flows: a case study of the Kuroshio Current". *Nonlin. Processes Geophys.*, **19**, 449–472.

Mendoza, C., Mancho, A. M., and Rio, M.-H. (2010). The turnstile mechanism across the Kuroshio current: analysis of dynamics in altimeter velocity fields. *Nonlin. Proc. Geophys.*, **17**(2), 103–111.

Mendoza, C., Mancho, A. M., and Wiggins, S. (2014). Lagrangian Descriptors and the Assesment of the Predictive Capacity of Oceanic Data Sets. *Nonlin. Proc. Geophys.*, **21**, 677–689.

Mezic, I. and Wiggins, S. (1999). A method for visualization of invariant sets of dynamical systems based on the ergodic partition. *Chaos*, **9**(1), 213–218.

Miller, P. D., Jones, C. K. R. T., Rogerson, A. M., and Pratt, L. J. (1997). Quantifying transport in numerically generated velocity fields. *Physica D.*, **110**, 105–122.

Moser, J. (1973). *Stable and Random Motions in Dynamical Systems.*, volume 77. Annals of Mathematical Studies (Princeton University Press).

Nese, J. M. (1989). Quantifying local predictability in phase space. *Physica D*, **35**, 237–250.

Nusse, H. E. and Yorke, J. A. (1989). A procedure for finding numerical trajectories on chaotic saddles. *Physica D Nonlinear Phenomena*, **36**(1), 137–156.

Ottino, J. (1989a). *The Kinematics of Mixing: Stretching, Chaos, and Transport*. Cambridge University Press, Cambridge,.

Ottino, J. M. (1989b). The mixing of fluids. *Scientif. Am.*, **260**, 56–67.

Poincaré, H. (1890). Sur le problème des trois corps et les équations de la dynamique. *Acta Mathematica*, **13**, 1–270.

Rempel, E. L., Chian, A. C.-L., Brandenburg, A., Munuz, P. R., and Shadden, S. C. (2013). Coherent structures and the saturation of a nonlinear dynamo. *Journal of Fluid Mechanics*, **729**, 309–329.

Rom-Kedar, V., Leonard, A., and Wiggins, S. (1990). An analytical study of transport, mixing and chaos in an unsteady vortical flow. *Journal of Fluid Mechanics*, **214**, 347–394.

Rypina, I. I., Scott, S. E., Pratt, L. J., and Brown, M. G. (2011). Investigating the connection between complexity of isolated trajectories and Lagrangian coherent structures. *Nonlin. Proc. Geophys.*, **18**, 977–987.

Shadden, S. C., Lekien, F., and Marsden, J. E. (2005). Definition and properties of Lagrangian Coherent structures from finite-time Lyapunov exponents in two-dimensional aperiodic flows. *Physica D*, **212**, 271–304.

Shadden, S. C., Lekien, F., Paduan, J. D., Chavez, F. P., and Marsden, J. E. (2009). The correlation between surface drifters and coherent structures based on high-frequency radar data in Monterey Bay. *Deep-Sea Res. Pt. II*, **56**, 161–172.

Smale, S. (1967). Differentiable dynamical systems. *Bull. Amer. Math. Soc.*, **73**(6), 747–817.

Smith, M. and Mc Donald, A. J. (2014). A quantitative measure of polar vortex strength using the function M. *J. Geophys. Res.*, **119**, 5966–5985.

Stoffer, D. (1988a). Transversal homoclinic points and hyperbolic sets for non-autonomous maps I. *J. Appl. Math. Phys. (ZAMP)*, **39**, 518–549.

Stoffer, D. (1988b). Transversal homoclinic points and hyperbolic sets for non-autonomous maps II. *J. Appl. Math. Phys. (ZAMP)*, **39**, 783–812.

Sturman, R., Ottino, J. M., and Wiggins, S. (2006). *The Mathematical Foundations of Mixing*, volume 22. Cambridge Monographs on Applied and Computational Mathematics.

Tew Kai, E., Rossi, V., Sudre, J., Weimerskirch, H., Lǿpez, C., Hernández-García, E., Marsac, F., and Garçon, V. (2009). Top marine predators track Lagrangian Coherent Structures. *P. Natl. Acad. Sci. USA*, **106**, 8245–8250.

Wiggins, S. (1992). *Chaotic Transport in Dynamical Systems*. Springer-Verlag, New York.

Wiggins, S. (1999). Chaos in the dynamics generated by sequences of maps, with applications to chaotic advection in flows with aperiodic time dependence. *Z. angew. Math. Phys. (ZAMP)*, **50**, 585–616.

Wiggins, S. (2003). *Introduction to Applied Nonlinear Dynamical Systems and Chaos.* Springer, 2nd edition.

Wiggins, S. (2005). The Dynamical Systems Approach to Lagrangian Transport in Oceanic Flows. *Annu. Rev. Fluid Mech.*, **37**, 295–328.

Wiggins, S. and Mancho, A. M. (2014). Barriers to tranport in aperiodically time-dependent two dimensional velocity fields: Nekhoroshev's Theorem and 'Nearly Invariant' Tori. *Nonlin. Proc. Geophys.*, **21**, 165–185.

Wiggins, S. and Ottino, J. (2004). Foundations of Chaotic Mixing. *Phil. Trans. Roy. Soc.*, **362 (1818)**, 937–970.